**The Dissertation Committee for Krista Marie Angileri Certifies that this is the approved version of the following dissertation:**

# Genetic and Epigenetic Regulation of Ocular Development and Homeostasis

**Committee:**

Steven A. Vokes, Supervisor

Jeffrey M. Gross, Co-Supervisor

Jonghwan Kim

Kyle M. Miller

Haley Tucker

# Genetic and Epigenetic Regulation of Ocular Development and Homeostasis

**by**

**Krista Marie Angileri**

**Dissertation**

Presented to the Faculty of the Graduate School of

The University of Texas at Austin

in Partial Fulfillment

of the Requirements

for the Degree of

**Doctor of Philosophy**

**The University of Texas at Austin**

**May 2020**

# Dedication

To those who have always supported my endeavors, my parents: Mike and Mary Angileri. You are my constant source of strength, guidance, and love. You taught me how to persevere and to “play the game”. I would not be the person I am today without you.

Love always.

# Acknowledgements

I would first like to thank my advisor, Dr. Jeffrey M. Gross for his endless guidance, support, and patience throughout my sixteen-months-too-long graduate career. Through his mentorship, I now feel ready to tackle any obstacles that lie ahead. Thank you to the members of my dissertation committee: Dr. Steven A. Vokes, Dr. Jonghwan Kim, Dr. Kyle M. Miller, and Dr. Haley Tucker for their invaluable insight and advice.

Thank you to all members of the Gross lab, past and present. You all have been a constant source of motivation, scientific criticism, and wealth of knowledge throughout the years, many of whom survived our lab-pocalypse upon arrival in Pittsburgh. Your comradery and helped to push me through this arduous adventure to completion. Thank you to my colleagues from the Molecular Biosciences department at the University of Texas at Austin and the Ophthalmology and Developmental Biology departments at the University of Pittsburgh. You all have contributed so much to my growth as a scientist.

I would like to thank my chosen families away from home, both in Austin and Pittsburgh, who have been a wealth of energy, fun, and laughter through the years. To my kung fu students, thank you for subconsciously knowing when to push and when to make me proud. Your constant waves of growth and progress are memories that will stay with me forever.

Finally, I would like to thank my biological family. To my father who taught me to "play the game" and has been a shining beacon of patience through the years. To my mother, for her unconditional love, understanding, and support as I pursue my dreams. To my siblings who have helped mold me into the person I am today. You all inspire me to be a better version of myself, and I would be nothing without you all.

# Genetic and Epigenetic Regulation of Ocular Development and Homeostasis

Krista Marie Angileri, PhD

The University of Texas at Austin, 2020

Supervisor: Steven A. Vokes

Co-Supervisor: Jeffrey M. Gross

Vertebrate retinogenesis is a complex developmental process that requires the dynamic orchestration of multiple tissues and cell types, morphological changes, and intrinsic and extrinsic cellular signaling. Intertwined with these processes are coordinated genetic and epigenetic mechanisms that function to regulate cellular state, proliferation, differentiation, and maintenance of retinal progenitor cells and neurons. Disruption of the DNA methylome or micro-RNA pathways, the regulatory pathways examined in this study, results in aberrant cellular proliferation, differentiation, and retinal homeostasis. Additionally, defects in these pathways are known to result in tumorigenesis, embryonic lethality, and neurodegenerative disease. Data presented in this thesis address the role of maintenance and *de novo* DNA methylation in the retina. Utilizing the zebrafish as a model for vertebrate retinal stem cell (RSC) maintenance and development, I demonstrated a requirement for *dnmt1*, the maintenance DNA methyltransferase, in RSC maintenance through the regulation of cell cycle genes, cell survival, and dysregulation of retroviral elements (RE). Additionally, I generated combinatorial mutants for the six *de novo* DNA methylation genes using TALEN and CRISPR/Cas9 mutagenesis to assess the function of these enzymes during retinogenesis. The tested combinations of mutant alleles lack overt

phenotypes, however further analyses will be critical for determining their gene-specific and likely overlapping roles within the retina. Finally, I aimed to characterize the role of the dual-specificity phosphatase enzyme, Dusp11, within the retina. Utilizing a Dusp11, splice-mutant mouse line, I lay the groundwork for characterizing this enzyme *in vivo* and assessing its roles in retinal maintenance and potential contribution to retinal degeneration diseases. Through the use of Spectral Domain Optical Coherence Tomography (SD-OCT), I performed longitudinal experiments to assess retinal lamination and structure. Additionally, preliminary immunohistochemistry unveiled potential cell type-specific localization of Dusp11. These findings require further validation, but provide a first glimpse into ocular requirements for Dusp11 function and potentially revealing a unique genetic regulator that contributes to retinal degenerative diseases.

# Table of Contents

# List of Tables

# List of Figures

# List of Illustrations

# CHAPTER 1: INTRODUCTION TO EYE DEVELOPMENT AND DISEASE.

Table 1.1. Common Abbreviations

| Definition | Abbreviation |
|---|---|
| Retinal Stem Cell | RSC |
| Ciliary Marginal Zone | CMZ |
| Ganglion Cell Layer | GCL |
| Retinal Neural Fiber Layer | RNFL |
| Inner Nuclear Layer | INL |
| Inner Plexiform Layer | IPL |
| Outer Nuclear Layer | ONL |
| Outer Plexiform Layer | OPL |
| Inner Segments | IS |
| Outer Segments | OS |
| Retinal Pigmented Epithelium | RPE |
| 5-methylcytosine | 5mC |
| Bruch's Membrane | BM |
| Age-Related Macular Degeneration | AMD |
| Choroidal Neovascularization | CNV |
| DNA methyltransferase | Dnmt |
| Dual-Specificity Phosphatase | Dusp |
| Retroelements | RE |
| Micro-RNA | miRNA |
| Tri-phosphorylated RNA | 3pRNA |
| Gap junctions | GJ |

1.1 Ocular development and maturation.

The vertebrate retina is a complex organ, which derives from the embryonic forebrain. The overall development and structure of the human eye is recapitulated in other vertebrate model organisms such as the mouse and zebrafish[1–3]. The genetic and morphological similarities found in these models provide the necessary tools for studying retinal development and disease through genetic perturbations and analyses.

Retinal development begins when evagination from the diencephalon forms the optic vesicles[2]. Once the optic vesicle contacts the overlying ectoderm, its morphology changes and starts the invagination process to create the optic cup (Illustration 1.1)[3]. Once the optic cup is formed, cells within the inner layer begin to differentiate into the neural retina and those in the outer layer form the retinal pigmented epithelium (RPE). At early time points, the neural retina is comprised of retinal stem cells (RSCs) in a pseudo-stratified epithelial structure[4]. Over time, embryonic RSCs begin to differentiate into six neural cell types and one glial cell type[5–7] beginning in the central retina and fanning outward toward the retinal periphery[8].

Eventually, mammalian RSCs become confined to the ciliary margin at the most peripheral edge of the retina, transition into a quiescent state, and remain inactive throughout life[9]. By comparison, zebrafish RSCs, though also restricted to the peripheral region of the retina termed the Ciliary Marginal Zone (CMZ), remain proliferative throughout life allowing for continued growth[8,10,11]. The CMZ contains a mixed population of RSCs and retinal progenitor cells that are fated for differentiation and incorporation into the neural retina[10,12,13]. Newly formed neurons and glia first integrate into the neural retina

apposed to the CMZ, and as younger neurons continue to be generated, the older cells are shifted inward toward the central region of the retina, creating newly differentiated neurons in concentric rings[4,14,15]. The ability of the zebrafish to maintain these RSC populations throughout life, and in combination with their genetic tractability, fecundity, and ease of genetic manipulation, provides scientists with a unique opportunity to understand RSC maintenance and particularly the epigenetic modifications that influence this cell state.

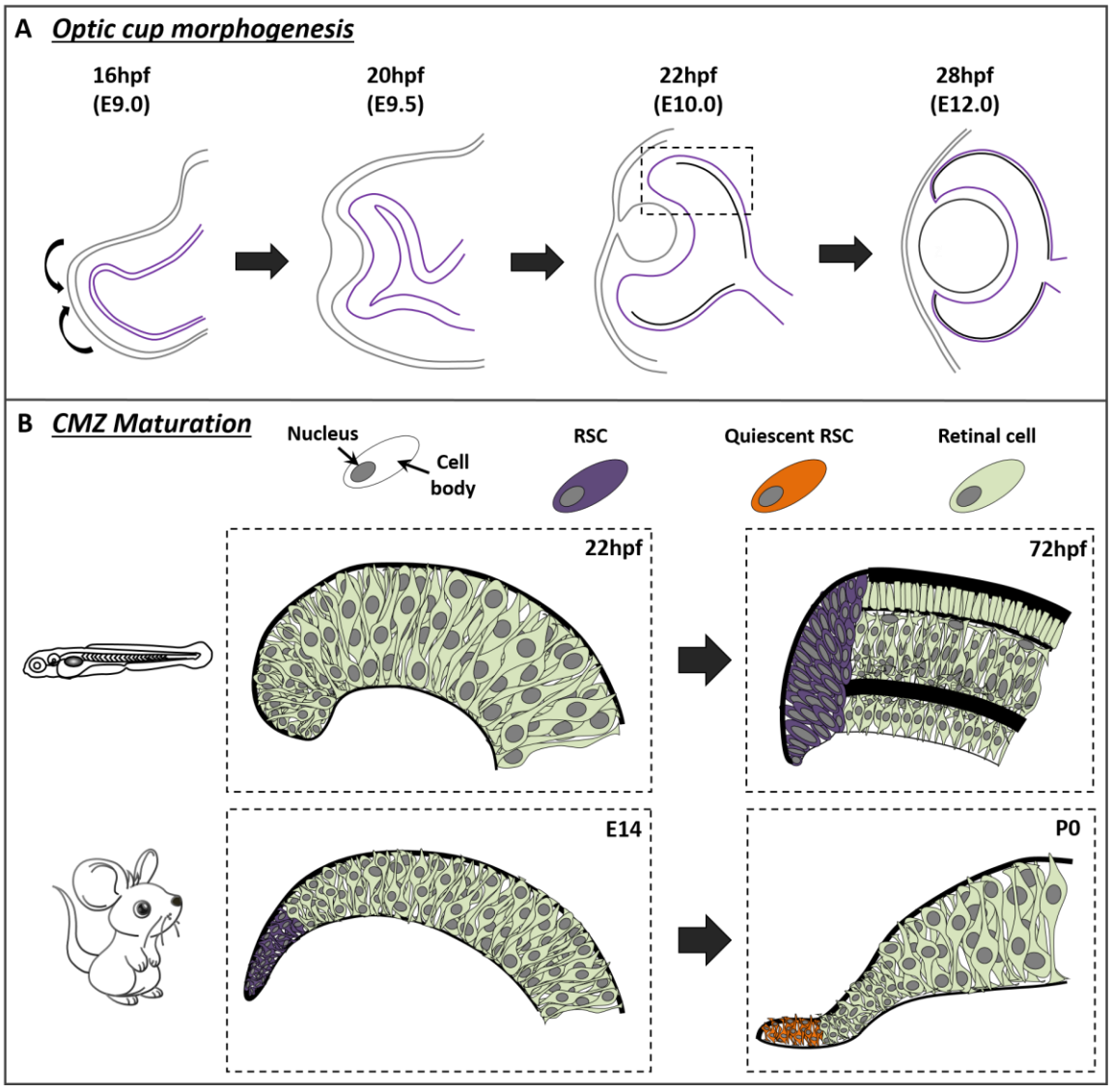


Illustration 1.1. Diagram of vertebrate optic cup morphogenesis and CMZ maturation. **A.** The optic vesicle begins to invaginate around 16hpf (zebrafish) or E9.0 (mouse) to create the optic cup by 22hpf (or E10.0). Cells within the retina begin to differentiate between 22-28hpf (E12.). Neural ectoderm (gray). Optic vesicle/cup (purple). **B.** Enlarged diagrams of the dotted square in A. *Top*: The zebrafish CMZ matures by 72hpf. Note the differences in cell and nuclear shape of the CMZ compared to the differentiated neural retina at 72hpf. *Bottom*: The mouse ciliary margin is proliferative during embryonic development, and RSCs become quiescent in the ciliary margin. Hours post fertilization (hpf), Embryonic day (E), Postnatal day (P), retinal stem cell (RSC), Ciliary Marginal Zone (CMZ).

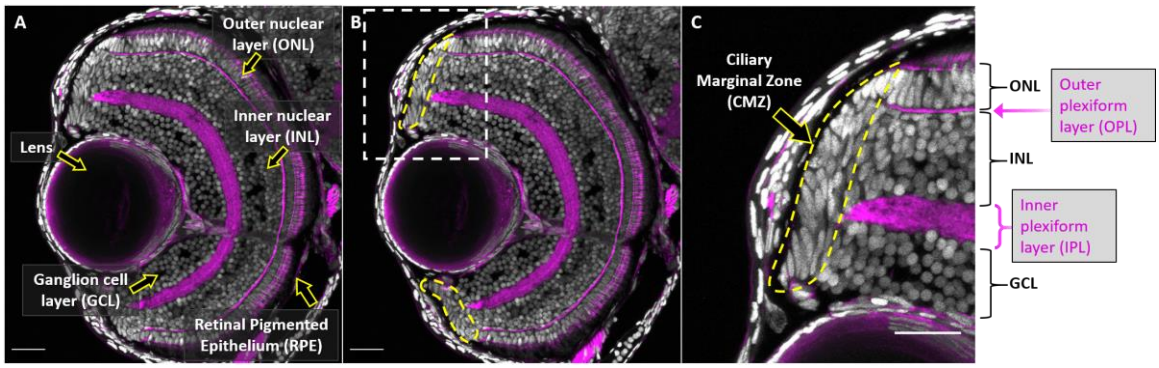


Figure 1.1. Zebrafish Ciliary Marginal Zone morphology.
**A-B.** Transverse cross-section of the zebrafish eye defining the lens and neural retinal layers (A) and the Ciliary Marginal Zone (B). **C.** Enlarged image of the CMZ (white dotted rectangle from B). The CMZ is located at the retinal periphery (yellow dotted line). Nuclei labeled with DAPI (gray). F-actin labeled with Phalloidin (magenta). Scale bars: 30 μm.

## 1.2 Age-related macular degeneration

Degenerative ocular diseases affect millions of people worldwide, and within developed countries, one of the more predominant diseases reported is age-related macular degeneration (AMD)[16,17]. AMD can be categorized as geographic atrophy (dry AMD) or exudative (wet AMD). Dry AMD is the more common form of the disease, and its pathology is first characterized through degeneration of the RPE in the central retina, closely followed by death and degeneration of the apposed photoreceptors[18]. Wet AMD however, denoted by infiltration of the choroidal vasculature into the retina, termed choroidal neovascularization (CNV)[16]. The most prominent indication of AMD onset and correlated geographic atrophy is the buildup of drusen, membrane-rich deposits between the RPE and Bruch's membrane[19], or as reticular pseudodrusen between photoreceptors and the RPE[20,21]. Although the mechanisms underlying the development of AMD are still unclear, scientists in the field theorize that this is caused by chronic inflammation[22,23], a common correlating phenotype associated with epigenetic dysregulation[24–26]. This study focuses on both an epigenetic pathway, DNA methylation, and genetic perturbation of the microRNA (miRNAs) pathway within the eye.

## 1.3 Epigenetic and genetic regulation of the retina.

A common trait of many degenerative diseases is aberrant epigenetic regulation[27,28]. The concept of epigenetics denotes the potential of a single genomic sequence producing one or more differing phenotypes[29,30]. These alterations can be driven by a variety of cellular signals including histone methylation[31] and DNA methylation[32]. These epigenetic

mechanisms work in combination to regulate tissue development[33,34], differentiation[35,36], and maintenance[37–39].

### 1.3.1 DNA methylation pathway

DNA methylation involves the addition of a methyl group to the 5$^{th}$ position of the cytosine bases to create 5-methylcytosine (5mC). This process is catalyzed by a family of enzymes termed DNA methyltransferases (dnmts) (Illustration 1.2) .[40,41] Removal of DNA methylation is accomplished through a variety of proposed pathways extending from replication-dependent passive dilution to enzymatic removal[42,43]. Although this part of the DNA methylation pathway has been shown to be important for intercellular signaling and differentiation[44,45], the processes of demethylation are not addressed within this study. Instead, this study (specifically Chapters 2 and 3) focuses on the enzymes responsible for defining these landscapes.

DNA methyltransferases fall within two main categories: *de novo* and maintenance. *De novo* dnmts (*Dnmt3* family) function to add the initial methylation mark to cytosine bases[46,47], and the maintenance of this mark is propogated by *Dnmt1* during DNA replication (Illustration 1.2).[48–50] Previous studies have identified numerous processes that are affected by changes in the DNA methylome, for example gene expression[51,52], chromatin accessibility[53], transcription factor binding[54,55], and silencing of transposable elements[56,57]. Additionally, the location of 5mC marks within the genome also partially determines how this epigenetic mark will modulate gene expression.

Genes containing high levels of 5mC at their transcription start sites and enhancer elements are inversely correlated with expression[54,58], whereas intragenic 5mC is positively correlated with expression[59,60]. This creates a cell-type specific methylome that is specific to the identity of that particular cell and tissue. In mammals, DNA methylation is critical for development[61–64], and loss-of-function mutations in Dnmt3a and Dnmt3b often result in tumorigenic phenotypes[65–69]. Moreover, genomic hypomethylation *in vitro* is correlated with premature differentiation[70,71] and defects in chromosomal organization, which can have wide-ranging effects on gene expression and regulation[72–74]. Studies have also demonstrated cross-talk between DNA methylation and miRNA pathways [75–77].

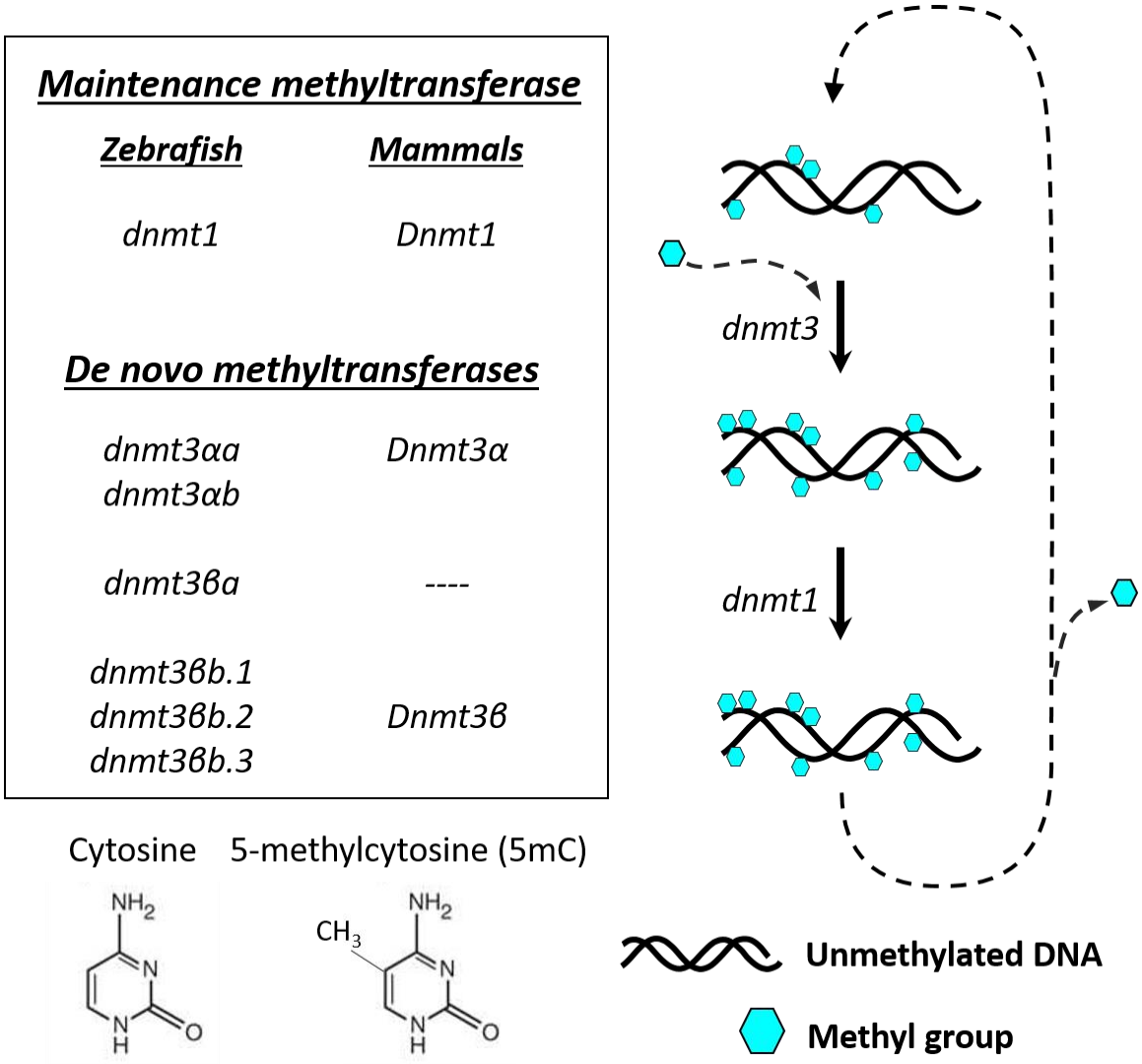


Illustration 1.2. DNA methylation pathway.
*Box*: List of DNA methyltransferase genes in the zebrafish (*left*) across from the mammalian orthologue (*right*). The addition of methyl groups to DNA catalyzed by dnmt3 enzymes and propagated by the dnmt1 enzyme.

### 1.3.2 Regulation of microRNA and endogenous retroviral expression

Small noncoding RNAs function to cooperate with epigenetic modifications to regulate gene expression through either specific or non-specific targeting of genic mRNAs[78]. These consist of 1) small interfering (si)RNAs and miRNAs produced through the Dicer pathway[79] and 2) the gonadal-specific PIWI-associated (pi)RNAs[80] which act to repress endogenous retroelement (RE)[81–83] activity.

Canonical miRNAs originate from a single poly-cistronic RNA containing multiple primary miRNA templates[84] (Illustration 1.3) and are typically transcribed by the RNA Polymerase II enzyme[85]. However, non-canonical miRNAs often lie within REs which contain sequence elements that are specific to RNA Polymerase III activity[86]. Early processing of primary miRNAs occurs in the nucleus where they are trimmed by the microprocessor complex containing the Drosha and DGCR8 proteins[87,88]. This produces a precursor miRNA product that is exported from the nucleus and processed by the Dicer complex to yield the final ~22 nucleotide double-stranded miRNA[89]. Previous work has demonstrated that effective processing of miRNA requires Dicer's ability to recognize and bind the 5' tail[90]. Once associated with Dicer, the duplex associates with the Argonaute (Ago) protein to form the RNA-induced silencing complex (RISC)[91–93]. While in this complex, one of the two RNA strands is selected to remain associated with Ago and the other is released for degradation. The Ago protein is then guided by the final miRNA product to target and downregulate gene transcripts[94,95].

The degree to which a miRNA modulates gene expression is dependent upon its sequence specificity. miRNAs with perfect sequence complementarity, when bound to the

Ago complex, will lead to cleavage of the target mRNAs. Alternatively, if miRNAs are not perfectly complementary, then their association with the Ago complex will sequester the target mRNAs from translational machinery[96,97]. It is through this sequence specificity that miRNAs are able to modulate gene expression, including mRNA levels of epigenetic regulators whether it is of histone modifiers[98–100] or DNA methylation enzymes[95,101,101–103], demonstrating a link between these two mechanistic pathways. Disruption of miRNA association with either the nuclear Drosha/DGCR8 complex or cytoplasmic Dicer/Ago complex can result in aberrant gene expression and differentiation[104–106], tumorigenesis[107], or degenerative diseases[108–111]. Furthermore, the Dicer/miRNA pathway has been implicated in control of RE expression and activity[83,112].

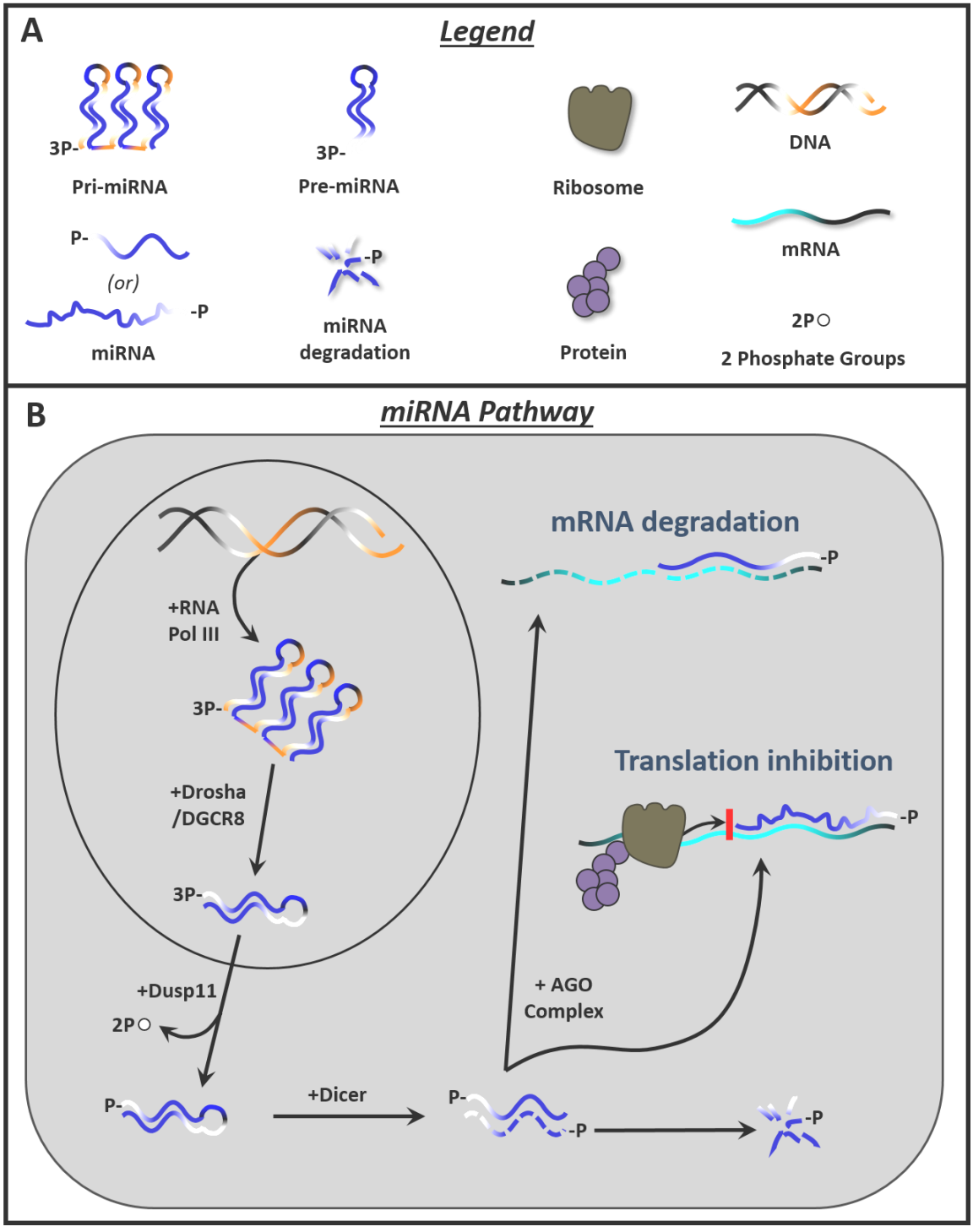


Illustration 1.3. RNA polymerase III generated miRNA pathway.
**A:** Legend of the miRNA pathway components. **B.** Diagram of the miRNA pathway..

### 1.3.3 Retroelement contribution to neurodegenerative disease

miRNAs and epigenetics play a crucial role in how the genome functions and genes are regulated and, in doing so, ultimately affect how a cell responds to stress. As stated previously, DNA methylation and miRNAs are crucial players in these processes and disruption of either are known to have detrimental effects[61,108,113]. Critically, they are also required for proper regulation of REs. REs are a subset of ancient viral sequences contained within mammalian DNA and constitute over 40 percent of the human genome[114]. Many REs maintain the potential to "jump" or transpose themselves into novel locations in the genome thus having detrimental effects on cellular function. Additionally, overexpression of REs is causal to increases in inflammation, a feature of multiple neurodegenerative disorders to include Alzheimer's[115,116], hereditary sensory and autonomic neuropathy type IE[117], and Creutzfeldt-Jakob disease[118].

Previous reports have demonstrated a requirement for DNA methylation[113,119,120] and miRNAs[104,121,122] in proper gene regulation within the retina. Defects in either of these regulatory pathways are tightly correlated with RE overexpression, increased inflammation, and the onset of degenerative eye diseases to include retinoblastoma[107] and age-related macular degeneration (AMD)[108,123]. Currently, there are no known cures for AMD and therapies are limited. Therefore it is necessary to increase our understanding of how these pathways contribute to degenerative eye disease and can inform the ophthalmology field when developing novel therapeutic strategies.

# CHAPTER 2: DNMT1 IS REQUIRED TO MAINTAIN RETINAL STEM CELLS IN THE CILIARY MARGINAL ZONE:

Portions of this Chapter are modified with permission from the following article:
*Angileri, K.M., Gross, J.M., 2020. dnmt1 function is required to maintain retinal stem cells within the ciliary marginal zone of the zebrafish eye. Scientific Reports (in revision). KMA conducted all experiments. KMA wrote and KMA and JMG edited the manuscript.*

## 2.1 Introduction

The distal region of the vertebrate retina, termed the ciliary marginal zone (CMZ), contains a population of resident retinal stem cells (RSCs). The CMZ remains proliferative throughout the life of fish, but it proliferates to a more limited extent during the lifetime of amphibians and birds[8,10,124–127]. Whether an analogous structure exists in mammals is debated, but there are distinct, progenitor-like cells in the periphery of the retina that are active during embryogenesis[5,7,128]. Mammalian RSCs can also be isolated from the adult ciliary margin, cultured *in vitro*, and stimulated to produce retinal neurons[129–132]. However, this activity has not been demonstrated in the mature mammalian retinae *in vivo*.

Studies of the CMZ have primarily focused on zebrafish and *Xenopus* models to determine genetic pathways required for RSC identity[13,125,133,134] and to characterize the epigenetic networks which regulate RSC function[135,136]. By comparison, the mechanisms mediating RSC maintenance *in vivo* remain unknown. In studies of RSCs, the zebrafish has been advantageous given that it possesses a highly active RSC population and is tractable for genetic and pharmacological manipulations, transgenesis and *in vivo* imaging[137,138].

DNA methylation, a frequently studied epigenetic modification, is the process through which a methyl group is added to the fifth carbon of cytosine nucleotides and is commonly found at CpG dinucleotide sequences[139]. Members of the family of DNA methyltransferase (Dnmt) enzymes[41,140] catalyze this epigenetic modification. Dnmt1 serves as a maintenance methyltransferase, copying the methylation pattern from parent to daughter strand during DNA replication and its function is required for cell cycle progression[35,141,142]. Loss of Dnmt1 function results in genomic hypomethylation[70,120,143] and in developmental contexts and specific organ systems, this often compromises progenitor cell maintenance[35,120,144–147] through numerous cellular mechanisms. These include: inducing cell cycle arrest[148,149], retroelement activation[56,57,150,151], inflammatory responses[24,56,147], aberrant differentiation[70,74,145,152–154] and/or *p53*-mediated apoptosis[148,149].

Utilizing the *dnmt1*$^{s872}$ mutant zebrafish allele[144], a widely used catalytically inactive point mutant, we establish an *in vivo* requirement for dnmt1 in RSCs. Through our analyses, we identify a decrease in overall RSC numbers, reduced RSC proliferation and aberrant gene expression patterns within the dnmt1-deficient CMZ. Additionally, we note increased retroelement expression and increased retrotransposition activity in *dnmt1*$^{-/-}$ embryos. Remarkably, RSCs in *dnmt1*$^{-/-}$ embryos are eliminated in a p53-independent manner, suggesting that dnmt1 represses alternative, non-apoptotic cell death pathways in RSCs. Taken together, these data highlight a novel function for dnmt1 in maintaining stem cell populations in the vertebrate retina.

## 2.2. Results

### 2.2.1. *DNMT1* MUTANTS POSSESS DEFECTS IN THE CILIARY MARGINAL ZONE.

Previously, we identified a requirement for dnmt1 in maintaining lens epithelial cell viability using *dnmt1*$^{s872}$ mutant zebrafish[120]. During these previous studies, we also detected photoreceptor layer abnormalities, similar to those documented in *Dnmt1*$^{-/-}$ conditional knockout mice[113,119], and an apparent defect in the CMZ. With an interest in the role that dnmt1 plays in maintaining RSCs *in vivo*, here, we focused further on the CMZ phenotype. Using DAPI to label and count retinal nuclei, we confirmed a progressive degeneration of CMZ morphology beginning at 4 days post fertilization (dpf; Figure 2.1A-F) and a significant decline in retinal cell numbers through 5dpf (Figure 2.1G).

The total number of cells present within central retina sections are equivalent between *dnmt1*$^{-/-}$ and sibling larvae at 3dpf; however, numbers in *dnmt1*$^{-/-}$ larvae diminish significantly between 4 and 5dpf (18.8% and 26.6% reduction respectively; $p$ <0.0005; Figure 2.1G). Additionally, we compared the proportions of nuclei within the ganglion cell layer (GCL), inner nuclear layer (INL), outer nuclear layer (ONL), and CMZ between *dnmt1*$^{-/-}$ larvae and siblings from 3-5dpf (Figure 1H). Interestingly, the proportions of cells in all three retinal laminae (GCL, INL, & ONL) remained equivalent over time in *dnmt1*$^{-/-}$ larvae when compared to siblings, with only a slight increase in the ONL at 4dpf (Figure 2.1H and Figure 2.2A-C; $p$ <0.005). In contrast, the CMZ proportion decreased significantly from 3-5dpf suggesting that dnmt1 function in the retina is required within the CMZ to maintain the RSC population (Figure 2.1H and Figure 2.2D; $p$ <0.0005).

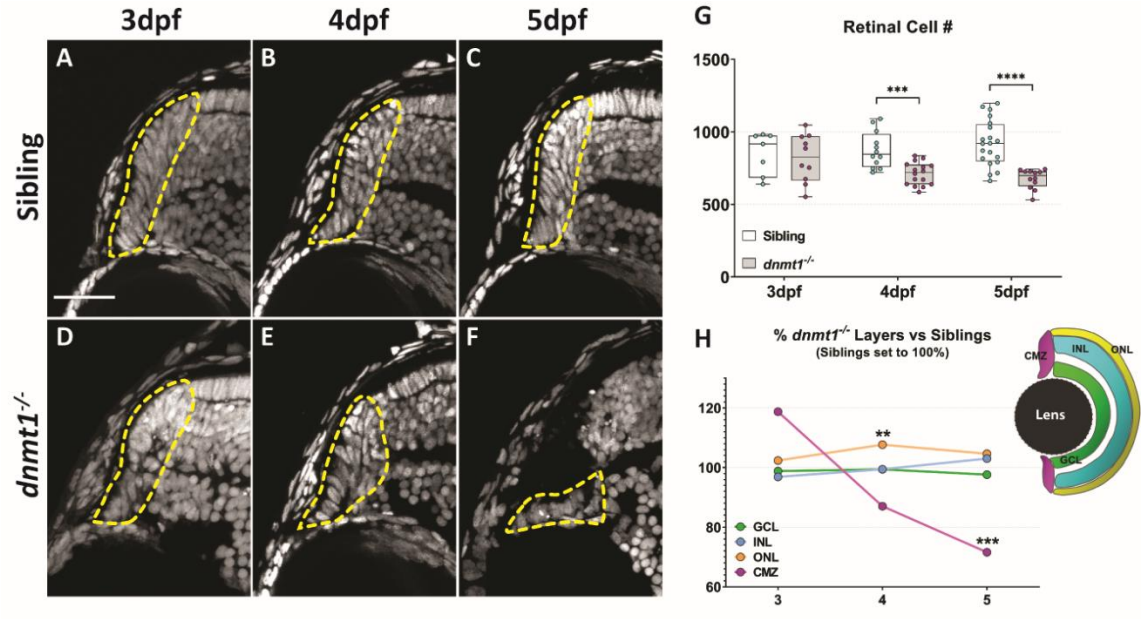


Figure 2.1. Disruption of dnmt1 function results in CMZ defects.

**A-F.** DAPI staining of nuclei (gray) within the CMZ (white dotted lines delineate CMZ boundaries) of siblings (**A-C**) and *dnmt1*$^{-/-}$ (**D-F**) larvae from 3-5dpf. **G.** Average number of all nuclei within the central retina of siblings and mutants. Each data point is the average of cell counts from three different 12 µm sections in one eye of a single larva. **H.** Proportional changes of *dnmt1*$^{-/-}$ retinal domains (GCL, INL, ONL, & CMZ) relative to siblings (set to 100%). Colors correspond with retinal domains in diagram. Scale bars = 30 µm. ** $p$ <0.005, *** = $p$ <0.0005; **** = $p$ <0.00005. Dorsal is up in all images.

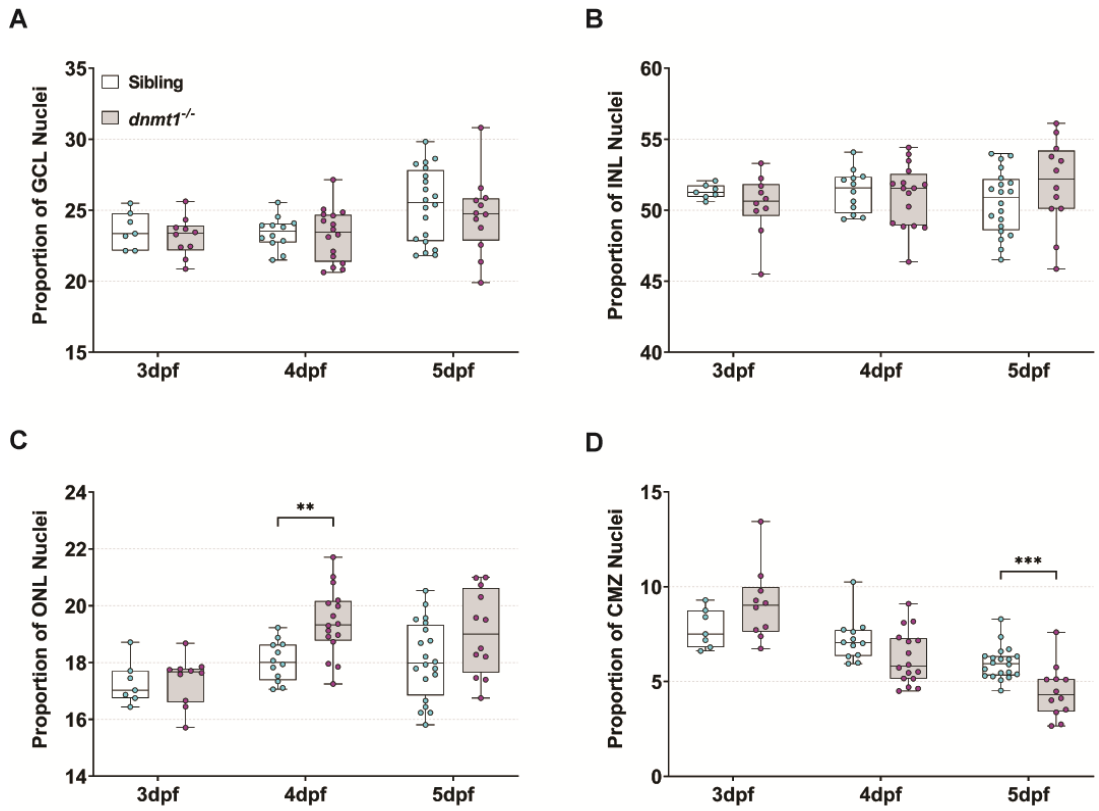


Figure 2.2. Loss of dnmt1 function results in a decline of RSC number.

**A-D.** Graphs of retinal domain proportions over time between siblings and *dnmt1*$^{-/-}$ larvae. ** $p$ <0.005, *** = $p$ <0.0005.

### 2.2.2 CELL DEATH IS ELEVATED IN THE *DNMT1*$^{-/-}$ CMZ IN A *P53*-INDEPENDENT MANNER.

Previous publications have demonstrated increased *p53* expression and TUNEL$^{+}$ cells in Dnmt1-deficient tissues and cell types[144,148,149,155] suggesting a *p53*-dependent apoptotic mechanism for cell loss. Based on these studies, we hypothesized that *dnmt1*$^{-/-}$ RSCs would similarly undergo p53-dependent apoptosis. To test this hypothesis, we first assayed for the presence of DNA double-strand breaks in *dnmt1*$^{-/-}$ and sibling retinae using TUNEL (Figure 2.3A-F). *dnmt1* siblings displayed few TUNEL$^{+}$ cells between 3-5dpf (Figure 2.3L-N), whereas the *dnmt1*$^{-/-}$ retina contained increased proportions of TUNEL$^{+}$ cells at 3, 4, and 5dpf in the INL (+0.5-2.3%, $p < 0.05$), ONL (+0.01-1.8%, $p < 0.05$) and at 5dpf in the GCL (+1.3%, $p < 0.05$; Figure 2.3H-I). Within the CMZ, we detected a 4.5% increase in TUNEL$^{+}$ cells at 3dpf ($p < 0.005$, Figure 2.3J) prior to the onset of CMZ disorganization. This proportion decreased to 1% at 4dpf ($p < 0.05$) and increased again to 3.7% at 5dpf ($p < 0.05$; Figure 2.3J), a time at which *dnmt1*$^{-/-}$ larvae begin to display severe systemic defects. During this 3-5dpf period, the majority of TUNEL$^{+}$ cells in *dnmt1*$^{-/-}$ larvae were located within the retina proper, not within the CMZ (Figure 2.3K and Figure 2.5). In concordance with the TUNEL data, immunofluorescence of the pro-apoptotic marker, active-caspase3, displayed similar patterns to TUNEL (data not shown). Together, these data are consistent with those seen in previous studies; dnmt1 deficiency results in increased cell death[144,149,155].

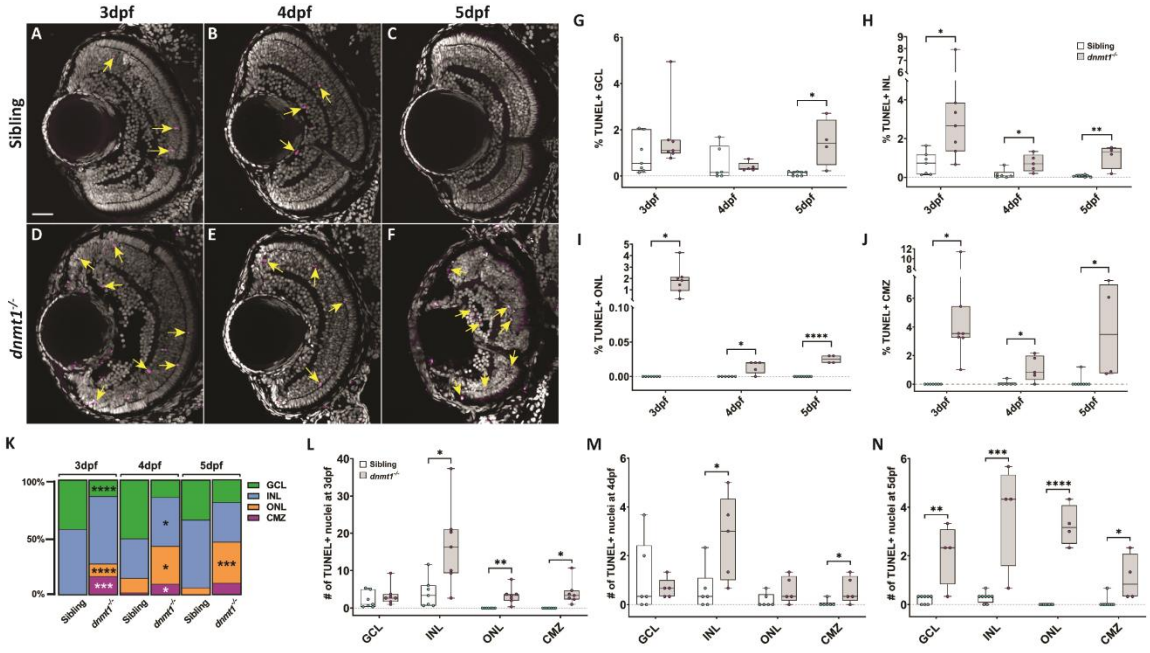


Figure 2.3. Cell death is elevated in the *dnmt1*$^{-/-}$ CMZ.

**A-F.** dnmt1 sibling (**A-C**) and mutant (**D-F**) retinae labeled with DAPI (gray; nuclei) and TUNEL (magenta; dsDNA breaks) from 3-5dpf. **G-J.** Proportion of retinal layers (GCL, INL, ONL, and CMZ) labeled by TUNEL staining. **K.** Proportion of TUNEL$^{+}$ cells within each layer from 3-5dpf. **L-N.** Average number of TUNEL$^{+}$ cells in each retinal layer of siblings and *dnmt1*$^{-/-}$ larvae from 3-5dpf. Yellow arrows in **A-F** indicate TUNEL$^{+}$ nuclei. Scale bars = 30 µm. **p* <0.05, ***p* <0.005, ****p* <0.0005, *****p* <0.00005. Dorsal is up in all images.

To identify if dnmt1 deficient RSCs are lost via *p53*-dependent apoptosis, we generated *dnmt1;p53* double mutants using the $p53^{zdf1}$ allele, which is defective in *p53*-dependent apoptosis[156,157]. We hypothesized that *p53*-dependent apoptosis was the driving mechanism of RSC loss in $dnmt1^{-/-}$ mutants and therefore loss of p53 activity would rescue the CMZ phenotype. To test this hypothesis, we quantified nuclei in $dnmt1^{+/+}$;$p53^{+/+}$, $dnmt1^{+/+}$;$p53^{-/-}$, $dnmt1^{-/-}$;$p53^{+/+}$ and $dnmt1^{-/-}$;$p53^{-/-}$ retinae (Figure 2.4).

Loss of p53 function did not affect retinal morphology (Figure 2.4A,E,I compared to Figure 2.4B,F,J) and $dnmt1^{+/+}$; $p53^{-/-}$ mutants possessed equivalent retinal cell numbers as $dnmt1^{+/+}$;$p53^{+/+}$ siblings (Figure 2.4Q-T and Figure 2.5D) at 3, 4 and 5dpf. When considering $dnmt1^{-/-}$;$p53^{-/-}$ larvae, we predicted an increase in CMZ cell numbers and a rescue of the CMZ-specific phenotype when compared to $dnmt1^{-/-}$; $p53^{+/+}$ larvae. Surprisingly, the $dnmt1^{-/-}$;$p53^{-/-}$ CMZ displayed similar morphology (Figure 2.4C,D,G,H,K,L) and was proportional to the $dnmt1^{-/-}$; $p53^{+/+}$ sibling retina (Figure 2.4P) across all three time points. These results suggest that *p53*-dependent apoptosis is not responsible for $dnmt1^{-/-}$ RSC loss.

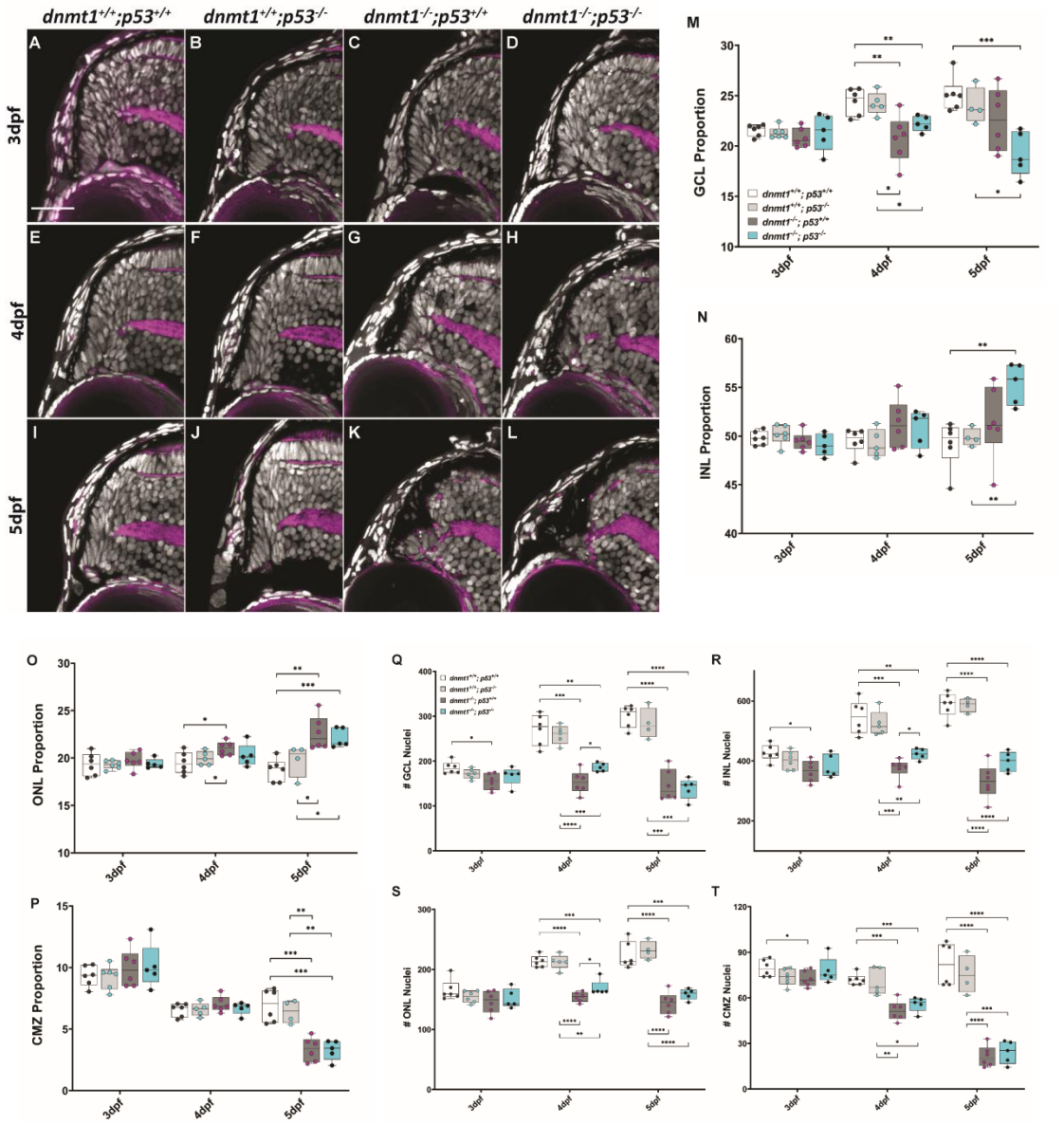


Figure 2.4. Loss of p53 function does not rescue the *dnmt1*$^{-/-}$ CMZ phenotype.

**A-L.** Transverse sections of the dorsal CMZ in wildtype (**A, E, I**), *dnmt1*$^{+/+}$*;p53*$^{-/-}$ (**B, F, J**), *dnmt1*$^{-/-}$*;p53*$^{+/+}$ (**C, G, K**), *dnmt1*$^{-/-}$*;p53*$^{-/-}$ (**D, H, L**) larvae from 3-5dpf. Nuclei labeled with DAPI (gray) and F- actin labeled with phalloidin (magenta). **M-P.** Graphs depicting changes in retinal domain proportions over time. **Q-T.** Number of nuclei in each retinal domain of *dnmt1*$^{+/+}$*;p53*$^{+/+}$, *dnmt1*$^{+/+}$*;p53*$^{-/}$, *dnmt1*$^{-/-}$*;p53*$^{+/+}$, and *dnmt1*$^{-/-}$*;p53*$^{-/-}$ larvae from 3-5dpf. GCL: ganglion cell layer; INL: inner nuclear layer; ONL: outer nuclear layer; CMZ: ciliary marginal zone. Scale bars = 25 μm. **p* <0.05; ***p* <0.005; ****p* <0.0005; *****p* <0.00005. Dorsal is up in all images.

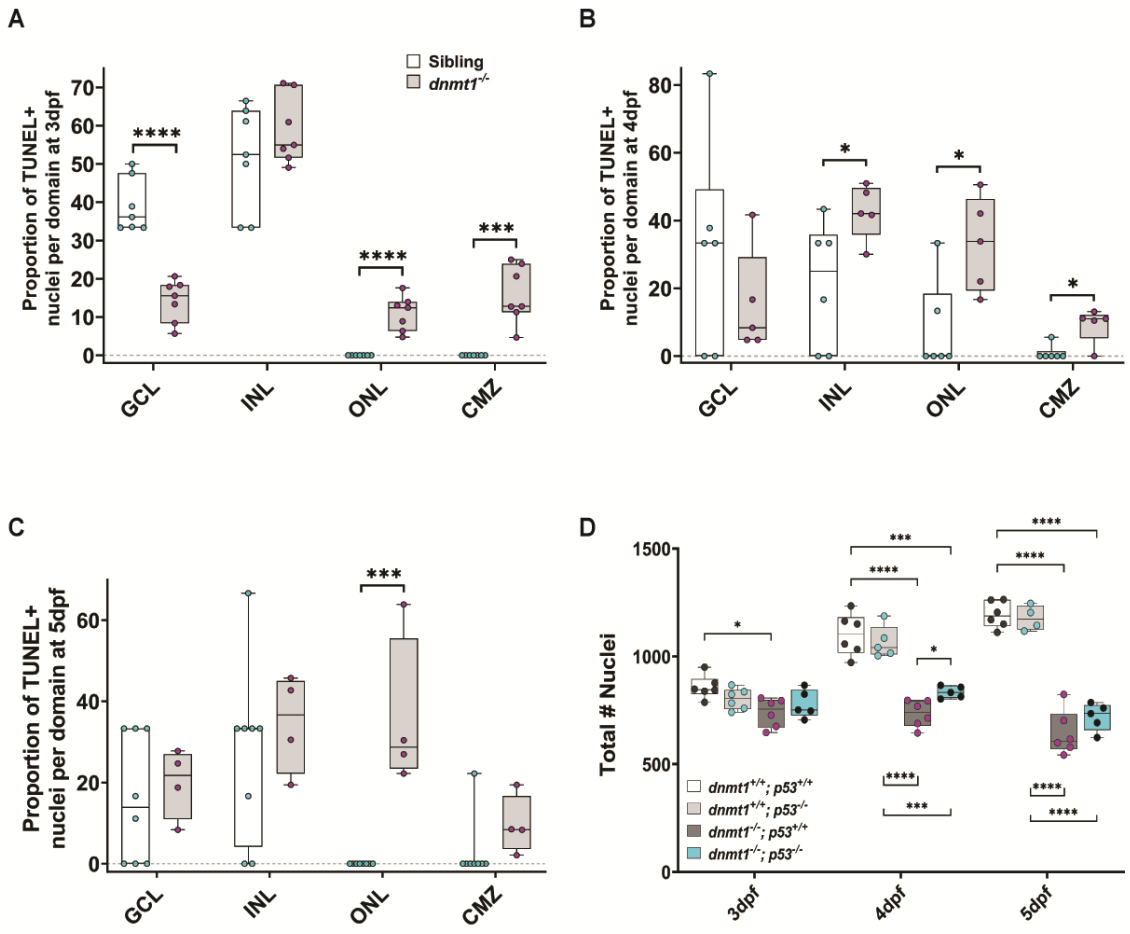


Figure 2.5. p53-mediated apoptosis is not responsible for *dnmt1*$^{-/-}$ RSC loss.

**A-C.** Proportion of TUNEL$^{+}$ nuclei in each retinal domain of *dnmt1*$^{-/-}$ larvae (gray bars) compared to sibling controls (white bars) at 3dpf (**A**), 4dpf (**B**), and 5dpf (**C**). D. Total number of retinal nuclei between *dnmt1*$^{+/+}$;*p53*$^{+/+}$ (white bars), *dnmt1*$^{+/+}$;*p53*$^{-/-}$ (light gray bars), *dnmt1*$^{-/-}$;*p53*$^{+/+}$ (dark gray bars), *dnmt1*$^{-/-}$;*p53*$^{-/-}$ (blue bars) larvae from 3-5dpf. GCL: ganglion cell layer; INL: inner nuclear layer; ONL: outer nuclear layer; CMZ: ciliary marginal zone. *$p$ <0.05, ***$p$ <0.0005, ****$p$ <0.00005. Dorsal is up in all images.

### 2.2.3 *DNMT1* IS REQUIRED TO MAINTAIN RSC GENE EXPRESSION.

*dnmt1* is expressed in RSCs at 4dpf (Figure 2.6I,J), consistent with dnmt1's known requirements in stem cell populations *in vivo*[37,120,144,145,158]. Loss of Dnmt1 function results in aberrant gene expression in a number of contexts[117,119,158,159] and therefore we wanted to determine if CMZ-specific gene expression was altered in the *dnmt1*$^{-/-}$ CMZ. Previous reports have characterized the expression/distribution of the CMZ-specific genes: *col15a1b*, *cyclinD1*, *cdkn1c*, and *atoh7*[133,134,160]. To determine if CMZ expression of these genes was altered in *dnmt1*$^{-/-}$ larvae, we utilized whole-mount *in situ* hybridization at 4dpf when the morphological defects in the CMZ begin to manifest (Figure 2.1). All sibling controls displayed normal CMZ-specific gene expression at 4dpf (Figure 2.6). Expression of *col15a1b* and *atoh7* were normal in *dnmt1*$^{-/-}$ larvae (Figure 2.6C,D,S,T); however, the expression of *ccnD1* and *cdkn1ca*, which function to regulate cell cycle progression, were disrupted (Figure 2.6G,H,O,P). The majority of 4dpf *dnmt1*$^{-/-}$ CMZs maintained *dnmt1* expression (Figure 2.6K,L). These data suggest that RSCs are present at the onset of morphological defects in the *dnmt1*$^{-/-}$ CMZ, but could be impaired in their ability to progress through the cell cycle and self-renew.

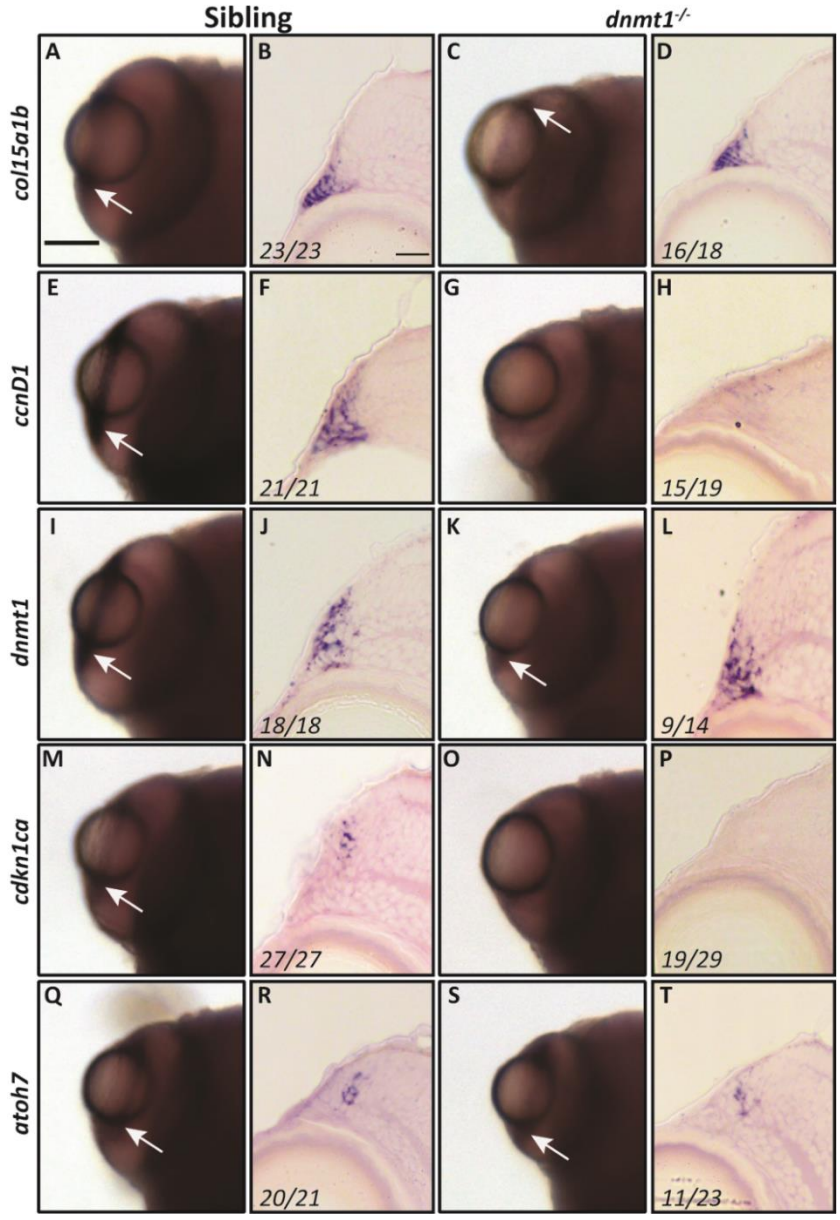


Figure 2.6. dnmt1 is required to maintain RSC gene expression.

Gene expression shown in whole mount (**A, C, E, G, I, K, M, O, Q, S**) and transverse cryosections (**B, D, F, H, J, L, N, P, R, T**) between siblings and *dnmt1*$^{-/-}$ *larvae*. **A-D.** *col15a1b* expression. **E-H.** *ccnD1* expression. **I-L.** *dnmt1* expression. **M-P.** *cdkn1ca* expression. **Q-T.** *atoh7* expression. Numbers in transverse cryosections designate the number of larvae that showed the displayed expression pattern vs. the total number of larvae analyzed. Scale bars = 75 mm (whole mount) and 10 μm (transverse sections). Anterior is up in all whole-mounts and dorsal is up for all section images.

### 2.2.4 Loss of *DNMT1* activity results in decreased RSC proliferation.

RSCs within the teleost CMZ remain proliferative throughout the lifespan of the animal[4,10,14] and Dnmt1 is known to be required for cell cycle progression within stem cells of various tissue types[35,141,161]. Based on the significant loss of RSCs in *dnmt1*$^{-/-}$ larvae between 3-5dpf (Figure 2.1) and the inability of *dnmt1*$^{-/-}$ RSCs to maintain expression of cell cycle genes (Figure 2.6), we hypothesized that *dnmt1*$^{-/-}$ RSCs would be defective in their proliferative capacity. To test this hypothesis, larvae were incubated for 2 hours in BrdU at 3, 4, and 5dpf, fixed immediately thereafter, and immunolabeled for BrdU and phosphohistone-H3-serine10 (pH3) to identify RSCs in late G2/M. *dnmt1* siblings maintained a constant proportion of BrdU$^{+}$ cells within the CMZ between 3-5dpf (Figure 2.7A-C,H).

Notably, the proportion of BrdU$^{+}$ *dnmt1*$^{-/-}$ RSCs at 3dpf was comparable to sibling controls (compare images in Figure 2.7A and 2.7D and nuclear proportions in Figure 2.7G). However, beginning at 4dpf, the percentage of BrdU$^{+}$ *dnmt1*$^{-/-}$ RSCs is significantly reduced when compared to controls (Figure 2.7B,E,H; $p < 0.00001$), and this proportion continues to decrease through 5dpf (Figure 2.7C,F,H; $p < 0.0001$). Additionally, the proportion of cells in late G2/M phase (pH3$^{+}$) was significantly reduced at 3 and 4dpf in the *dnmt1*$^{-/-}$ CMZ when compared to siblings (Figure 2.7G,I) indicating potential cell cycle defects in *dnmt1*$^{-/-}$ RSCs that manifest as early as 3dpf.

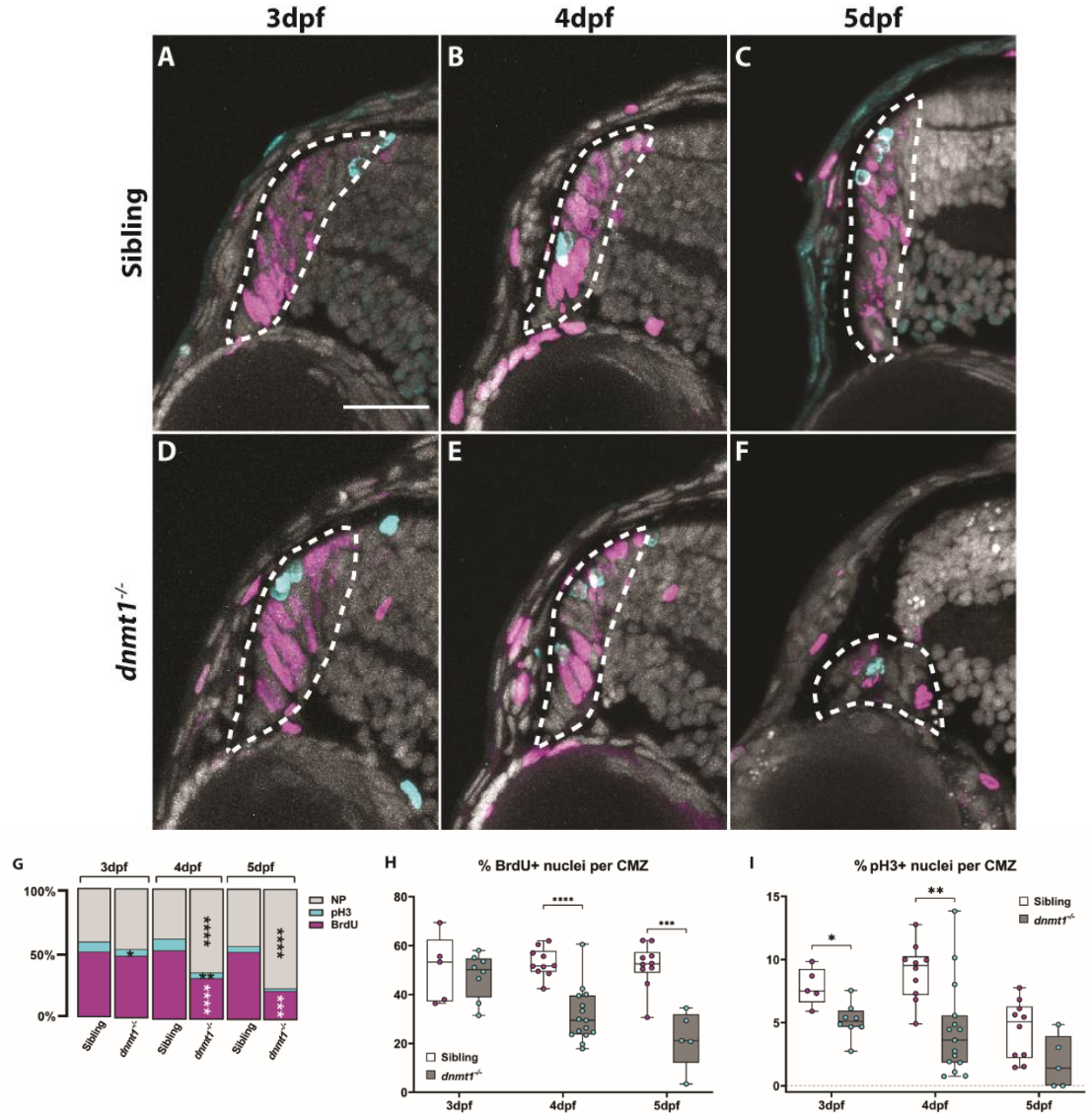


Figure 2.7. RSCs require dnmt1 function to maintain proliferation.

**A-F.** Transverse sections of siblings (**A-C**) and *dnmt1*$^{-/-}$ (**D-F**) larvae from 3-5dpf. Nuclei labeled with DAPI (gray). Cells in S-phase indicated by BrdU incorporation (magenta). Mitotic cells are labeled by a pH3(ser10) antibody (cyan). **G.** Proportions of CMZ cells in S-phase (magenta), G2/M-phase (cyan), or not proliferating (gray) of both siblings and *dnmt1*$^{-/-}$larvae from 3-5dpf. **H.** Proportion of CMZ cells labeled with BrdU from 3-5dpf between controls and *dnmt1*$^{-/-}$larvae. **I.** Proportion of CMZ cells labeled with pH3 from 3-5dpf between controls and *dnmt1*$^{-/-}$larvae. White dotted lines designate CMZ (**A-F**). Scale bars: 30 μm *$p$ <0.05, **$p$ <0.005, ***$p$ <0.0005, ****$p$ <0.00005. Dorsal is up in all images.

### 2.2.5 *DNMT1* IS REQUIRED FOR RSC DIFFERENTIATION AND INCORPORATION INTO THE NEURAL RETINA.

Potential cell cycle progression defects coupled to the fact that the vast majority of *dnmt1*$^{-/-}$ RSCs elude *p53*-dependent apoptosis (Figures 2.3 & 2.4) led us to hypothesize that *dnmt1*$^{-/-}$ RSCs might instead be undergoing premature differentiation, as has been shown *in vitro*[70]. To test this hypothesis, we performed a BrdU birth-dating assay[162]. Our aim was to saturate RSCs with BrdU for a 12-hour period (3-3.5dpf) and quantify the average starting number of proliferating cells at 3.5dpf and determine the final position of daughter cells at 5dpf, once they incorporated into the retina (Figure 2.8A). Initial analysis of these samples revealed that most BrdU$^{+}$ nuclei in both sibling and *dnmt1*$^{-/-}$ larvae were located within the CMZ after the 12hr incubation (Figure 2.8C,E,G). However, there were a few BrdU$^{+}$ cells that had incorporated into the neural retina at this time (Figure 2.8G). By comparing the number of BrdU$^{+}$ nuclei of each retinal domain (CMZ, GCL, INL, ONL, Figure 2.8B) to the total number of BrdU$^{+}$ nuclei (Figure 2.8H) at 3.5dpf, we noted a significant increase in the proportion of BrdU$^{+}$ nuclei in the *dnmt1*$^{-/-}$ CMZ (79.5%, $p < 0.05$) compared to controls (71.7%, Figure 2.8G; Figure 2.9A). Additionally, we found that the proportion of BrdU$^{+}$ cells in the *dnmt1*$^{-/-}$ ONL (7.8%, $p < 0.05$) was significantly reduced compared to siblings (10.9%, Figure 2.8G; Figure 2.9A) at 3.5dpf.

At 5dpf, all BrdU$^{+}$ cells in the sibling controls had exited the cell cycle and incorporated into the neural retina (Figure 2.8D,G), whereas *dnmt1*$^{-/-}$ larvae retained 19.8% ($p = 0.05$) of BrdU$^{+}$ nuclei within the CMZ and had fewer BrdU$^{+}$ cells overall within the retina (Figure 2.8F,G). Additionally, there was a significant decrease in the proportion of BrdU$^{+}$ nuclei

in the GCL (9.8%, $p$ <0.0005) (Figure 2.8G; Figure 2.9B) compared to controls (21.4%). Surprisingly, among the cells that remained in the 5dpf *dnmt1*$^{-/-}$ CMZ, there was an increase in the BrdU$^{+}$ proportion when compared to siblings (19.76% vs. 0.9% respectively, $p$ =0.05; Figure 2.8G; Figure 2.9B) suggesting an inability for some RSCs to either successfully complete the cell cycle or to integrate into retinal laminae. These data also show that daughter cells produced from the *dnmt1*$^{-/-}$ CMZ proportionally incorporate into the INL and ONL at similar levels to those detected in controls (Figure 2.8G; Figure 2.9B) supporting the notion that *dnmt1*$^{-/-}$ RSCs are still capable of producing neurons that can successfully integrate into these two layers of the retina.

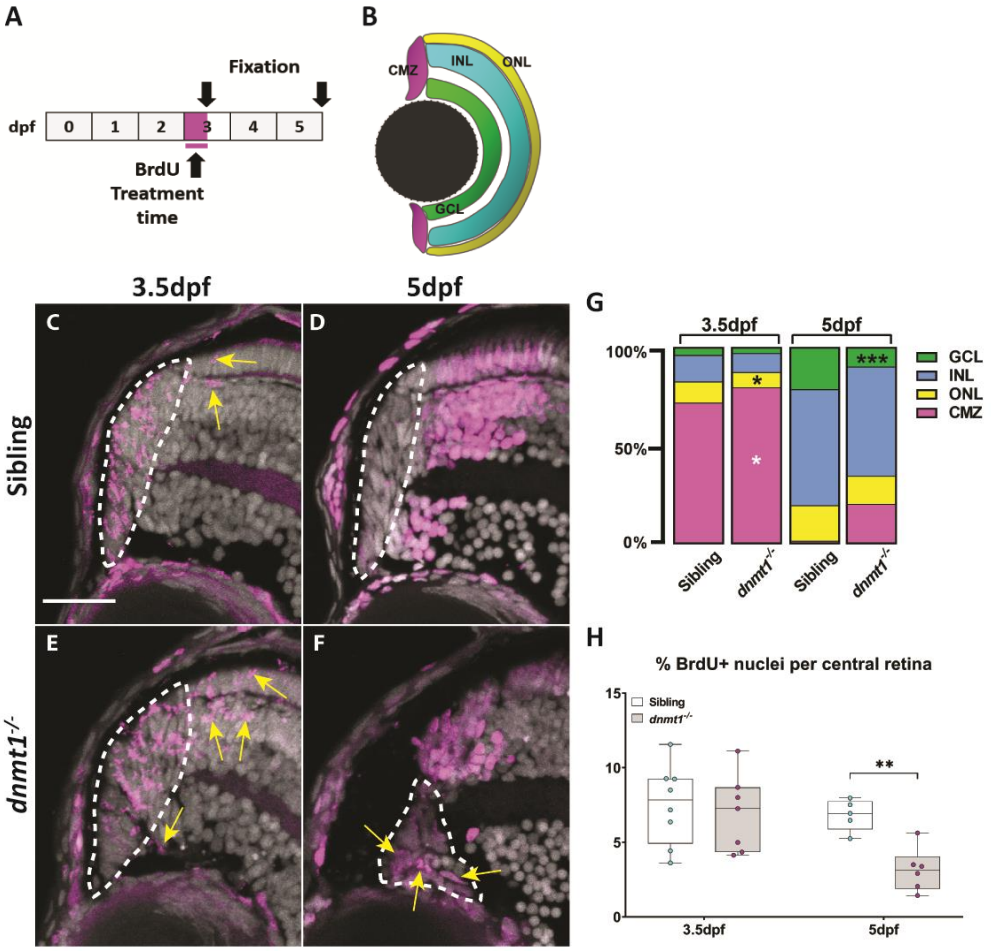


Figure 2.8. Neurons produced by *dnmt1*$^{-/-}$ RSCs fail to integrate into the neural retina.

**A.** Experimental paradigm depicting BrdU incorporation from 3-3.5dpf. Fixations occurred at 3.5 & 5dpf. **B.** Diagram of the four retinal domains (CMZ, GCL, INL, and ONL) whose colors correlate with the data presented in G. **C-F.** Transverse sections of BrdU pulses from 3-3.5dpf (C,E) and pulse-chase assay from 3-5dpf (D,F) (Siblings: A-B; *dnmt1*$^{-/-}$ C-D). Nuclei labeled with DAPI (gray). Cells in S-phase indicated by BrdU incorporation (magenta). Mitotic cells are labeled by a pH3(ser10) antibody (cyan). **G.** Proportion of BrdU+ cells located in each retinal layer at 3.5dpf and 5dpf of *dnmt1*$^{-/-}$ and control larvae. **H.** Proportion of total BrdU$^{+}$ cells within the central retina of the pulse-chase experiment. White dotted lines designate the CMZ (**C-F**). Yellow arrows = BrdU$^{+}$ nuclei outside the CMZ (**C,E**). Scale bars: 20 μm. **p* <0.05, ***p* <0.005, ****p* <0.0005. Dorsal is up in all images.

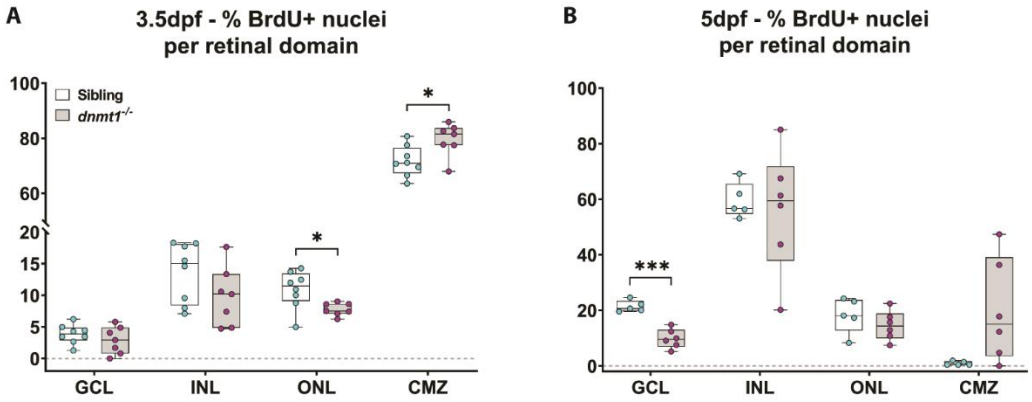


Figure 2.9. dnmt1-deficient RSCs fail to incorporate into the neural retina.

**A.** Data points collected of the proportion of cells labeled with BrdU in each retinal domain at 3.5dpf divided by the number of total $BrdU^{+}$ cells. **B.** Data points collected of the proportion of cells labeled with BrdU in each layer at 5dpf divided by the number of total $BrdU^{+}$ cells. Sibling controls = white bars; *dnmt1*$^{-/-}$ = gray bars. Dorsal is up in all images.

### 2.2.6 Loss of dnmt1 activity leads to altered Long Terminal Repeat retroelement expression within the CMZ.

Half of the zebrafish genome is comprised of endogenous viral elements known as transposons[163,164], and dnmt1 is required for repressing the retroelement (RE) lineage of transposons[56,165–167]. Though many REs have lost their ability to "jump" throughout evolution, some still retain this ability[168,169]. These studies led us to hypothesize that aberrant DNA methylation resulting from loss of dnmt1 activity in RSCs would result in upregulation of RE expression within the *dnmt1*$^{-/-}$ CMZ. To identify RE expression within the CMZ, we performed *in situ* hybridizations targeting several REs that belong to the Long Terminal Repeat (LTR) class of retrotransposons, specifically *Bel20*, *ERV1*, *ERV1-N5*, *ERV4*, and *Gypsy10* LTRs. We noted endogenous expression of *Bel20*, *ERV4*, and *Gypsy10* REs within the CMZ but not the neural retina of control larvae at 4dpf (Figure 2.10A,D,E).

This result was unexpected since REs can be deleterious to cellular function[56,170–172]. However, not all of the LTR REs were detected within control CMZs; *ERV1* and *ERV1-N5* expression was not detected in the CMZ of siblings (Figure 2.10B,C), but rather *ERV1-N5* seemed to be expressed within the ONL of some control larvae (Figure 2.11O). Remarkably, *dnmt1*$^{-/-}$ larvae had increased expression of *ERV1-N5* in the CMZ and within the overlying retinal pigmented epithelium (Figure 2.10H). The expression domains of *Bel20* and *ERV4* were expanded beyond the CMZ and into the neural retina of *dnmt1*$^{-/-}$ larvae (Figure 2.10F,I) when compared to controls. Of note, we also identified several non-ocular tissues that displayed altered RE expression between *dnmt1*$^{-/-}$ and sibling control

larvae (Figure 2.11). Interestingly, these LTR RE expression patterns were larvae-dependent, suggesting that not all RSCs respond uniformly to loss of dnmt1 function.

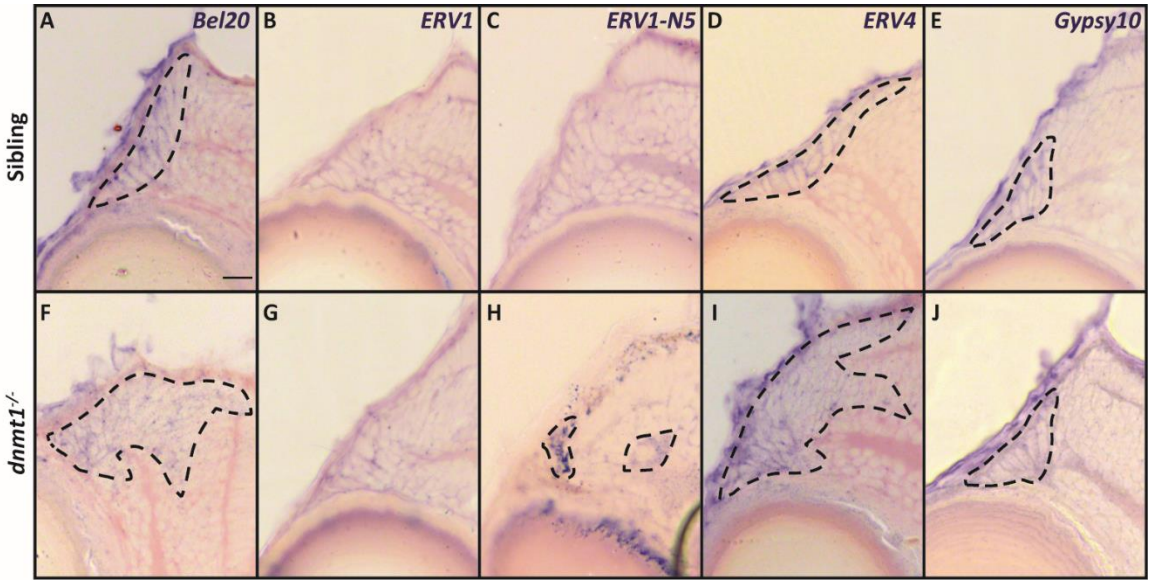


Figure 2.10. Loss of dnmt1 function results in misregulation of retroelement expression.

**A-J.** Transverse cryosections of sibling (**A-E**) and *dnmt1*$^{-/-}$ (**F-J**) larvae at 4dpf. **A, F.** Expression of *Bel20 LTR*. **B, G.** Expression of *ERV1 LTR*. **C, H.** Expression of *ERV1-N5 LTR*. **D, I.** Expression of *ERV4 LTR*. **E, J.** Expression of *Gypsy10 LTR*. Dotted lines: domains of retroelement expression. Scale bars = 10 μm. Dorsal is up in all images.

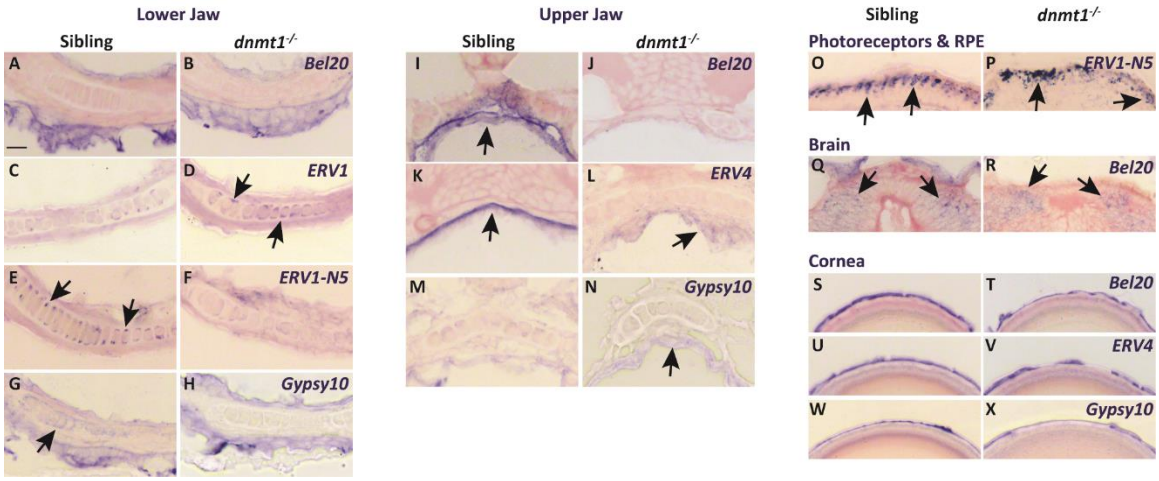


Figure 2.11. Loss of dnmt1 function results in misregulation of LTR RE expression across numerous tissues.

**A-X.** Transverse cryosections of larvae analyzed by *in situ* hybridization. All sibling and *dnmt1*$^{-/-}$ larvae are 4dpf. **A-H.** Expression of indicated REs within the lower jaw. **I-N.** Expression of indicated REs within the upper jaw. **O-P.** Expression of *ERV1-N5 LTR* in photoreceptors (**O**; sibling) and the RPE (**P**; *dnmt1*$^{-/-}$). **Q-R.** Expression of *Bel20 LTR* within the brain. **S-X.** Expression of indicated REs within the cornea. Arrows delineate expression changes of specified REs. Scale bar (A) = 10 μm. All images were taken at the same magnification. RPE = retinal pigmented epithelium.

### 2.2.7 A *L1RE3-EGFP* TRANSGENE REPORTS INCREASED *LINE1* RETROTRANSPOSITION ACTIVITY IN *DNMT1*$^{-/-}$ CMZ.

To expand our analysis of RE expression in *dnmt1*$^{-/-}$ RSCs, and more specifically, visualize retrotransposition activity *in vivo*, we generated a non-LTR, *LINE1* element transgenic reporter line by modifying the *pLRE3-EGFP* plasmid[173,174] (referred to as *L1RE3-EGFP* for the remainder of this study). The *L1RE3-EGFP* construct contains a human-derived *LINE1* RE sequence that requires retrotransposition for EGFP to be expressed and translated into a functional protein[173]. p53 is known to repress REs and when used transiently in *p53*$^{-/-}$ zebrafish, *L1RE3-EGFP* was shown to have increased transposition activity and EGFP expression[172]. We validated the stability and effectiveness of the *L1RE3-EGFP* transgenic using again *p53* mutants[156,172] and immunolabeling for EGFP (Figure 2.12A).

When *L1RE3-EGFP* was incorporated into the *dnmt1*$^{s872}$ genetic background, ectopic EGFP expression could be seen within the *dnmt1*$^{-/-}$ eye when compared to control siblings (Figure 2.13B,C). Notably, we detected ectopic EGFP expression more frequently within the *dnmt1*$^{-/-}$ CMZ at both 3dpf (Figure 2.13C) and 4dpf (Figure 2.13D) time points when compared to controls (Figure 2.13A,B). However, like RE expression, clonal EGFP expression patterns were variable, both within and between sibling controls and *dnmt1*$^{-/-}$ larvae, again suggesting that the effects of dnmt1 loss is variable from cell to cell and larva to larva.

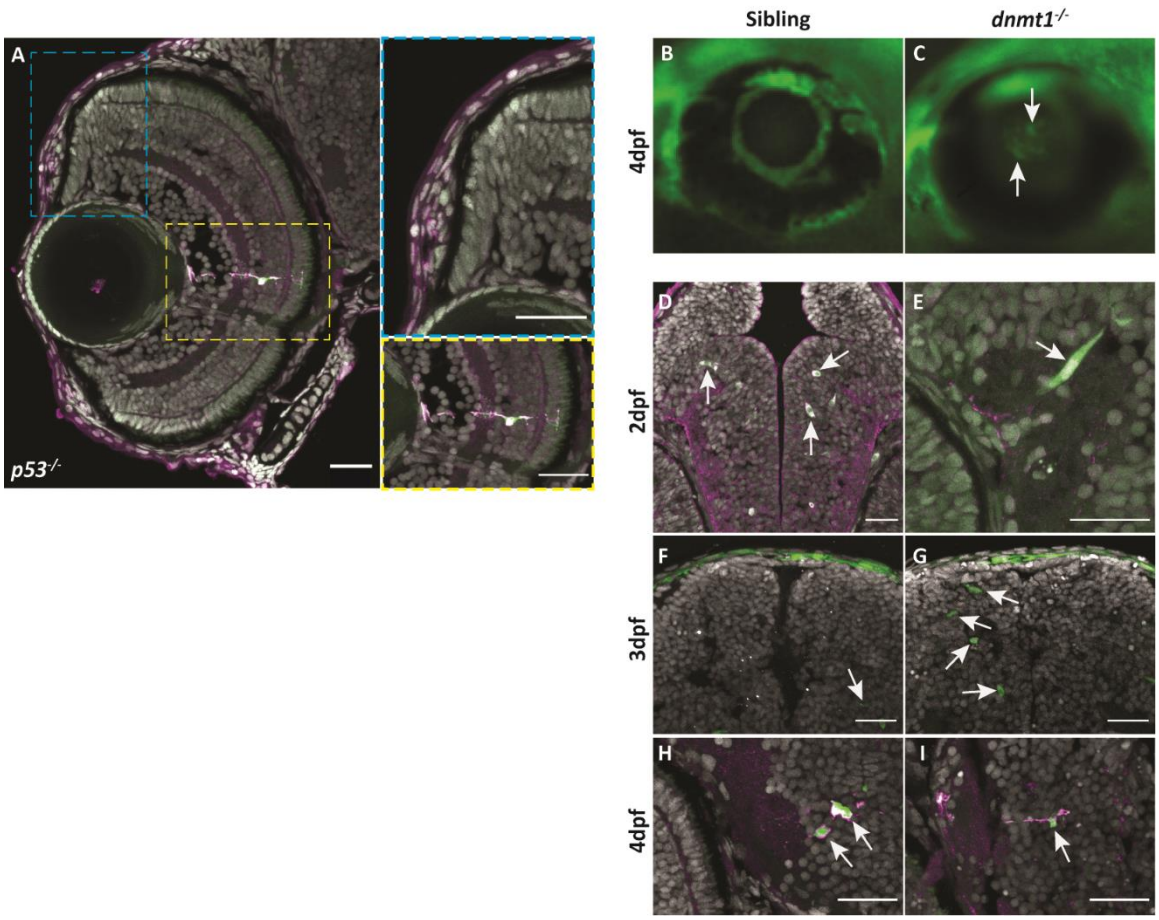


Figure 2.12. L1RE3-EGFP transgene expression is more prominent in *dnmt1*$^{-/-}$ larvae.

**A-A''.** Transverse section of *Tg(CMV:Hsa.L1RE3,EGFP,myl7:EGFP;p53*$^{-/-}$*)* larvae at 4dpf. **A.** L1RE3-EGFP$^{+}$ retinal cells labeled with endogenous EGFP. Cyan (A') and yellow (A'') dotted boxes indicate magnified images to the right of panel A. **A'.** Magnified image of *Tg(CMV:Hsa.L1RE3,EGFP,myl7:EGFP;p53*$^{-/-}$*)* CMZ showing no expression of the L1RE3-EGFP transgene. **A''.** Magnified image of retinal neuron expressing L1RE3-EGFP transgene. **B-I.** All images are taken from *Tg(CMV:Hsa.L1RE3,EGFP,myl7:EGFP)* larvae that are either *dnmt1*$^{+/+}$ (B,D,F,H) or *dnmt1*$^{-/-}$ (C,E,G,I). **B-C.** Whole-mount images of 4dpf eyes demonstrating L1RE3-EGFP transgene activation seen through the lens of *dnmt1*$^{-/-}$ larvae and not siblings. **D,F,H.** Sibling larvae expressing the L1RE3-EGFP transgene in the brain. **E,G,I.** *dnmt1*$^{-/-}$ larvae expressing the L1RE3-EGFP transgene in the brain. Nuclei labeled with DAPI (gray). Endogenous L1RE3-activated EGFP labeled in green. EGFP antibody is magenta. Scale bars: 30 μm in all images. Dorsal is up in all images.

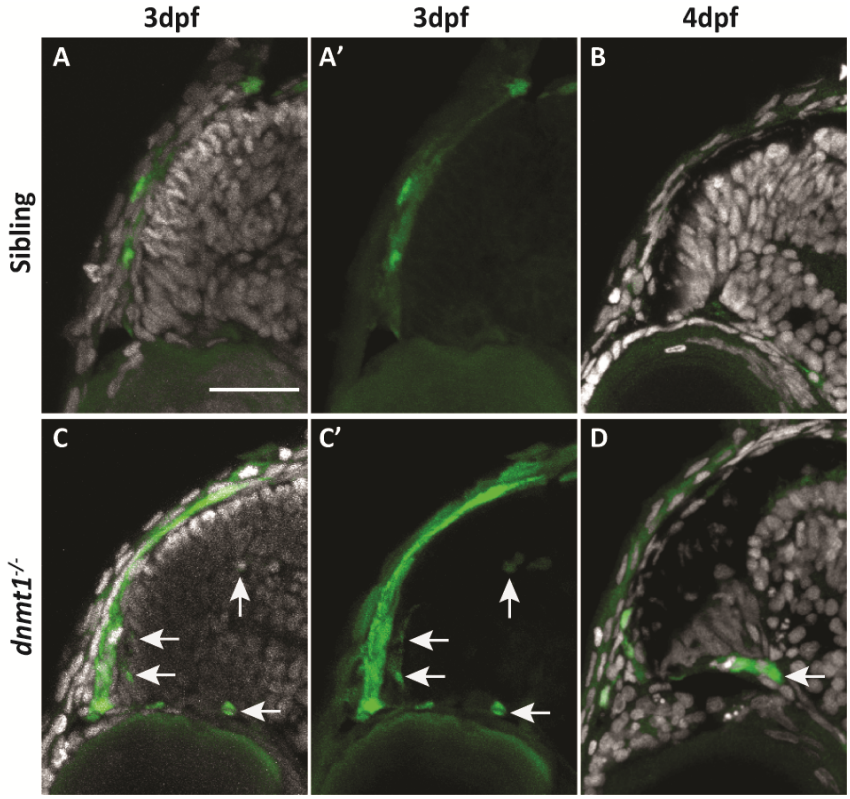


Figure 2.13. RSCs require dnmt1 function to repress L1RE3-EGFP transposition.

**A-D.** Transverse sections of *Tg(CMV:Hsa.L1RE3,EGFP,myl7:EGFP;dnmt1$^{+/+}$)* (**A-B**) and *Tg(CMV:Hsa.L1RE3,EGFP,myl7:EGFP;dnmt1$^{-/-}$)* (**C-D**) larvae at 3dpf (**A, A', C, C'**) and 4dpf (**B, D**). Nuclei labeled with DAPI (gray). Endogenous EGFP expression activated after L1RE3-EGFP transposition labeled in green. Arrows delineate EGFP+ cells. Scale bars: 30 μm. Dorsal is up in all images.

## 2.3 Discussion:

The zebrafish, with its lifelong, actively cycling RSCs within the CMZ, is a powerful model through which we can address how epigenetic regulators function to maintain these stem/progenitor cell populations *in vivo*. This study focused on the role of the DNA maintenance methyltransferase, *dnmt1,* within the CMZ, with the goal of determining how dnmt1 activity facilitates RSC maintenance. Previous work has shown that loss of dnmt1 function results in ocular defects[113,119,120,159], but no studies have yet analyzed RSC populations and determined whether dnmt1 activity modulates their behavior.

Here, we demonstrate that *dnmt1* is essential for RSC homeostasis by maintaining CMZ-specific gene expression (Figure 2.6), facilitating cell cycle progression (Figure 2.7), and incorporation of CMZ-derived cells into the retina (Figure 2.8). These data are consistent with Dnmt1 functions described in other *in vivo* progenitor models such as the lens[120], hippocampus[158], kidney[166], pancreas[144] and intestine[37]. RSCs in S- and G2/M-phases of the cell cycle were detected in reduced proportions in the *dnmt1*$^{-/-}$ CMZ and this correlated with a reduction in CMZ expression of genes encoding proteins that function in cell cycle progression, namely *ccnD1* (Figure 2.6G-H) and *cdkn1ca* (Figure 2.6O-P). Defects in cell cycle progression may also contribute to aberrant daughter cell integration into retinal laminae detected in *dnmt1*$^{-/-}$ larvae (Figure 2.8). Although our data demonstrate an overall loss of RSCs and their progeny, this RSC depletion is independent of the p53-driven apoptotic pathway (Figures 2.3 and 2.4) signifying additional mechanisms of cell loss are at play.

While loss of *p53* function in the *dnmt1*$^{-/-}$ background significantly rescued cell death within the laminated retina, validating that the *p53*$^{zdf1}$ allele is in fact inhibiting *p53*-driven apoptosis, loss of p53 in the *dnmt1*$^{-/-}$ CMZ had no effect on CMZ cell numbers suggesting a *p53*-independent cell death pathway is likely modulated by dnmt1 in the CMZ[175]. Recent reports have demonstrated an upregulation of an innate inflammatory response in *dnmt1*$^{-/-}$ larvae[56]. Necroptosis, a programmed cell death pathway tightly linked to a cell's innate viral detection system and inflammatory responses, also results in DNA fragmentation and, in its later stages, is detected by TUNEL[175]. Accordingly, we considered the possibility that *dnmt1*$^{-/-}$ RSCs were instead lost via necroptosis. We tested this hypothesis using several chemical inhibitors of necroptosis, some of which have been reported to function in the zebrafish[176,177]; however, we were unable to replicate necroptotic inhibition nor validate drug efficacy. None the less, we predict that either necroptosis or pyroptosis (a programmed cell death pathway triggered by intracellular bacterial infections[178,179]) are the most likely mechanisms of cell death in dnmt1-deficient RSCs, but this will require the development of new tools to enable further analysis.

Alterations in RE expression activity the *dnmt1*$^{-/-}$ CMZ (Figures 2.10 and 2.13) are exciting given Dnmt1's known roles in repressing RE activity[56,57,150,151]. RE expression was aberrant in most *dnmt1*$^{-/-}$ CMZs examined (Figure 2.10); however, expression changes and levels were variable between larvae, suggesting that the location and extent of genomic hypomethylation resulting from loss of dnmt1 function is inherently variable between cells of each larva. Previous reports demonstrated innate RE activity within healthy somatic neural tissue[168,169,180–182]. Indeed, we detected retrotransposition activity within the larval

zebrafish brain (Figure 2.13D-I) of both siblings and *dnmt1*$^{-/-}$ larvae from 2-4dpf, similar to activity detected in human hippocampal neurons[168,169,182]. Notably, some REs were found to be expressed within sibling control tissues and down-regulated in the *dnmt1*$^{-/-}$ larvae (Figure 2.11). These data, along with the recent studies in the human brain[168,169,180,182], suggest that expression of some REs is a normal occurrence. Moreover, it is increasingly apparent that certain REs have functional roles within the cell[183,184], indicating a vertebrate cooption of RE acquisitions throughout evolutionary history.

Detection of active RE retrotransposition using the *CMV:Hsa.L1RE3,EGFP* construct is highly variable between larvae (Figure 2.13), and is likely a result of 1) its starting location within the transgenic line, 2) levels of genomic methylation at that locus, and 3) cell type-specific factors and response to loss of DNA methylation. Further studies will be required to determine what cellular processes might sensitize a cell- or tissue-type to upregulate REs and whether these REs have a mechanistic purpose within the cell.

In conclusion, our results demonstrate that dnmt1 functions to maintain RSC proliferation, gene expression, and integration of RSC daughters into the retina. Additionally, some REs are innately expressed within RSCs, however dnmt1 function is required to maintain tight control of these viral elements. Without dnmt1 activity, *LTR* expression remains active within the retina and *L1RE3-EGFP* retrotransposition activity is increased. Interestingly, RE activity within RSCs does not result in p53-mediated apoptosis, supporting a model in which *dnmt1*$^{-/-}$ RSCs are lost through another mechanism of cell death. As discussed above, we predict that this increase in RE activity most likely activates necroptotic or pyroptotic cell death pathways, which are both known to result

from intracellular responses to invading pathogens[175,178,179]. Regarding the innate *LTR* expression within *dnmt1*$^{+/+}$ RSCs, in conjunction with previous reports of inherent RE activity within human neural tissue, it is worth considering how RE activity may contribute to neural stem cell biology. It is well known that dysregulation of REs is a hallmark of many human neurodegenerative diseases[27,171,185–187]. Future evaluations regarding the innate cost-to-benefit ratio of RE activity could provide crucial evidence for the development of neurodegenerative therapies.

# CHAPTER 3: DISRUPTION OF *DE NOVO DNMT* PARALOGS DOES NOT AFFECT RETINAL DEVELOPMENT:

## 3.1 Introduction to *de novo* DNA methylation.

As discussed in the previous chapter, *dnmt1* is responsible for copying DNA methylation patterns from parent to daughter strands of DNA during replication. However, nascent methyl groups can be added to cytosine bases through the catalytic action of *de novo* DNA methyltransferases[140,188]. The *Dnmt3α* and *Dnmt3β* family of enzymes mediate this catalytic reaction[61]. Disruption of the methylome can result in aberrant gene and miRNA expression[76,95,101,189], premature differentiation[68,71,190], activation of endogenous retroelements[191,192] (REs), tumorigenesis[66,69,193], and embryonic lethality[61,71].

Although there are numerous studies of DNA methylation function *in vitro* and *in vivo*, those regarding studies of eye development, differentiation, and disease are limited. Within the eye, tissue-specific disruption of combinatorial mutants for *Dnmt1*, *Dnmt3α*, and/or *Dnmt3β* function leads to aberrant photoreceptor differentiation and synapse formation[113,119]. Moreover, *dnmt1* is known to be required for lens progenitor cell maintenance[120]. Nonetheless, our current understanding of *de novo* methyltransferase function within the mammalian eye has been limited, and studies using non-mammalian model organisms have been limited to chemical manipulation[50,141,194] or morpholino-based gene knockdowns[159,195].

Due to genome duplication events in the evolutionary history of the zebrafish, its genome contains six paralogs of *dnmt3* in comparison to the two paralogues found in mammals[41,196]. Of these, two are orthologues of *Dnmt3α*, three are orthologues of *Dnmt3β*, and the last is distinct from mammalian *Dnmt3*s (Illustration 1.2)[197,198]. Recently, our laboratory published a study on *de novo dnmts* demonstrating that all six paralogs are expressed within the developing zebrafish eye and display tissue-specific expression patterns[199]. Of note, four of the dnmts (*dnmt3βa, dnmt3ββb.1, dnmt3ββb.2, and dnmt3ββb.3*) are expressed within the zebrafish CMZ, suggesting they might play a role in RSC maintenance and/or function. Additionally, *de novo* dnmts play a role in gene expression changes and cellular differentiation[71,190]. Based on this knowledge, we hypothesized that *dnmt3* methyltransferases would provide critical insight into their role of *de novo* methylation during retinal development and differentiation.

Taking advantage of the genetic tractability and fecundity of the zebrafish to our advantage, we generated mutant alleles in five of the six *de novo dnmt* genes using transcription activator-like effector nucleases (TALENs)[200] and clustered regularly interspaced short palindromic repeats (CRISPR)-Cas9 mutagenesis[201]. TALEN- and CRISPR/Cas9-directed mutagenesis are common genome-editing tools for creating site-specific mutations and both are utilized in a variety of model organisms[190,202–204]. To disrupt the function of the remaining *de novo dnmt* paralogue, *dnmt3αa*, we acquired the *dnmt3αa*$^{sa617}$ allele from the Zebrafish International Resource Center (ZIRC) and created combinatorial genetic mutants of the *dnmt3* alleles described in this chapter. Through the creation of frameshift mutants and whole gene knockouts (KOs), we generated different

combinations of triple, quadruple, and quintuple mutants. The single and compound alleles generated for this dissertation are listed in Table 3.1.

## 3.2 Results

### 3.2.1 FUNCTIONAL ANALYSIS OF *DE NOVO DNMTS* WITHIN THE CILIARY MARGINAL ZONE.

To determine how *de novo dnmts* may be functioning during retinal development, I collaborated with Dr. Pawat Seritrakul to create null mutations in five of the *dnmt3* genes [190] ( Figure 3.1). I designed TALEN constructs targeting the 5' end of both *dnmt3βb.2* and *dnmt3βb.3* genes (Figure 3.1). We hypothesized that since the early zebrafish embryo repairs DNA breaks through non-homologous end-joining (NHEJ), the most likely mutation to be generated by the TALEN constructs would be frameshift mutations that would result in premature stop codons[205].

Table 3.1: List of single and compound mutant alleles used in this study.

| Gene target(s) | Allele designation | Brief allelic description | Mutagenesis Method |
|---|---|---|---|
| *dnmtβb.2* | *pt702* | 5bp deletion | TALEN |
| *dnmtβb.3* | *pt703* | 8bp deletion | TALEN |
| *dnmtβb.3* | *pt704* | 17,540bp deletion; gene knockout | 2xCRISPR/Cas9 target sites |
| *dnmtβb.1-3* | *pt705* | 115,375bp deletion & 352bp insertion; triple gene knockout | CRISPR/Cas9 Target site 1: Target site 2: |
| *dnmtαb*[#] | *au62* | 4bp deletion | TALEN |
| *dnmtβa*[#] | *au63* | 8bp deletion | TALEN |
| *dnmtαa* | *sa617*[*] | Point mutant (G>T) | N/A |

* – Allele acquired through ZIRC.

[#] – Allele generated by Dr. Pawat Seritrakul

$F_0$ founders were identified through PCR and Sanger sequencing, then outcrossed to create stable lines for the *dnmt3βb.2*$^{pt702}$ and *dnmt3βb.3*$^{pt703}$ genes (Figure 3.2). Initial analyses of both *dnmt* mutations demonstrated a lack of retinal phenotype (Figure 3.3B-C). These results were consistent with those reported previously in the *dnmt3αb, dnmt3βa, and dnmt3βb.1* genes[190]. Additionally, it was reported that frameshift mutations generated through TALEN- and CRISPR-induced frameshift mutations often result in nonsense-mediated decay (NMD) of the unstable, mutant mRNA transcripts. The zebrafish NMD pathway triggers in-frame exon skipping for continued expression[206]. To bypass the nonsense-mediated decay response, I generated a CRISPR/Cas9-mediated gene knockout in the *dnmt3βb.3*$^{pt704}$ gene (Figure 3.2) by targeting both the 5' and 3' end of the gene. This would theoretically bypass the mRNA instability associated with the NMD response.

I successfully generated a stable *dnmt3βb.3* knockout (KO) using CRISPR/Cas9 mutagenesis, which deleted 17,805bp from the genomic sequence of *dnmt3βb.3* on Chromosome 23. Surprisingly, *dnmt3βb.3* KO larvae retained a phenotypically normal retina (Figure 3.3C). We hypothesized that the *de novo dnmts* were functionally redundant based on the lack of phenotypes in single genetic mutants and gene expression patterns previously reported[190].

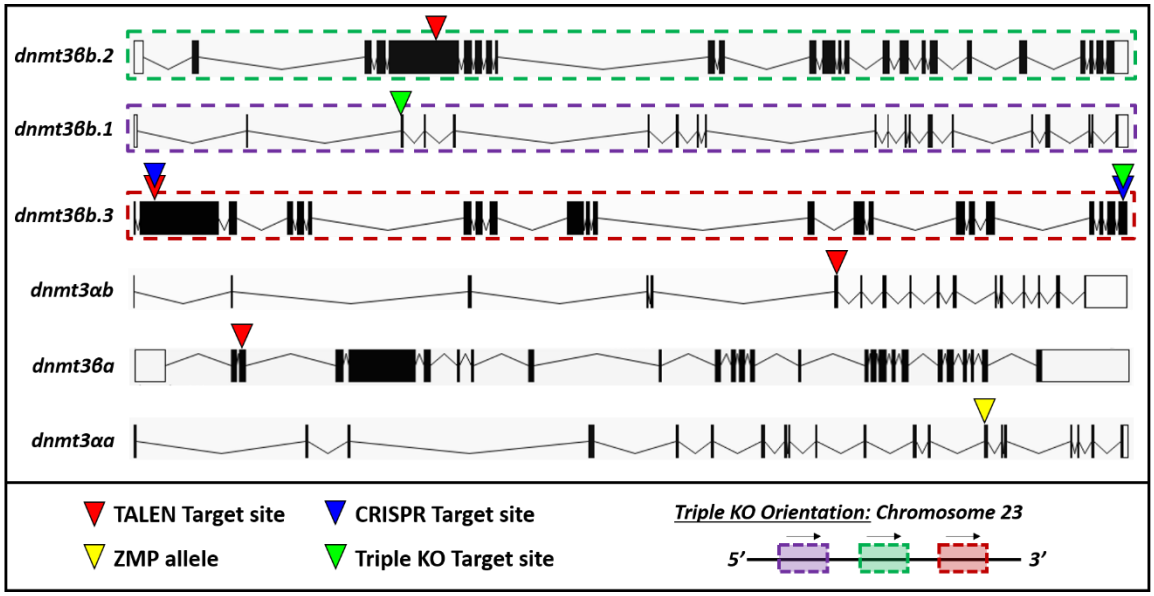


Figure 3.1. Diagram depicting the six *de novo dnmt* genes and target sites used in this collaborative study.

Each gene diagram, represented by annotated exons (black boxes) and introns (lines), was acquired from the Ensembl genome browser. Genetic distances are not to scale. Colored arrowheads depict TALEN or CRISPR/Cas9 target sites used for mutagenesis. The ZMP allele (yellow arrowhead) was acquired through the Zebrafish International Resource Center. All three *dnmt3ββ* genes annotated with colored dotted lines, which correspond to their genetic orientation within Chromosome 23 diagrammed at the bottom of this figure. Arrows depict the directionality of the *dnmt3ββ* gene transcripts.

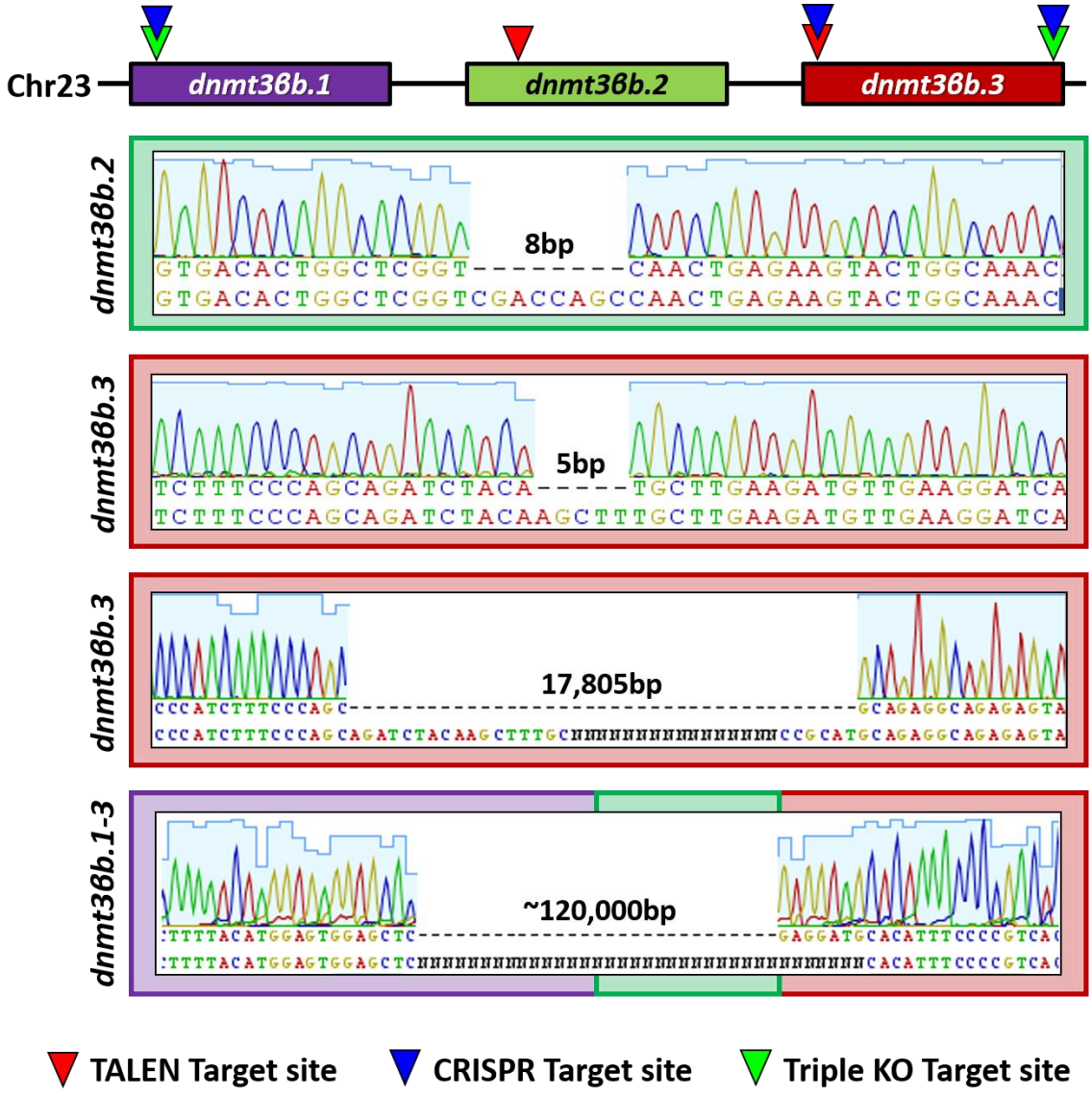


Figure 3.2. Diagram of the *de novo dnmt* alleles generated.

All three *dnmt3βb* genes are oriented consecutively along Chromosome 23. Arrowheads depict the target sites and method of mutagenesis based on color. Triple KO sites generated using CRISPR/Cas9. Sanger sequencing of each allele is shown (mutant sequence is aligned on top of the wildtype sequence) and designates the number of base pairs missing from the original genetic sequence.

### 3.2.2 *DNMT3* QUINTUPLE MUTANTS LACK A RETINAL PHENOTYPE.

Based on the *de novo* dnmt gene expression patterns, our lab had previously demonstrated that four of the six *de novo dnmts* were not required in a pair-wise manner for retinal development[190]. Although these double dnmt mutants did not present with a phenotype, this did not negate the possibility that all six *de novo dnmts* were capable of compensating for the loss of another. Thus, we hypothesized that these studies would require all six *de novo* paralogs to be non-functional in order for the larvae to present with a phenotype. To begin addressing this possibility, we took advantage of the three *dnmt3βb* genes located in succession along Chromosome 23 (diagrammed in Figures 3.1 and 3.2). We generated CRISPR/Cas9 small guide RNAs (sgRNAs) to target the 5' end of *dnmt3βb.1* and the 3' end of the *dnmt3βb.3* gene. Injection of both sgRNAs with Cas9 mRNA into the 1-cell embryo resulted in the deletion of approximately 120,000bp of DNA on Chromosome 23. A founder identified by PCR and Sanger sequencing was outcrossed to create a stable mutant line, referred to as *dnmt3βb.1-3*$^{pt705}$ for the remainder of this dissertation (Figure 3.2). Interestingly, *dnmt3βb.1-3*$^{-/-}$ larvae did not present with any apparent phenotype within the retina (Figure 3.3D) nor systematically (data not shown).

Based on these results, I continued outcrossing each *de novo dnmt* allele with another in an effort to create a sextuple mutant line. I successfully generated adult zebrafish that were *dnmt3βb.1-3*$^{+/-}$, *dnmt3αa*$^{+/-}$, *dnmt3αb*$^{+/-}$ and *dnmt3βa*$^{+/-}$ alleles (Figure 3.1). Surprisingly, larvae generated from these adults looked phenotypically normal to wildtype controls. These larvae were genotyped, and I identified quintuple mutants which also lacked a retinal phenotype (Figure 3.3H). We were unable to identify sextuple mutant

larvae from these genetic crosses, and clutch sizes were small making the likelihood of identifying a sextuple mutant larva difficult.

The analyses reported in this chapter reveal a lack of overt phenotypes among combinatorial *de novo dnmt* mutants suggesting that these enzymes are functioning redundantly. Despite the overtly normal development of quintuple dnmt mutants, the lack of phenotypic and/or functional evidence warrants further analyses to determine how these enzymes may function in eye development and differentiation. Any conclusive results in the future will require continued efforts to generate a sextuple null *de novo dnmt* line and validation of gene disruptions.

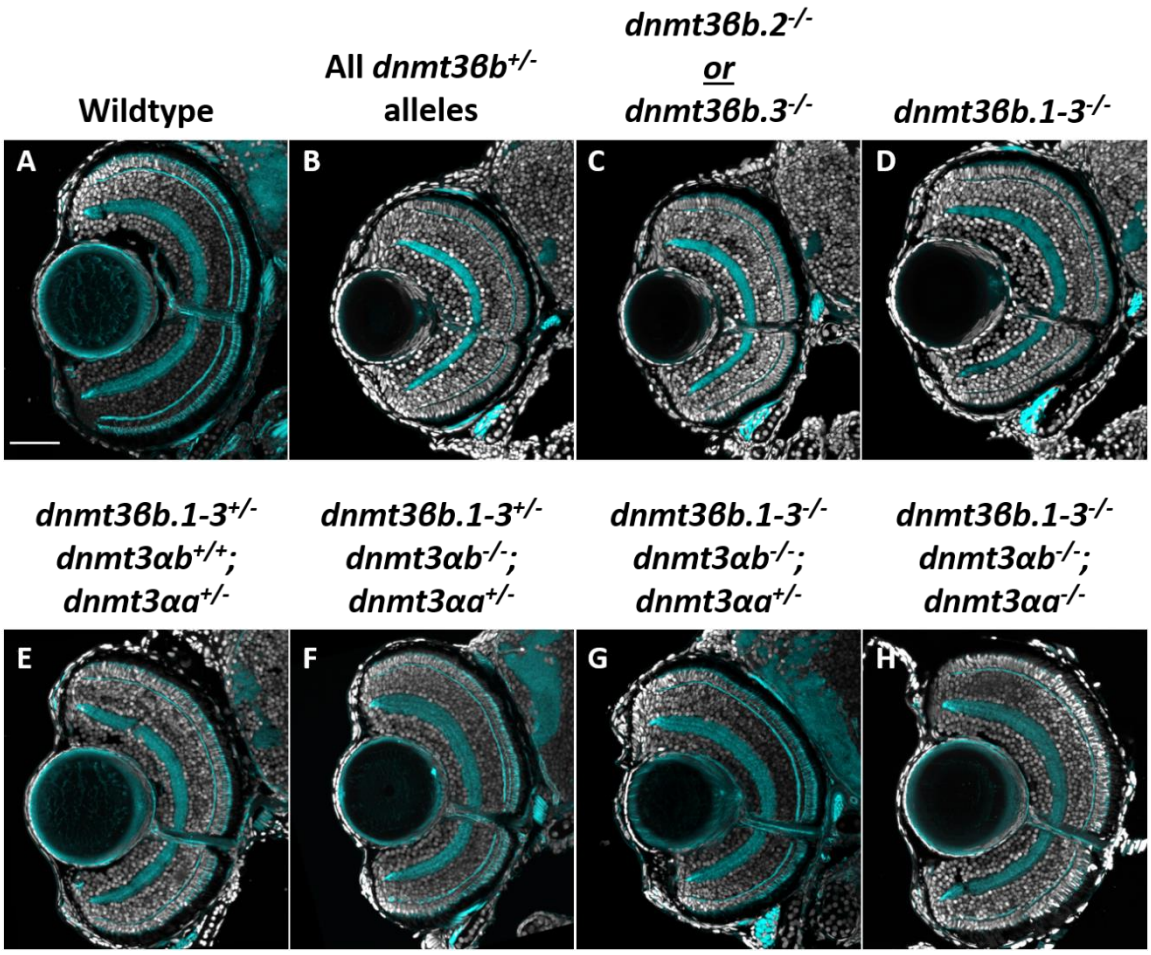


Figure 3.3. Combinatorial *de novo* mutants do not display aberrant retinal phenotypes.

**A, B, E.** Control retinas of wildtype (**A**), all heterozygous *dnmt3ββ* alleles (*dnmt3ββ.2, dnmt3ββ.3*, and *dnmt3ββ.1-3*) (**B**), and a combination of the quintuple alleles (*dnmt3ββ.1-3, dnmt3αa*, and *dnmt3αb*) (**E**). **C.** Example of *dnmt3ββ.2*$^{-/-}$ or *dnmt3ββ.3*$^{-/-}$ retinae. **D.** Retina of the *dnmt3ββ.1-3*$^{-/-}$ (triple KO) allele. **F.** *dnmt3αb*$^{-/-}$ allele as an additional control. **G.** Retina of quadruple *dnmt* mutant. **H.** Retina of quintuple *dnmt* mutant. All images taken of 5dpf larvae. Nuclei labeled with DAPI (gray). F-actin labeled with phalloidin (cyan). Scale bar = 50µm.

## 3.3 Discussion:

Regulation of gene expression and chromosomal interactions across multiple organisms, tissues, and cell types is an inherent function of DNA methylation[207–209]. *De novo Dnmt* genes have been shown to be critical for embryonic development[61], yet the field is still lacking in our understanding of how precisely this family of dnmts alters the genomic landscape in specific tissues or during development. Any malfunction in these proteins, and ultimately how that affects genomic methylation patterns, often leads to misregulation of gene expression[210,211], tumorigenesis[65,212], or even cell death[213]. Known mutations within mammalian *de novo Dnmts* correlate with embryonic lethality[61,69,214]. Moreover, disruption of the methylome is correlated with multiple neurodegenerative diseases, for example Alzheimer's, Parkinson's[215], and age-related macular degeneration[165].

### 3.3.1 *DE NOVO DNMT3S* ARE FUNCTIONALLY REDUNDANT.

Our findings in this chapter are inconclusive, in that we were unable to determine a specific role that *de novo dnmt3* family members play during retinal development. The possibility exists that this is a result of functional redundancy between the *dnmt3* paralogs. However, there are many unanswered questions in this regard. Firstly, it has not been established that all of the mutant alleles are functionally inactive and have bypassed the NMD trigger for compensation[206]. Validating *de novo dnmt3* transcript and protein levels will provide strong evidence for future analysis, though the sequence and protein similarities between these paralogs will require careful consideration. Secondly, if there is

functional redundancy, it will be essential to determine if these enzymes work to target the same regions of the genome or have site-specific differences. Cofactors that bind *Dnmt3*s could also play a large part in how these proteins are functioning retinal development. However, the fact that quintuple mutants lacked any obvious phenotype supports a model in which these enzymes are functionally redundant (Figure 3.3). Future studies aimed at determining *dnmt3* family member function will require careful preparation and genotypic analyses, because successful propagation of these combined mutant alleles is a long and time-consuming process.

Knockout of the three *dnmt3βb* genes lying in tandem on Chromosome 23 enables maintenance of these mutants as a single allele (*dnmt3βb.1-3*$^{pt705}$). However, maintaining and propagating four separate alleles still only produces one sextuple mutant per 256 embryos. Even with the zebrafish's high fecundity, the amount of genetic screening requires an excessive amount of work. It was attempted to propagate these alleles as mutant lines in progressively larger combinations since single and double mutant zebrafish were viable. Despite these efforts, the pool of adults carrying the necessary mutant alleles was small, and breeding these fish together was much less fruitful than wildtype controls. This limited the number of embryos available for experiments and increased the difficulties of propagating these mutant alleles together. Whether these breeding inadequacies were due to the inbreeding (to acquire the necessary mutant allele combinations), an effect of the mutant allelic combinations upon larval development, or fecundity remains to be elucidated. Our understanding of how each of these six *de novo dnmts* may be functioning,

either similarly or otherwise, within a cell and how that translates to tissue development and function will be critical for progress in both the epigenetic and evolutionary fields.

# CHAPTER 4: CHARACTERIZATION OF DUSP11 FUNCTION IN THE MURINE RETINA:

## 4.1: Introduction

### 4.1.1: THE DUAL-SPECIFICITY PHOSPHATASE (DUSP) FAMILY OF ENZYMES

It is widely known that many proteins are modified by the addition of (via kinases) or removal of (via phosphatases) phosphate groups and that this modification can alter the function of a protein. The Dual-specificity phosphatase (Dusp) family is unique in that they have the ability to dephosphorylate both tyrosine and serine/threonine residues[216] and have demonstrated roles in various cellular processes[217–219]. Dusp variants are numerous and grouped into two main categories: Map-kinase phosphatases and atypical phosphatases[220]. Additionally, reports of Dusp family members have been implicated in activation of the innate inflammatory response or increased susceptibility to infection[220,221].

Dusp11 falls within the atypical category, and is the sole member of the Dusp protein family that has a unique affinity for 5'-triphosphorylated-RNA substrates (herein referred to as 3pRNA)[216,222]. Dusp11 binds 3pRNAs and removes two of the phosphate groups to create mono-phosphorylated RNA (pRNA)[222,223]. This activity is essential for micro-RNAs (miRNAs) to bind to the RNA-induced silencing complex (RISC) complex and regulate gene expression[90]. Recent *in vitro* studies have demonstrated a critical role for Dusp11 in limiting RNA virus replication[221,224]. Additionally, reported evidence demonstrates an

increased inflammatory response *in vitro* in response to decreased levels of *Dusp11* mRNA[225]. Indeed, this correlative trend in inflammatory response and Dusp11 mRNA levels has been reported in cases of human inflammatory bowel disease patients[226], though no *in vivo* mechanistic studies have been demonstrated to date.

### 4.1.2: Intracellular detection and response to self and non-self 3pRNAs

3pRNAs are transcribed by RNA Polymerase III and are a common indicator of adenoviral or retroviral RNAs[216,220]. 3pRNAs located within the cytoplasm are therefore common indicators of viral infections[224,227,228]. Once viral RNA is detected, the Pattern Recognition Receptors (PRRs) trigger an immune response[225,227]. Interestingly, RNA Pol III also transcribes endogenous REs within the mammalian genome, which consequently are labeled by triphosphate groups[229,230]. This shared feature between REs and infectious viral RNAs introduces a conundrum within the cell in which it must distinguish between self and non-self elements.

Pattern Recognition Receptors are part of a cell's defense against pathogens, and these PRRs will trigger an immune response if 3pRNAs are detected[227]. *Alu* elements are an example of endogenous, non-autonomous REs that are transcribed by RNA Pol III[229,229], and, if left unchecked, can be detrimental to cellular processes[108,111,123]. In homeostatic conditions, *Alu* elements are processed by Dusp11 to remove the diphosphate group[231], in essence inhibiting the cell's ability to recognize these endogenous elements as viral. Recent studies have demonstrated that Dusp11 loss-of-function mutations lead to increased levels of *Alu*-derived REs *in vitro*[232], and overexpression of *Alu* elements is a common hallmark

of neurodegenerative diseases[111,233]. In collaboration with the lab of Dr. Chris Sullivan at the University of Texas at Austin, we aim to determine if Dusp11 function in the murine RPE results in a similar AMD-type phenotype as that seen in *Dicer1*-deficient mice[233–235].

## 4.2: Results

*Dusp11*$^{Tm1a(EUCOMM)Wtsi}$ mice (hereafter referred to as *Dusp11*) were previously generated by the International Mouse Phenotyping Consortium in the C57BL/6N mouse strain. This strain harbors a mutation within the *Crb1* gene (*rd8* allele) which causes a retinal degeneration phenotype[236]. To begin our studies using these mice, we first had to breed out the *Crb1*$^{rd8}$ allele. Sperm from *Dusp11*$^{Tm1a}$ male mice were used to rederive the *Dusp11*$^{Tm1a}$ allele in wildtype C57BL/6J pseudo-pregnant females, generating pups heterozygous for *Crb1*$^{rd8}$. We eliminated the *Crb1*$^{rd8}$ allele within two subsequent generations however, the data reported in this chapter were generated using mice which contained both *Crb1*$^{+/+}$ and *Crb1*$^{+/rd8}$ alleles.

*Dusp11*$^{Tm1a}$ mice harbor a promoter-less selection cassette that functions to create an mRNA splicing defect within the *Dusp11* gene body and were reported to have smaller eyes than their wildtype counterparts[237], but no analysis has validated those findings. This study aimed to characterize the *Dusp11*$^{Tm1a/Tm1a}$ phenotype, specifically within the retina and RPE. It is important to note that all results reported in this chapter are derived from an ongoing longitudinal study and will continue past the publication date of this document.

### 4.2.1 CHARACTERIZATION OF *DUSP11*$^{Tm1a/Tm1a}$ PHENOTYPE

*Dusp11*$^{Tm1a/Tm1a}$ mice are viable, survive into adulthood, and are capable of producing offspring. *Dusp11*$^{Tm1a/Tm1a}$ mice have a noticeably shorter muzzle length compared to their siblings by the weanling stage (P21) which continues through adulthood (data not shown). Although some *Dusp11*$^{Tm1a/Tm1a}$ pups appear smaller at birth, they generally reach the same body size and weight as their siblings by P60 and do not vary from their siblings through P270 (Figure 4.1). The shortened muzzle and smaller eye phenotypes are apparent throughout adult life and are independent of sex (data not shown). After noting these general differences, we began assessing Dusp11 localization within the eye and characterizing the retina and RPE morphologies.

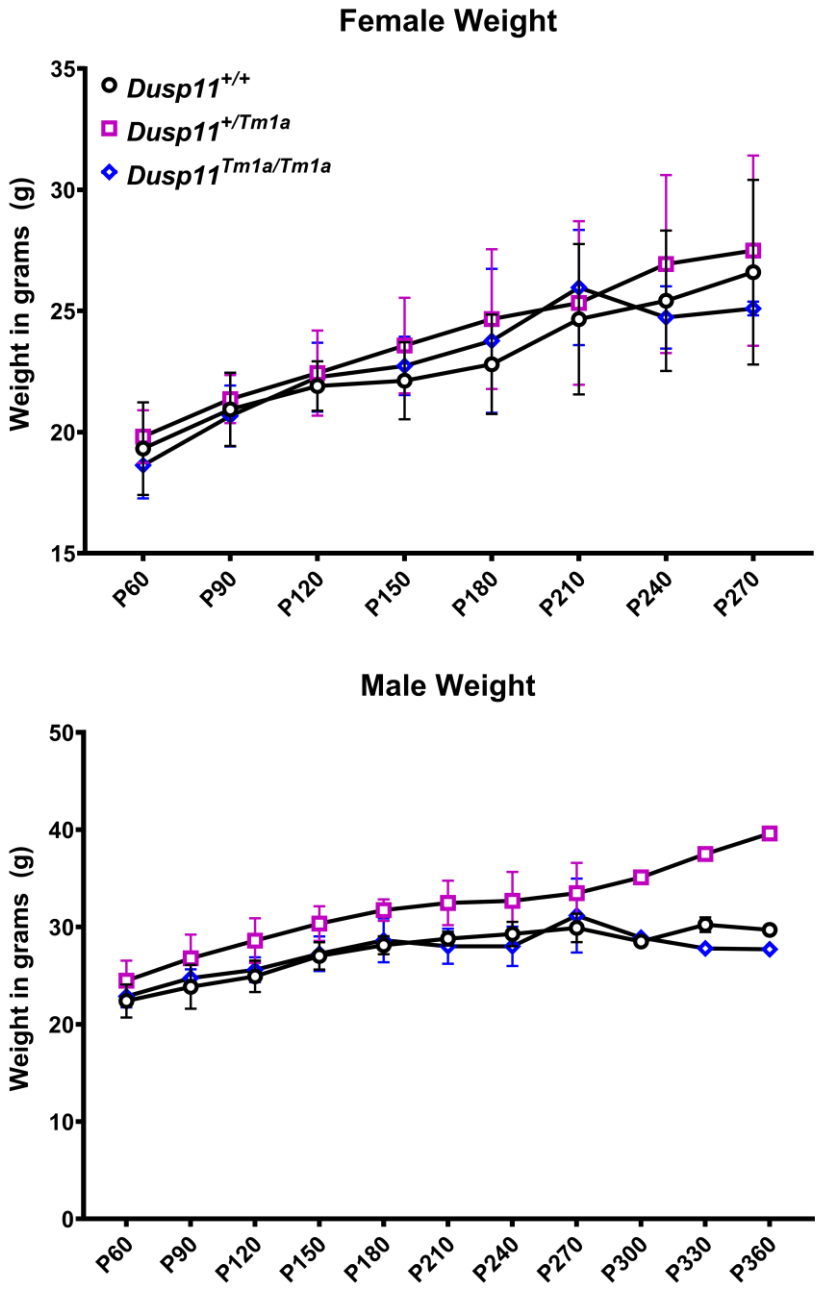


Figure 4.1. Dusp11 function is not required to maintain body weight.

**Top:** Weight in grams (g) of female mice from P60 to P270. **Bottom:** Weight of male mice from P60 to P360. *Dusp11*$^{+/+}$ = Black circle; *Dusp11*$^{+/Tm1a}$ = Magenta square; *Dusp11*$^{Tm1a/Tm1a}$ = Blue diamond. n $\geq$ 3 between P60 & P270; weights of P300+ mice are not yet quantifiable.

### 4.2.1: *Dusp11*$^{Tm1A/Tm1A}$ mice display retinal lamination defects by P210.

Previous work demonstrated the requirement for Dicer-mediated miRNA processing within the retina, and Dicer loss-of-function mutants developed retinal lamination defects and the buildup of drusen deposits under the RPE[108,235]. These retinal abnormalities, commonly associated with AMD, began to emerge by approximately three months of age[108,235]. Since 3pRNAs require processing by Dusp11 in order for their association with Dicer and the AGO complex, we hypothesized that our Dusp11 mice would produce a similar AMD-like phenotype and age of onset.

To determine the presence and/or age of onset of any retinal phenotype, we performed a longitudinal experiment using Spectral Domain Optical Coherence Tomography (SD-OCT). 37 mice were used in this study (*Dusp11*$^{+/+}$ n=9, *Dusp11*$^{+/Tm1a}$ n=17, *Dusp11*$^{Tm1a/Tm1a}$ n=11), and each mouse was imaged approximately every 30 days from P60-P360. Contrary to our hypothesis, no obvious retinal lamination defects were detected within the first six months of age (Figure 4.2 and 4.3). Beginning around P270 however, *Dusp11*$^{Tm1a/Tm1a}$ mice presented with lamination abnormalities (Figure 4.2C). In particular, the ONL appeared thinner, having a pinched-like appearance between the RPE and INL (arrow in Figure 4.2C) compared to the smooth lamination pattern seen in sibling controls (Figure 4.2B). To validate these findings, we used proprietary software developed by Bioptigen Inc. to automatically segment the SD-OCT images, measuring for retinal thickness (Figure 4.2) and lamination (Figure 4.3)[238–241]. All measurements obtained were analyzed for statistical significance using GraphPad Prism 8.0.

Total retinal thickness measurements remained constant between *Dusp11*$^{Tm1a/Tm1a}$ mice and controls through P150 (Figure 4.2D). By P180$^{+}$, *Dusp11*$^{Tm1a/Tm1a}$ retinae began to show an overall reduction in thickness compared to their sibling controls (Figure 4.2D). Total retinal thickness was comparable between *Dusp11*$^{Tm1a/Tm1a}$ and sibling controls through P150 (Figure 4.3C). However, *Dusp11*$^{Tm1a/Tm1a}$ mice began to display an overall thinning of the retina starting at P180 (Figure 4.3C, $p < 0.05$). To ascertain if these measurements were a result of overall retinal thinning or layer-specific changes, we compared measurements of the inner (RNFL, IPL, and INL), middle (OPL and ONL), and outer retina (IS/OS and RPE) across all time points. Strikingly, the inner and outer retinal thicknesses were consistent between sibling controls and *Dusp11*$^{Tm1a/Tm1a}$ mice across all time points (Figure 4.3E,G). In comparison, the middle retina is statistically thinner in the *Dusp11*$^{Tm1a/Tm1a}$ compared to controls from P180-P240 (Figure 4.3F). These measurements indicate a thinning of the ONL, which is a characteristic of AMD[242].

We then broke down these measurements into each of the retinal layers to determine whether the thinning within the middle retina is due to changes in the OPL, ONL, or both. Indeed, the proportion of the ONL within the *Dusp11*$^{Tm1a/Tm1a}$ shows a similar decreasing trend (Figure 4.3E) alongside the OPL reduction at P180 and P210 (Figure 4.3D). This reduction in OPL and ONL proportions correlates with increases of the RNFL (Figure 4.3A) and IS (Figure 4.3F) layers of the retina. All other layers show no significant changes across all time points. The onset of these aberrations within the *Dusp11*$^{Tm1a/Tm1a}$ are possibly consistent with degenerative retinal diseases, however this model requires further analyses through SD-OCT, histology, and immunohistochemistry.

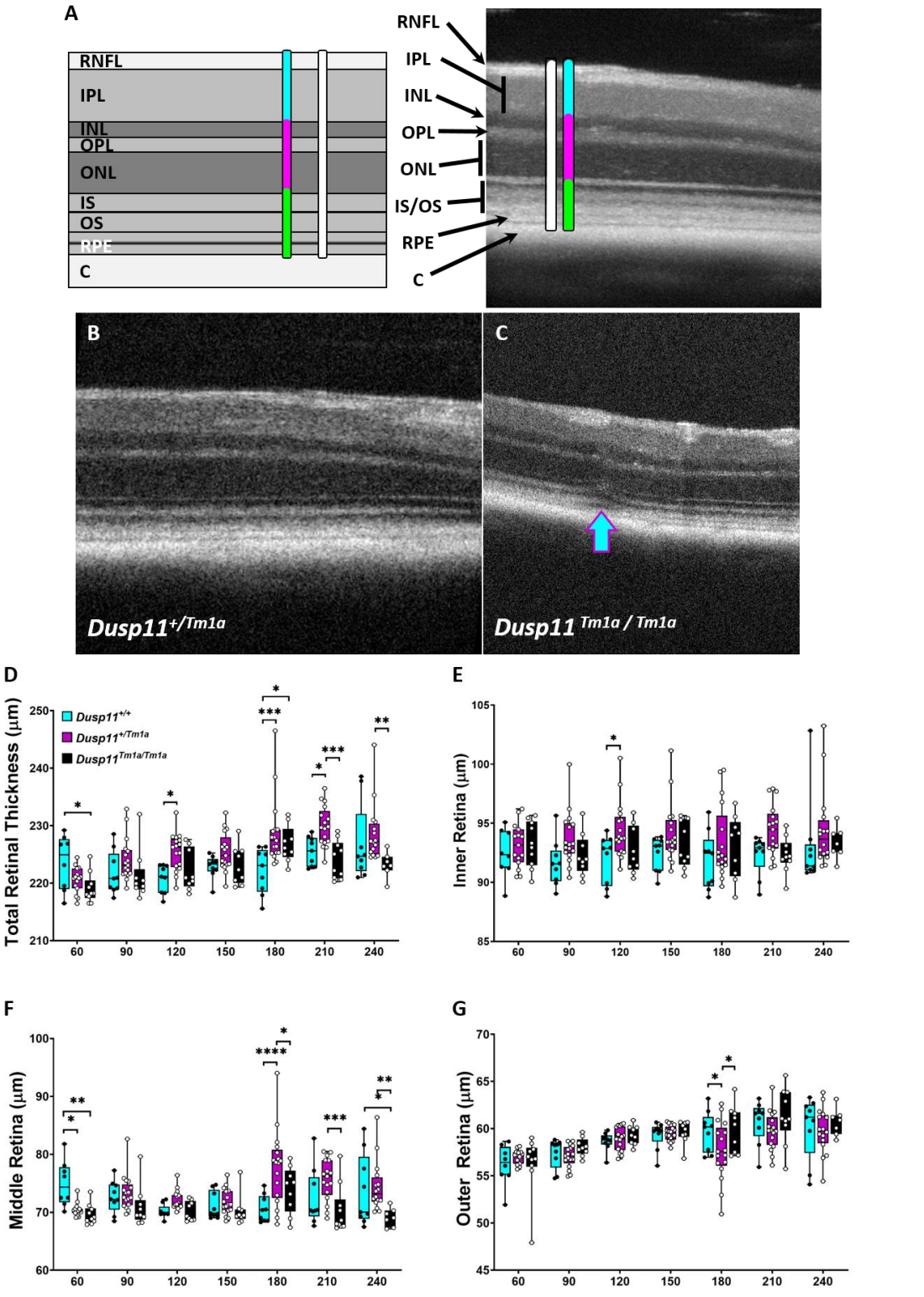


*(Figure 4.2 continued on next page)*

Figure 4.2. *Dusp11*$^{Tm1a/Tm1a}$ mice begin to display retinal thinning by P180.

**A.** Diagram (*left*) and example OCT image (*right*) of the murine retina and the corresponding layers indicated in the center. Vertical lines depict measurements of the inner retina (*cyan*), middle retina (*magenta*), outer retina (*green*), and total retinal thickness (*white*). **B.** *Dusp11*$^{+/Tm1a}$ control with normal retinal lamination. **C.** *Dusp11*$^{Tm1a/Tm1a}$ showing retinal deformation within the middle retina domain (arrow). **D.** Average total retinal thickness over time of all samples measured. **E-G.** Average inner (**E**), middle (**F**), and outer (**G**) retinal thicknesses over time from P60-P240 (x-axis). *Note:* images in B,C are not cropped to the same scale. n $\geq$ 7. **p* <0.05, ***p* <0.005, ****p* <0.0005, *****p* <0.00005.

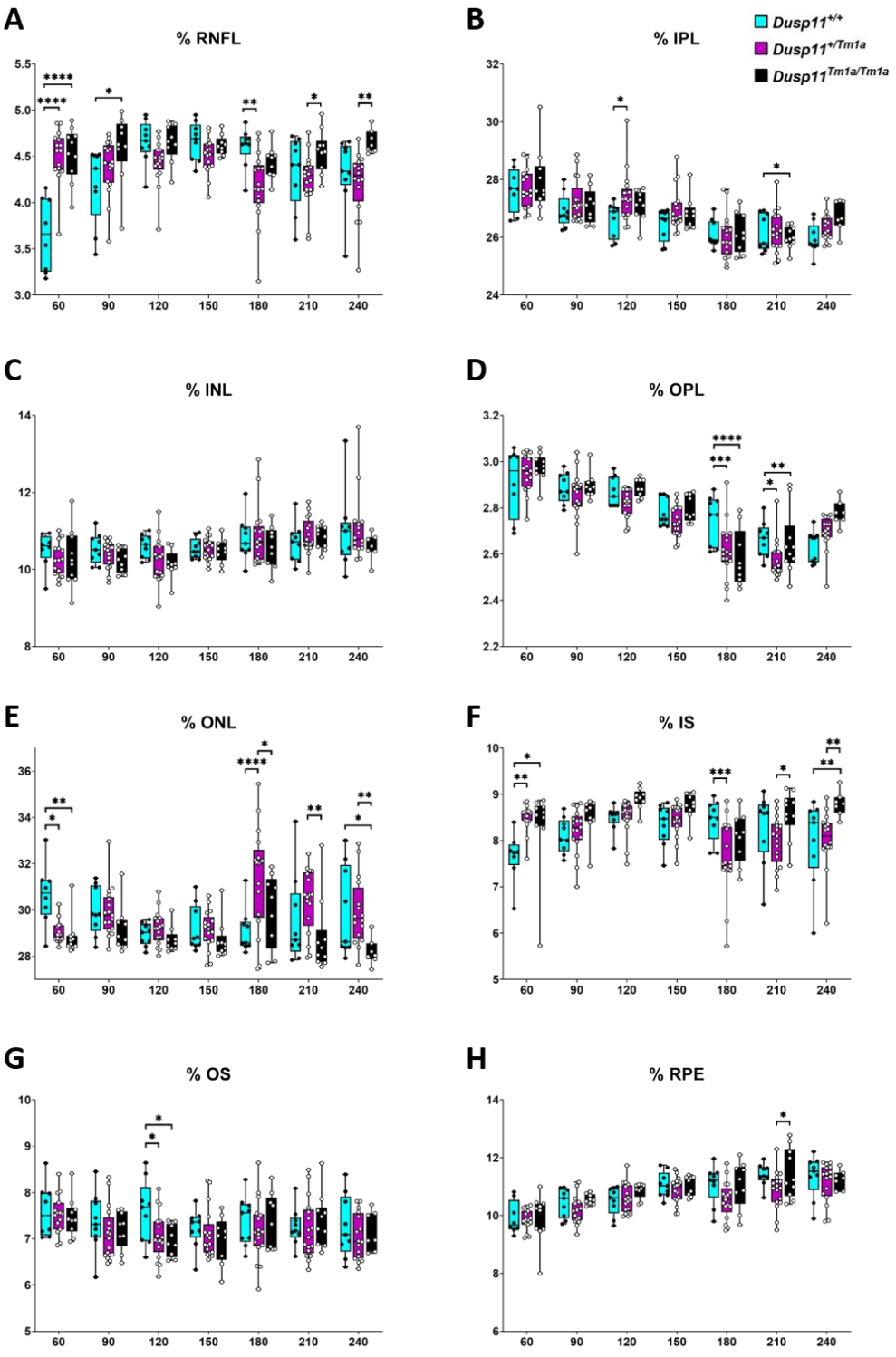


*(Figure 4.3 continued on next page)*

Figure 4.3. *Dusp11*$^{Tm1a/Tm1a}$ display quantifiable changes in retinal lamination by P210.

**A.** Proportion of the RNFL layer of the total retinal thickness. **B.** Proportion of the IPL layer. **C.** Proportion of the INL layer. **D.** Proportion of the OPL layer. **E.** Proportion of the ONL layer. **F.** Proportion of the IS layer. **G.** Proportion of the OS layer. **H.** Proportion of the RPE layer. All data collected approximately every 30 days from P60-P240 (x-axis). $n \geq 7$. **p* <0.05, ***p* <0.005, ****p* <0.0005, *****p* <0.00005.

## 4.3: Discussion

Results reported in this chapter lay the groundwork for future studies of Dusp11 function within the retina. Although Dusp11 is not critical for normal development and viability of the mouse, its requirement within the retina is becoming apparent. Indeed, our results show that Dusp11 function is required to maintain retinal lamination in older mice (Figure 4.2 and 4.3). Of note, the lamination defects identified here (Figure 4.2 and 4.3) are suggestive of retinal degeneration, and the pinched-like deformity seen in Figure 4.2C is similar in pattern to reports of choroidal neovascularization[235,243] though continued analyses through P360 will be necessary to verify these results. Interestingly, *Dusp11*$^{+/Tm1a}$ mice were occasionally found to have a more dramatic change in their retinal layer measurements than *Dusp11*$^{Tm1a/Tm1a}$ mice. Since the SD-OCT analysis was conducted using earlier generations after the rederivation mentioned previously, we suspect that the differences seen in heterozygous mice are indicative of mouse strain backgrounds variations.

Despite these initial reports of *Dusp11*$^{Tm1a/Tm1a}$ retinal phenotypes, these defects arise at later time points than those seen in Dicer mutants[235]. It is important to note the Dusp11 is only known to affect the processing of 3pRNAs, a small component of the miRNA pathway[231], whereas Dicer is critical for much of the pre-miRNA processing[244]. These vast differences in miRNA governance is likely a reason for the delayed onset of an AMD-like phenotype in *Dusp11*$^{Tm1a/Tm1a}$ retinae (Figure 4.2 and 4.3) compared to controls. These

results implicate Dusp11 as a potential regulator of retinal homeostasis and lends a unique view of neurodegenerative disease regulation.

Localization of Dusp11 from previous reporting *in vitro* have identified Dusp11 within the nucleus and cytoplasm[222,231], however, no evidence has been reported of Dusp11 localization *in vivo* and if there are tissue-specific differences in its localization or function. We have begun characterizing Dusp11 localization *in vivo* through immunohistochemistry using a Dusp11 polyclonal antibody on RPE flat mounts (data not shown). Notably, we detected Dusp11$^{+}$ puncta along the cellular membranes suggesting a potential role at cell-to-cell junctions. These unexpected results have led us to hypothesize that Dusp11 may have tissue-specific localization and function.

Accordingly, we collected various organs to determine if Dusp11 localization was tissue-dependent. Remarkably, we found Dusp11 localization was as varied as the tissues analyzed (data not shown). Of note, Dusp11 displayed 1) diffused localization throughout the cytoplasm and nuclei of the liver and corneal endothelium, 2) nuclear-specific localization within the corneal epithelium, 3) cytoplasmic localization within the heart, and 4) restricted localization to cell-to-cell junctions within hair follicles of the skin. When considering Dusp11 localization within the liver and corneal endothelium, it is possible that this non-specific binding is due to tissue autofluorescence. It will be essential to compare these stain patterns between controls and *Dusp11*$^{Tm1a/Tm1a}$ tissues and to ensure minimal autofluorescence using established tissue-clearing protocols[245,246]. Although these results are promising and suggest the potential for cell type-specific localization or function, more in-depth analyses are required to determine Dusp11 function *in vivo*.

Nonetheless, these Dusp11$^{+}$ puncta along epithelial cell membranes are thought-provoking and require experimental validation.

Previous reports have identified the intercellular transfer of miRNAs through gap junctions (GJs)[247,248]; more recently demonstrating that these GJ-mediated miRNAs function to regulate gene expression within the neighboring cell[249]. Disruption of GJ-mediated miRNA transfer within the developing cochlea was shown to result in a developmental hearing disorder in mice[250]. Additionally, gliomas have demonstrated the capacity to transfer miRNAs across GJs with astrocytes and ultimately affect the invasiveness of this aggressive disease[251,252]. Considering Dusp11's ability to identify and modify 3pRNAs, one could hypothesize that RPE cells proactively stage this enzyme at cell-to-cell junctions with the purpose of identifying and processing viral-like RNAs as they travel between cells. Indeed, retroviruses like HIV are capable of coopting GJs for the transfer of viral particles between cells[253]. Therefore, positioning Dusp11 at GJs could act as an early warning system for the RPE, a highly sensitive and critical tissue for maintaining vision.

Investigations into Dusp11 function have been limited and only recently shown to bind 3pRNAs[223,232]. Its ability to bind RNA is unique among the Dusp family members[231] and will challenge our views on how these enzymes function *in vivo* to modify gene expression and regulate retroviruses, and more specifically how Dusp11 functions in a tissue-dependent fashion. Undoubtedly, evidence provided in this dissertation and future experiments will inspire novel ideas on how Dusp11 modulates gene expression, retroviral activity, and how this may contribute to the onset of AMD or other retinal degenerative

diseases. The results reported within this study, and those still ongoing, will provide unique insights into Dusp11's function *in vivo* and trigger new ideas for studying the relationships between epigenetics, non-coding RNAs, and retinal degeneration.

# CHAPTER 5: FUTURE DIRECTIONS.

## 5.1 Summary of work

This dissertation focuses on epigenetic regulation during retinal development and disease, particularly through the DNA methylation and miRNA pathways. DNA methylation is a critical mechanism through which our cells regulate gene expression, cellular identity, and survival. miRNAs work in conjunction with DNA methylation to modulate these epigenetic signatures and promote cellular homeostasis and differentiation. In Chapter 2, I demonstrate a role for dnmt1 function in the maintenance of retinal stem cells (RSCs) within the zebrafish retina. Disruption of dnmt function resulted in depletion of the RSC population through disruption of the cell cycle, increased cell death, and overexpression of retroelements (REs) (Illustration 5.1). In Chapter 3, I generated and established combinatorial *de novo dnmt* mutants to assess their contribution to retinal development and differentiation. Although these mutants did not develop any obvious retinal abnormalities, further validation is required to parse out redundant versus allele-specific defects. In Chapter 4, I conduct the first *in vivo* characterization of potential eye functions for the unique dual-specificity phosphatase enzyme, Dusp11, to determine its contribution to retinal development, differentiation, and disease. Although the evidence presented in Chapter 4 is preliminary, future analyses of this pathway will be critical for expanding our current understanding of the epigenetics field and Dusp11's function in the retina. Furthermore, the mutant and transgenic alleles generated in this thesis will expand

the current repertoire of tools available for future investigations of retinal development and disease.

## 5.2 Determining the contribution of maintenance DNA methylation to retinal stem cell homeostasis

In Chapter 2, I presented evidence demonstrating a requirement for dnmt1 function in RSCs maintenance, without which RSCs are lost. Although the data provided clearly support this conclusion, the exact mechanism of RSC loss was not established. As discussed in Chapter 2.3, a likely mechanism of *dnmt1*$^{-/-}$ RSC loss occurs through a non-p53-mediated cell death pathway. To determine which cell death pathway is regulated by maintenance DNA methylation and responsible for RSC loss, it will be necessary to continue these studies through gene expression studies and cell death pathway modulation. In Chapter 2.3, I hypothesized that pyroptosis and necroptosis are likely cell death pathways contributing to *dnmt1*$^{-/-}$ RSC loss. However, attempts to modify necroptotic processes via pharmacological manipulation were unsuccessful and genetic tools to assess this pathway within the zebrafish require further development. In contrast, tools for assessing the role of pyroptosis, an alternative mode of cell death, in zebrafish development and tissue function are available[254]. Previous reports demonstrate a role for autophagy, a common trait of the pyroptotic pathway, in the clearance of damaged cellular organelles and debris and has been shown to be independent of p53 function[255,256]. Defects within autophagy and lysosomal biogenesis pathways were also shown to result in neurodegenerative disease phenotypes[257,258].

To address this possibility, I acquired both the *Tg(CMV:EGFP-map1lc3b)*$^{zf155}$ and *Tg(CMV:mCherry-map1lc3b)*$^{scf4}$ transgenic lines (kindly donated by Dr. Donghun Shin's lab[254] and mated them into the *dnmt1*$^{s872}$ background. These transgenic lines provide *in vivo* detection and tracking of intracellular autophagic and lysosomal processes within the zebrafish[254]. A known repressor of autophagy is mTOR, a key effector of multiple cellular processes including cell growth, proliferation, and aging[255]. Biochemical inhibitors of the mTOR pathway, namely Rapamycin, have been shown increase cellular autophagy[259,260]. Additionally, 3-methyladenine (3-MA) inhibits autophagy in the zebrafish[260]. Thus, the use of the *dnmt1;map1lc3b* transgenic lines in combination with pharmacological manipulations, will elucidate any aberrant autophagic processes within *dnmt1*$^{-/-}$ RSCs and if this contributes to RSC loss via pyroptosis.

In parallel, we are developing multiple experimental tools to determine the function of REs within *dnmt1*$^{-/-}$ RSCs. We aim to 1) identify and characterize the expression levels of RE families when hypomethylated, 2) modulate RE activity through pharmacological inhibition of retroviral transcription, 3) utilize macrophage/microglia-deficient zebrafish to determine the requirement for *dnmt1*$^{-/-}$ RSC clearance via the innate immune system, and 4) to determine the contribution of RE transposition to DNA damage and chromosomal recombination. Results from these experiments will be crucial for narrowing in on the precise mechanism of RSC loss and potentially implicate these processes for the development of retinal therapies and regenerative treatments.

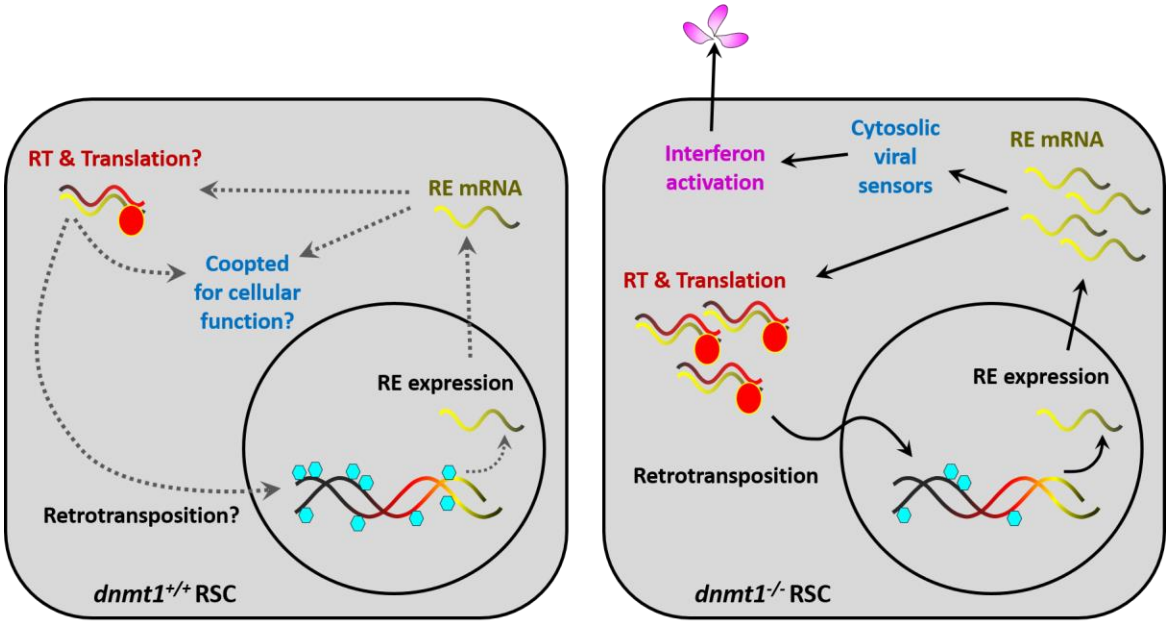


Illustration 5.1. Working model of dnmt1 function in RSCs.

*Left.* Wildtype dnmt1 functions to maintain the methylome of proliferating cell. This limits RE expression such that retrotransposition is limited. *Right.* *dnmt1*$^{-/-}$ RSCs are unable to maintain the methylome, thus allowing for increased RE expression. Endogenous viral sensors within the cytoplasm detect these viral elements and initiate an immune response. Increased numbers of RE transcripts become translated within the cytosol, transported into the nucleus, and then transposed into a new genomic location.

## 5.3 Elucidating the function of *de novo* DNA methyltransferases

Our original expectations that *de novo dnmts* would demonstrate pairwise functional redundancy was quickly challenged and determined to be incorrect. Indeed, the six *dnmt3* paralogs have suggested a more complex story which requires careful dissection. Experiments are currently underway to continue this project by first outcrossing these lines to ensure genetic diversity, thus limiting defects associated with inbreeding, and then attempting future incrosses to acquire a full panel of the six mutant *dnmt3* paralogs. However, the possibility exists that loss of *de novo dnmt* function is not detrimental to zebrafish development and viability. Recent studies have shown that this is true in the case of the red flour beetle[261262], and instead the over-expression of *dnmt3* or *dnmt3* gain-of-function alleles lead to cellular or tissue impairment[62,263]. Future experiments to address this possibility would include generating transgenic zebrafish that harbor inducible constructs to over express the *de novos* singularly or in combination and either systemically or tissue-specifically. Such methods will include the Gal4/UAS system[264–266], Tet-ON/OFF[267,268], or CRISPR/Cas9-activator and repressor constructs[269,270].

An alternate explanation for why the dnmt3 paralogs do not display overt phenotypes could be how they function in gonadal development. We know that *dnmt3* family members function in genomic imprinting[209,210,271], but the extent to their redundancy in this process is still unknown. Genomic imprinting is a process through which the established DNA methylome is passed down from parent to offspring, and disruption of these methylation patterns is known to have a detrimental impact on embryonic development[63,272].

The potential for developmental defects, specifically in gonadal development, in these combinatorial *dnmt3* mutants is high. DNA methylation, and more specifically its role in genomic imprinting, is known for its repression of REs during spermatogenesis[191,192,273] and oogenesis[274,275]. DNA hypomethylation within the developing gonads results in derepression of REs, which can cause a number of developmental defects arising from chromosomal breakages and recombinations[276–278]. Precise control of RE activity is achieved through the cooperation of both DNA methylation and Piwi-interacting RNA (piRNA) pathways[279]. The fact that we were unable to acquire offspring carrying all of the necessary *dnmt3* mutant alleles suggests that this is a likely possibility. Future in-depth analyses of gonadal development within these combinatorial mutants will be essential for teasing apart the redundant and/or exclusive functions of the *de novo dnmt3* family in regards to genomic imprinting and potentially guide further analysis to determine their retinal function.

## 5.4 Determining Dusp11 function in retinal degenerative disease

Studies of Dusp11 function are limited and primarily focus on its function in removing two phosphates from 3pRNAs, transcripts produced by RNA Pol III[280]. The data reported in Chapter 4 provides a novel, introductory glimpse into how this unique phosphatase potentially functions *in vivo*, and particularly within the retina. These results are preliminary and require further validation which is currently underway. In particular, these efforts are focused on identifying if Dusp11 loss-of-function phenocopies the AMD-like phenotype seen in Dicer-deficient retinas[108,235]. These analyses, first assessed through

longitudinal experiments using spectral domain optical coherence tomography (SD-OCT), of wildtype, heterozygous, and *Dusp11*$^{Tm1a/Tm1a}$ mice from P60-P360 demonstrate the emergence of retinal lamination defects (Figure 4.4 and 4.5) beginning around P180. The continuance of this longitudinal experiment will confirm if these defects arise solely within the *Dusp11*$^{Tm1a/Tm1a}$ retina if they result in retinal degeneration. Since we are collecting rectangular volume data via SD-OCT, we are able to take additional measurements of the sibling and *Dusp11*$^{Tm1a/Tm1a}$ retinal blood vessels. Should these results prove fruitful, then we also plan on assessing retinal blood flow in the *Dusp11*$^{Tm1a/Tm1a}$ retina and how that may contribute to a retinal degeneration phenotype.

A more in-depth characterization of Dusp11's intracellular function is underway and consists of histological and immunohistochemistry analyses to determine its expression pattern, localization, and retinal lamination defects. Functionality of these retinae will be tested through 1) electroretinography (ERG), a common methodology to assess photoreceptor function[281] and/or 2) intense light to induce cellular stress upon the photoreceptors. This methodology is frequently used to evaluate how photoreceptor stress can lead to ocular defects. This experimental setup will determine if Dusp11 function is required for a cellular response to photoreceptor stress. Taken together, the evidence supplied in this dissertation underscores the importance of epigenetic mechanisms required for retinal cell homeostasis. Future works will be critical for our understanding of how these processes intertwine and branch out to affect cellular change.

# APPENDICES

## Appendix A: dnmt Material and Methods

### A.1: ZEBRAFISH MAINTENANCE

Zebrafish (*Danio rerio*) were maintained at 28.5°C on a 14 h light/ 10 h dark cycle. All protocols used within this study were approved by the Institutional Animal Care and Use Committee of The University of Pittsburgh School of Medicine, and conform to the National Institutes of Health Guide for the Care and Use of Laboratory Animals. Mutant alleles used in this study were *dnmt1*$^{s872}$ and *tp53*$^{zdf1}$. *dnmt1*$^{s872}$ and *tp53*$^{zdf1}$ zebrafish were genotyped using BioRad's CFX Manager 3.1 and Precision Melt Analysis software (v4.0.52.0602). All genotyping primers are listed in Table A1. Transgenic *Tg(CMV:Has.L1RE3,EGFP,myl7:EGFP)*$^{pt701}$ zebrafish were generated as described[265] using constructs generously provided by Kristen Kwan and Chi-Bin Chien (University of Utah, Salt Lake City).

### A.2: BRDU LABELING

To assess cellular proliferation, larvae were incubated in 10mM BrdU for either 2 or 12 hours, after which the BrdU was washed out and larvae were either collected or used for BrdU pulse-chase experiments.

Table A.1. List of primer sequences and experimental purpose used in the *dnmt1* study.

| ***Gene / Target*** | **Fwd Primer Sequence** | **Rev Primer Sequence** | **Experimental Purpose** |
|---|---|---|---|
| *dnmt1*$^{s872}$ | GAATCAATGCACACCATATGCCTTATGTAC | CTCAGGGTGAAGGACACGTCC | HRM Genotyping in TL strain |
| *dnmt1*$^{s872}$ | AATGCTGTTCCTCCACCCC | CTTGACCTCCAGGCCAATGG | HRM Genotyping in AB strain |
| *tp53*$^{zdf1}$ | CTAAACTACATGTGCAATAGCAGCTGC | CTCCAGAGTGATGATTGTGAGGATGG | HRM Genotyping |
| *BEL20-LTR_DR* | AATGCAACGCAGTATCATCG | AGGTGCACTTCTCCGAGTGT | *In situ* hybridization probe; pGEM T-Easy Vector |
| *ERV1-1-LTR_DR* | TGAAGGATTTGATCTTCTCTCC | GCAATCGAGTCAGTGGGTCT | *In situ* hybridization probe; pGEM T-Easy Vector |
| *ERV1-N5-LTR_DR* | TGAGTATGCCTGCACAGGAG | TCAGACCGGAGGTTTTGAAT | *In situ* hybridization probe; pGEM T-Easy Vector |
| *ERV4_DR-I* | CCAAGACCGATCACACCTTT | ACTCCCATAATTCCCCCTTG | *In situ* hybridization probe; pGEM T-Easy Vector |
| *Gypsy10-LTR_DR* | TGCGGTTAACGCTTACAAAA | CACTCCCCCTAATCAGATACCA | *In situ* hybridization probe; pGEM T-Easy Vector |

### A.3: IMMUNOHISTOCHEMISTRY AND FLUORESCENT LABELING:

Immunohistochemistry performed as described previously[282]. The following antibodies and dilutions were used: anti-BrdU antibody (Abcam, ab6326, 1:250), anti-phospho-histone H3 (Ser10) (EMD Millipore, 06-570, 1:250), anti-GFP (Thermo Fisher Scientific, A-11122, 1:50), goat anti-rat Cy3 secondary (Jackson Immuno Research, 112-165-003, 1:500), goat anti-rabbit Cy3 secondary (Jackson Immuno Research, 111-165-144, 1:500), and goat anti-rabbit Cy5 secondary (Jackson Immuno Research, 711-035-152, 1:500). Nuclei were counterstained with DAPI using Vectashield with DAPI (Vector Laboratories, H-1200). F-actin was labeled using AlexaFluor 633 Phalloidin (Thermo Fisher Scientific, 1:33, A22284). TUNEL-labeling was accomplished using TMR-Red In situ Cell Death Detection Kit (Sigma Aldrich, 12156792910).

### A.4: CLONING AND PROBE SYNTHESIS

CMZ-specific probes have been published previously[120,133]. Retroelement probes were generated using reverse transcription-polymerase chain reaction (RT-PCR) on Trizol-isolated RNA from 24hpf and 5dpf embryos. Primer sequences were kindly provided by Dr. Kirsten Sadler (NYU Abu Dhabi), and PCR products were ligated into pGEM-T-easy vector (Promega Cat# PR-A1360) and verified by Sanger sequencing. Plasmids were linearized and used as templates to transcribe digoxigenin-labeled RNA probes *in vitro* (Roche).

### A.5: *IN SITU* HYBRIDIZATION

Hybridizations using digoxigenin labeled antisense RNA probes were performed essentially as described[283], except that they were pre-incubated with 1 mg/mL Collagenase type 1A (Sigma, C9891) to allow probe diffusion throughout the tissue. All probe primer sequences and plasmid construct information are listed in Table __.

### A.6: MICROSCOPY AND IMAGE PROCESSING

For sectioned embryos, imaging was performed with an Olympus FV1200 confocal microscope. Confocal Z-stacks were collected in 1µm optical sections. Z-stacks were max-projected using ImageJ (version 1.52r) software (National Institutes of Health) and quantification was conducted using the "Cell Counter" plugin. Figures were prepared using Adobe Illustrator CS6 (Adobe Systems). *In situ* cryosections were imaged utilizing a Leica DM2500 with a 100X oil immersion objective (NA: 1.25).

### A.7: CELL COUNTING AND QUANTIFICATION:

Each data point collected from an individual larva. Each larva was analyzed using three consecutive 12 µm sections of the central retina using the optic nerve and lens morphology as retinal landmarks. The average of the three consecutive sections was used as a single data point ($n \geq 4$ for all datasets). Proportions of retinal domains were calculated by dividing the number of DAPI-labeled nuclei in each domain over the total number of retinal nuclei.

### A.8: STATISTICS

For all statistical analysis, data were imported into GraphPad Prism 8 software. Quantification of nuclei and immunolabeled cells was statistically assessed using Student's two-tailed unpaired T-test with $p < 0.05$ as a significance threshold.

### A.9: GENERATION OF *TG(CMV:HSA.L1RE3,EGFP,MYL7:EGFP)*$^{PT701}$:

pLRE-mEGFPI plasmid was generously donated by Dr. John V. Moran (The University of Michigan School of Medicine)[173]. The *Hsa.L1RE3-EGFP* sequence was isolated from the pCEP4 backbone using NotI and SalI restriction enzymes and then inserted into pME-MCS plasmid from the Tol2 Gateway Kit. LR Clonase II Plus was used to carry out all Multisite Gateway assembly reactions[265] using p5E-MCS (19ng), pME-Hsa.L1RE3-EGFP (77ng), p3E-polyA (19ng), and pDestTol2CG2 (103ng) plasmids. Capped Tol2 mRNA was synthesized from pCS2FA-transposase using the Ambion mMessage mMachine Sp6 *in vitro* transcription kit (Thermo Fisher Scientific, AM1340). Tol2 mRNA (75pg) was co-injected with *pDEST- Hsa.L1RE3-EGFP* (40 pg) into *dnmt1*$^{+/-}$*;p53*$^{+/-}$ incross embryos at the 1-cell stage. Embryos displaying acceptable levels of mosaic *myl7*:EGFP expression were raised to adulthood, and outcrossed to screen for founders. $F_1$ embryos displaying ubiquitous *myl7*:EGFP expression were isolated and reared to generate the stable line *Tg(CMV:Hsa.L1RE3,EGFP,myl7:EGFP)*$^{pt701}$.

### A.10: TALEN- AND CRISPR/CAS9-MEDIATED MUTAGENESIS

TALEN sites were chosen based on sequence specificity and ease of genotyping via RFLP according to previous protocol[284]. TALEN constructs were assembled using the

Golden Gate platform[202,285] and injected into 1-cell stage embryos. Germline transmission was determined through sperm collection, PCR, RFLP, and Sanger sequencing to identify indels that was predicted to result in a non-functional protein product.

All mutant alleles generated using CRISPR/Cas9 mutagenesis were created following the protocol as described previously[204], and mutant alleles were validated as stated above for the TALEN generated alleles. Genotyping of all mutant alleles was conducted via RFLP or HRM analysis and larvae were processed for retinal phenotype analyses. All *de novo dnmt* primers used for genotyping and mutagenesis are listed in Table A2.

Table A.2. List of primer sequences used in the *de novo dnmt* study.

| **Gene target(s)** | **Allele** | **Forward Primer** | **Reverse Primer** |
|---|---|---|---|
| *dnmtβb.2* | *pt702* | GCCTGCTAACGGATGAGTTTTTGG | CAGCTCTGTTTGCCAGTACTTCTC |
| *dnmtβb.3* | *pt703* | GGACTTGCTGAGGAAGATCGGA | ATCCTCTAGAAGAAGGCAGACTGC |
| *dnmtβb.3* | *pt704* | GGACTTGCTGAGGAAGATCGGA | CAGCTCAATTTTATGAACACGCTAAACCA |
| *dnmtβb.1-3* | *pt705* | CTGTCACACATCTTTCCCAGATGAC | CAGCTCAATTTTATGAACACGCTAAACCA |
| *dnmtαb*[#] | *au62* | GGGCCGAACTGTGTAATATTCTTAGGA | GACCAATGATAGTGAGCAAGCATGC |
| *dnmtβa*[#] | *au63* | CTCTGGGTATTGCTGACATGCATTATTC | ACTACGCATAGAACTTAGTGTGCAAGG |
| *dnmtαa* | *sa617*[*] | GAAAATGGATCTAATGGCGTGTGTCGGAC | AGGAGGTCATCAGTTTTCAGGATTAAAAG |

* – Allele acquired through ZIRC.
[#] – Allele generated by Dr. Pawat Seritrakul

# Appendix B: Dusp11 Material and Methods

## B.1: Mouse colony maintenance

Healthy adult male mice from the transgenic line *Dusp11*$^{Tm1a(EUCOMM)Wtsi}$ were donated by Dr. Chris Sullivan's lab (University of Texas at Austin) and used for rederivation in C57BL/6J pseudo pregnant female mice at the Magee Women's Research Center, Pittsburgh, PA. Mice were maintained in the University of Pittsburgh Animal Facility in a 12-hour light/dark cycle and had free access to water and standard laboratory feed in accordance with the Institutional Animal Care and Use Committee. Mice were genotyped using the PCR protocol defined by the International Mouse Phenotyping Consortium (IMPC). Genotyping primers can be found in Table B1. The *Dusp11*$^{Tm1a}$ allele was generated at IMPC in the C57BL/6N mouse strain, which retains a known mutation (*rd8* allele) in the *Crb1* gene. *Crb1*$^{rd8/rd8}$ mice display retinal degenerative phenotypes, thus this mutation has been bred out to the C57BL/6J mouse strain for the past 3 generations.

## B.2: Spectral Domain - Optical Coherence Tomography

Spectral-domain optical coherence tomography (SD-OCT) scanning was adapted from the procedures described previously[286]. Before each session, mice were anesthetized with an intraperitoneal injection of ketamine and xylazine to prevent large movements during SD-OCT image acquisition. Mice were secured on a stage that allowed for free rotation to acquire images focusing on the retina. All images were acquired using SD-OCT (Bioptigen, Inc., Research Triangle Park, NC). All SD-OCT images were taken as rectangular volumes of 0.8 (W) x 0.8 (L) x 1.64 (H) mm and consisted of a 1000 A-scans

per B-scan, 200 B-scan frames, and 1024 samplings/A-scan in depth with an average of three volumes. SD-OCT images were then processed using the mouse automated segmentation function on the Bioptigen Diver 3.0 software to acquire retinal thickness measurements. Retinal lamination defects were detected using ImageJ[287], version 1.50e. SD-OCT files were loaded using the OCT Reader plugin, cropped, and sub-stacked around target location. Breathing and motion artifacts were processed using the StackReg plugin to create confluent frames which were then max-projected to create the final images. All data analyzed using SD-OCT were conducted on the second generation of *Dusp11*$^{Tm1a}$ mice bred into the C57BL/6J mouse strain.

### B.3: Statistical Analysis

All data collected for mouse weights and retinal thickness were imported into GraphPad Prism 8 software and analyzed for statistical significance using two-way ANOVA with Tukey's post hoc analysis using $p < 0.05$ as a significance threshold. Error bars show standard deviation.

Table B.1. List of mouse primer sequences used in the *Dusp11* study

| **IMPC Primer Name** | **Primer Sequence** |
|---|---|
| Wf | TTAAAACTAGATTCCACACAGG |
| Wr | CCCATCTTGAAAACAGATAC |
| Ef | ATTGAATTTGAGGTCTGTCAGCCAGTG |
| Kr | CTCCTACATAGTTGGCAGTGTTTGGG |
| L3f2 | GCCTGGGACTCGTTTCATTGCTT |
| Lxr | GAAGTTATCATTAATTGCGTTGCGCC |
| $Crb1^{rd8}$ Fwd | CCCCTGTTTGCATGGAGGAAAC |
| $Crb1^{rd8}$ Rev | GGGGCTAGAAAAGCACTCATCAATG |

# REFERENCES


1. Chow, R. L. & Lang, R. A. Early eye development in vertebrates. *Annual review of cell and developmental biology* **17**, 255–296 (2001).

2. Fuhrmann, S. Eye morphogenesis and patterning of the optic vesicle. in *Current topics in developmental biology* vol. 93 61–84 (Elsevier, 2010).

3. Schmitt, E. A. & Dowling, J. E. Early-eye morphogenesis in the zebrafish, Brachydanio rerio. *Journal of Comparative Neurology* **344**, 532–542 (1994).

4. Centanin, L. *et al.* Exclusive multipotency and preferential asymmetric divisions in post-embryonic neural stem cells of the fish retina. *Development* **141**, 3472–3482 (2014).

5. Bélanger, M.-C., Robert, B. & Cayouette, M. Msx1-Positive Progenitors in the Retinal Ciliary Margin Give Rise to Both Neural and Non-neural Progenies in Mammals. *Dev. Cell* **40**, 137–150 (2017).

6. Cepko, C. Intrinsically different retinal progenitor cells produce specific types of progeny. *Nature Reviews Neuroscience* **15**, 615–627 (2014).

7. Marcucci, F. *et al.* The ciliary margin zone of the mammalian retina generates retinal ganglion cells. *Cell reports* **17**, 3153–3164 (2016).

8. Marcus, R. C., Delaney, C. L. & Easter, S. S. J. Neurogenesis in the visual system of embryonic and adult zebrafish (Danio rerio). *Visual neuroscience* **16**, 417–424 (1999).

9. Kubota, R., Hokoc, J., Moshiri, A., McGuire, C. & Reh, T. A comparative study of neurogenesis in the retinal ciliary marginal zone of homeothermic vertebrates. *Developmental brain research* **134**, 31–41 (2002).

10. Raymond, P. A., Barthel, L. K., Bernardos, R. L. & Perkowski, J. J. Molecular characterization of retinal stem cells and their niches in adult zebrafish. *BMC*

*Developmental Biology* **6**, (2006).

11. Wan, Y. *et al.* The ciliary marginal zone of the zebrafish retina: clonal and time-lapse analysis of a continuously growing tissue. *Development* **143**, 1099–1107 (2016).

12. Tang, X. *et al.* Bipotent progenitors as embryonic origin of retinal stem cells. *J. Cell Biol.* **216**, 1833–1847 (2017).

13. Reinhardt, R. *et al.* Sox2, Tlx, Gli3, and Her9 converge on Rx2 to define retinal stem cells in vivo. *The EMBO journal* **34**, 1572–1588 (2015).

14. Tsingos, E. *et al.* Retinal stem cells modulate proliferative parameters to coordinate post-embryonic morphogenesis in the eye of fish. *Elife* **8**, (2019).

15. Centanin, L., Hoeckendorf, B. & Wittbrodt, J. Fate restriction and multipotency in retinal stem cells. *Cell stem cell* **9**, 553–562 (2011).

16. Mitchell, P., Liew, G., Gopinath, B. & Wong, T. Y. Age-related macular degeneration. *The Lancet* **392**, 1147–1159 (2018).

17. Berber, P., Grassmann, F., Kiel, C. & Weber, B. H. An eye on age-related macular degeneration: the role of microRNAs in disease pathology. *Molecular diagnosis \& therapy* **21**, 31–43 (2017).

18. Curcio, C. A., Zanzottera, E. C., Ach, T., Balaratnasingam, C. & Freund, K. B. Activated Retinal Pigment Epithelium, an Optical Coherence Tomography Biomarker for Progression in Age-Related Macular Degeneration. *Invest. Ophthalmol. Vis. Sci.* **58**, BIO211–BIO226 (2017).

19. Ferris, F. L. *et al.* Clinical classification of age-related macular degeneration. *Ophthalmology* **120**, 844–51 (2013).

20. Finger, R. P. *et al.* Reticular pseudodrusen: a risk factor for geographic atrophy in fellow eyes of individuals with unilateral choroidal neovascularization. *Ophthalmology* **121**, 1252–6 (2014).

21. Zhou, Q. *et al.* Pseudodrusen and Incidence of Late Age-Related Macular Degeneration in Fellow Eyes in the Comparison of Age-Related Macular Degeneration Treatments Trials. *Ophthalmology* **123**, 1530–40 (2016).

22. Gnanaguru, G., Choi, A. R., Amarnani, D. & D'Amore, P. A. Oxidized lipoprotein uptake through the CD36 receptor activates the NLRP3 inflammasome in human retinal pigment epithelial cells. *Investigative ophthalmology \& visual science* **57**, 4704–4712 (2016).

23. Parmeggiani, F. *et al.* Mechanism of inflammation in age-related macular degeneration. *Mediators of inflammation* **2012**, (2012).

24. Rajshekar, S. *et al.* Pericentromeric hypomethylation elicits an interferon response in an animal model of ICF syndrome. *Elife* **7**, (2018).

25. Kerur, N. *et al.* cGAS drives noncanonical-inflammasome activation in age-related macular degeneration. *Nature medicine* **24**, 50 (2018).

26. Kleinman, M. E. *et al.* Short-interfering RNAs induce retinal degeneration via TLR3 and IRF3. *Molecular therapy* **20**, 101–108 (2012).

27. Misiak, B., Ricceri, L. & Sąsiadek, M. M. Transposable Elements and Their Epigenetic Regulation in Mental Disorders: Current Evidence in the Field. *Front Genet* **10**, 580 (2019).

28. Baets, J. *et al.* Defects of mutant DNMT1 are linked to a spectrum of neurological disorders. *Brain* **138**, 845–61 (2015).

29. Allis, C. D. & Jenuwein, T. The molecular hallmarks of epigenetic control. *Nat. Rev. Genet.* **17**, 487–500 (2016).

30. Waddington, C. H. The epigenotype. *International journal of epidemiology* **41**, 10–13 (2012).

31. Bannister, A. J. & Kouzarides, T. Regulation of chromatin by histone modifications. *Cell Res.* **21**, 381–95 (2011).

32. Edwards, J. R., Yarychkivska, O., Boulard, M. & Bestor, T. H. DNA methylation and DNA methyltransferases. *Epigenetics \& chromatin* **10**, 23 (2017).

33. Gahurova, L. *et al.* Transcription and chromatin determinants of de novo DNA methylation timing in oocytes. *Epigenetics Chromatin* **10**, 25 (2017).

34. Aravin, A. A. *et al.* A piRNA pathway primed by individual transposons is linked to de novo DNA methylation in mice. *Molecular cell* **31**, 785–799 (2008).

35. Jacob, V. *et al.* DNA hypomethylation induces a DNA replication-associated cell cycle arrest to block hepatic outgrowth in uhrf1 mutant zebrafish embryos. *Development* **142**, 510–21 (2015).

36. Andl, T. *et al.* The miRNA-processing enzyme dicer is essential for the morphogenesis and maintenance of hair follicles. *Current Biology* **16**, 1041–1049 (2006).

37. Elliott, E. N., Sheaffer, K. L., Schug, J., Stappenbeck, T. S. & Kaestner, K. H. Dnmt1 is essential to maintain progenitors in the perinatal intestinal epithelium. *Development* **142**, 2163–72 (2015).

38. Liu, X. *et al.* UHRF1 targets DNMT1 for DNA methylation through cooperative binding of hemi-methylated DNA and methylated H3K9. *Nat Commun* **4**, 1563 (2013).

39. Houwing, S. *et al.* A role for Piwi and piRNAs in germ cell maintenance and transposon silencing in Zebrafish. *Cell* **129**, 69–82 (2007).

40. Jeltsch, A., Broche, J. & Bashtrykov, P. Molecular Processes Connecting DNA Methylation Patterns with DNA Methyltransferases and Histone Modifications in Mammalian Genomes. *Genes (Basel)* **10**, (2019).

41. Goll, M. G. & Halpern, M. E. DNA methylation in zebrafish. *Prog Mol Biol Transl Sci* **101**, 193–218 (2011).

42. Smith, Z. D. & Meissner, A. The simplest explanation: passive DNA demethylation in PGCs. *EMBO J.* **32**, 318–21 (2013).

43. Wu, H. & Zhang, Y. Reversing DNA methylation: mechanisms, genomics, and biological functions. *Cell* **156**, 45–68 (2014).

44. Zhang, X. *et al.* DNMT3A and TET2 compete and cooperate to repress lineage-specific transcription factors in hematopoietic stem cells. *Nat. Genet.* **48**, 1014–23 (2016).

45. Seritrakul, P. & Gross, J. M. Tet-mediated DNA hydroxymethylation regulates retinal neurogenesis by modulating cell-extrinsic signaling pathways. *PLoS Genet.* **13**, e1006987 (2017).

46. Chen, T., Ueda, Y., Xie, S. & Li, E. A novel Dnmt3a isoform produced from an alternative promoter localizes to euchromatin and its expression correlates with active de novo methylation. *J. Biol. Chem.* **277**, 38746–54 (2002).

47. Gujar, H., Weisenberger, D. J. & Liang, G. The Roles of Human DNA Methyltransferases and Their Isoforms in Shaping the Epigenome. *Genes (Basel)* **10**, (2019).

48. Vertino, P. M. *et al.* DNMT1 is a component of a multiprotein DNA replication complex. *Cell Cycle* **1**, 416–23.

49. Li, T. *et al.* Structural and mechanistic insights into UHRF1-mediated DNMT1 activation in the maintenance DNA methylation. *Nucleic Acids Res.* **46**, 3218–3231 (2018).

50. Milutinovic, S., Zhuang, Q., Niveleau, A. & Szyf, M. Epigenomic stress response. Knockdown of DNA methyltransferase 1 triggers an intra-S-phase arrest of DNA replication and induction of stress response genes. *J. Biol. Chem.* **278**, 14985–95 (2003).

51. Joseph, D. B. *et al.* Epithelial DNA methyltransferase-1 regulates cell survival, growth and maturation in developing prostatic buds. *Dev. Biol.* **447**, 157–169 (2019).

52. Rhee, K.-D., Yu, J., Zhao, C. Y., Fan, G. & Yang, X.-J. Dnmt1-dependent DNA methylation is essential for photoreceptor terminal differentiation and retinal neuron survival. *Cell Death Dis* **3**, e427 (2012).

53. Spektor, R., Tippens, N. D., Mimoso, C. A. & Soloway, P. D. methyl-ATAC-seq measures DNA methylation at accessible chromatin. *Genome Res.* **29**, 969–977 (2019).

54. Dekkers, K. F., Neele, A. E., Jukema, J. W., Heijmans, B. T. & de Winther, M. P. J. Human monocyte-to-macrophage differentiation involves highly localized gain and loss of DNA methylation at transcription factor binding sites. *Epigenetics Chromatin* **12**, 34 (2019).

55. Fu, X., Wu, X., Djekidel, M. N. & Zhang, Y. Myc and Dnmt1 impede the pluripotent to totipotent state transition in embryonic stem cells. *Nat. Cell Biol.* **21**, 835–844 (2019).

56. Chernyavskaya, Y. *et al.* Loss of DNA methylation in zebrafish embryos activates retrotransposons to trigger antiviral signaling. *Development* **144**, 2925–2939 (2017).

57. Jönsson, M. E. *et al.* Activation of neuronal genes via LINE-1 elements upon global DNA demethylation in human neural progenitors. *Nat Commun* **10**, 3182 (2019).

58. Andersen, I. S., Reiner, A. H., Aanes, H., Aleström, P. & Collas, P. Developmental features of DNA methylation during activation of the embryonic zebrafish genome. *Genome Biol.* **13**, R65 (2012).

59. Baubec, T. *et al.* Genomic profiling of DNA methyltransferases reveals a role for DNMT3B in genic methylation. *Nature* **520**, 243–7 (2015).

60. Duymich, C. E., Charlet, J., Yang, X., Jones, P. A. & Liang, G. DNMT3B isoforms without catalytic activity stimulate gene body methylation as accessory proteins in somatic cells. *Nat Commun* **7**, 11453 (2016).

61. Okano, M., Bell, D. W., Haber, D. A. & Li, E. DNA methyltransferases Dnmt3a and Dnmt3b are essential for de novo methylation and mammalian development. *Cell* **99**, 247–257 (1999).

62. Heyn, P. *et al.* Gain-of-function DNMT3A mutations cause microcephalic dwarfism and hypermethylation of Polycomb-regulated regions. *Nat. Genet.* **51**, 96–105 (2019).

63. Auclair, G., Guibert, S., Bender, A. & Weber, M. Ontogeny of CpG island methylation and specificity of DNMT3 methyltransferases during embryonic development in the mouse. *Genome Biol.* **15**, 545 (2014).

64. Kent, B., Magnani, E., Walsh, M. J. & Sadler, K. C. UHRF1 regulation of Dnmt1 is required for pre-gastrula zebrafish development. *Dev. Biol.* **412**, 99–113 (2016).

65. Yang, L. *et al.* DNMT3A Loss Drives Enhancer Hypomethylation in FLT3-ITD-Associated Leukemias. *Cancer Cell* **30**, 363–365 (2016).

66. Fomchenko, E. I. *et al.* DNMT3A co-mutation in an IDH1-mutant glioblastoma. *Cold Spring Harb Mol Case Stud* **5**, (2019).

67. Mudbhary, R. *et al.* UHRF1 overexpression drives DNA hypomethylation and hepatocellular carcinoma. *Cancer Cell* **25**, 196–209 (2014).

68. Ostler, K. R. *et al.* Truncated DNMT3B isoform DNMT3B7 suppresses growth, induces differentiation, and alters DNA methylation in human neuroblastoma. *Cancer research* **72**, 4714–4723 (2012).

69. Shah, M. Y. *et al.* DNMT3B7, a truncated DNMT3B isoform expressed in human tumors, disrupts embryonic development and accelerates lymphomagenesis. *Cancer research* **70**, 5840–5850 (2010).

70. Sen, G. L., Reuter, J. A., Webster, D. E., Zhu, L. & Khavari, P. A. DNMT1 maintains progenitor function in self-renewing somatic tissue. *Nature* **463**, 563–7 (2010).

71. Wu, Z. *et al.* Dnmt3a regulates both proliferation and differentiation of mouse neural stem cells. *Journal of neuroscience research* **90**, 1883–1891 (2012).

72. Merbs, S. L. *et al.* Cell-specific DNA methylation patterns of retina-specific genes. *PLoS ONE* **7**, e32602 (2012).

73. Jorgensen, B. G. *et al.* DNA methylation, through DNMT1, has an essential role in the development of gastrointestinal smooth muscle cells and disease. *Cell Death Dis* **9**, 474 (2018).

74. Hutnick, L. K. *et al.* DNA hypomethylation restricted to the murine forebrain induces cortical degeneration and impairs postnatal neuronal maturation. *Hum. Mol. Genet.* **18**, 2875–88 (2009).

75. Weber, B., Stresemann, C., Brueckner, B. & Lyko, F. Methylation of human microRNA genes in normal and neoplastic cells. *Cell Cycle* **6**, 1001–5 (2007).

76. Jin, C., Li, M., Ouyang, Y., Tan, Z. & Jiang, Y. MiR-424 functions as a tumor suppressor in glioma cells and is down-regulated by DNA methylation. *J. Neurooncol.* **133**, 247–255 (2017).

77. Shao, L. *et al.* Methylation of the HOXA10 Promoter Directs miR-196b-5p-Dependent Cell Proliferation and Invasion of Gastric Cancer Cells. *Mol. Cancer Res.* **16**, 696–706 (2018).

78. Fire, A. *et al.* Potent and specific genetic interference by double-stranded RNA in Caenorhabditis elegans. *nature* **391**, 806–811 (1998).

79. Wilson, R. C. & Doudna, J. A. Molecular mechanisms of RNA interference. *Annu Rev Biophys* **42**, 217–39 (2013).

80. Le Thomas, A., Tóth, K. F. & Aravin, A. A. To be or not to be a piRNA: genomic origin and processing of piRNAs. *Genome Biol.* **15**, 204 (2014).

81. Van den Beek, M. *et al.* Dual-layer transposon repression in heads of Drosophila melanogaster. *RNA* **24**, 1749–1760 (2018).

82. Le Thomas, A. *et al.* Transgenerationally inherited piRNAs trigger piRNA biogenesis by changing the chromatin of piRNA clusters and inducing precursor processing. *Genes \& development* **28**, 1667–1680 (2014).

83. Gainetdinov, I., Skvortsova, Y., Kondratieva, S., Funikov, S. & Azhikina, T. Two modes of targeting transposable elements by piRNA pathway in human testis. *RNA* **23**, 1614–1625 (2017).

84. Creugny, A., Fender, A. & Pfeffer, S. Regulation of primary micro RNA processing. *FEBS letters* **592**, 1980–1996 (2018).

85. Lee, Y. *et al.* MicroRNA genes are transcribed by RNA polymerase II. *EMBO J.* **23**, 4051–60 (2004).

86. Borchert, G. M., Lanier, W. & Davidson, B. L. RNA polymerase III transcribes human microRNAs. *Nat. Struct. Mol. Biol.* **13**, 1097–101 (2006).

87. Lee, Y. *et al.* The nuclear RNase III Drosha initiates microRNA processing. *Nature* **425**, 415–9 (2003).

88. Han, J. *et al.* The Drosha-DGCR8 complex in primary microRNA processing. *Genes Dev.* **18**, 3016–27 (2004).

89. Yates, L. A., Norbury, C. J. & Gilbert, R. J. The long and short of microRNA. *Cell* **153**, 516–519 (2013).

90. Park, J.-E. *et al.* Dicer recognizes the 5′ end of RNA for efficient and accurate processing. *Nature* **475**, 201–205 (2011).

91. Hammond, S. M., Boettcher, S., Caudy, A. A., Kobayashi, R. & Hannon, G. J. Argonaute2, a link between genetic and biochemical analyses of RNAi. *Science* **293**, 1146–50 (2001).

92. Mourelatos, Z. *et al.* miRNPs: a novel class of ribonucleoproteins containing numerous microRNAs. *Genes Dev.* **16**, 720–8 (2002).

93. Gregory, R. I., Chendrimada, T. P., Cooch, N. & Shiekhattar, R. Human RISC couples microRNA biogenesis and posttranscriptional gene silencing. *Cell* **123**, 631–40 (2005).

94. Martinez, J., Patkaniowska, A., Urlaub, H., Lührmann, R. & Tuschl, T. Single-stranded antisense siRNAs guide target RNA cleavage in RNAi. *Cell* **110**, 563–74 (2002).

95. Xie, H. *et al.* miR-377 induces senescence in human skin fibroblasts by targeting DNA methyltransferase 1. *Cell death \& disease* **8**, e2663–e2663 (2017).

96. Doench, J. G. & Sharp, P. A. Specificity of microRNA target selection in translational repression. *Genes Dev.* **18**, 504–11 (2004).

97. Brennecke, J., Stark, A., Russell, R. B. & Cohen, S. M. Principles of MicroRNA–Target Recognition. *PLoS Biology* **3**, (2005).

98. Taguchi, Y. Apparent microRNA-Target-specific histone modification in mammalian spermatogenesis. *Evolutionary Bioinformatics* **11**, EBO–S21832 (2015).

99. Noonan, E. *et al.* miR-449a targets HDAC-1 and induces growth arrest in prostate cancer. *Oncogene* **28**, 1714–1724 (2009).

100. Varambally, S. *et al.* Genomic loss of microRNA-101 leads to overexpression of histone methyltransferase EZH2 in cancer. *Science* **322**, 1695–9 (2008).

101. Wang, L. *et al.* MicroRNA-101 suppresses progression of lung cancer through the PTEN/AKT signaling pathway by targeting DNA methyltransferase 3A. *Oncol Lett* **13**, 329–338 (2017).

102. Fabbri, M. *et al.* MicroRNA-29 family reverts aberrant methylation in lung cancer by targeting DNA methyltransferases 3A and 3B. *Proceedings of the National Academy of Sciences* **104**, 15805–15810 (2007).

103. Duursma, A. M., Kedde, M., Schrier, M., Le Sage, C. & Agami, R. miR-148 targets human DNMT3b protein coding region. *Rna* **14**, 872–877 (2008).

104. Iida, A., Shinoe, T., Baba, Y., Mano, H. & Watanabe, S. Dicer plays essential roles for retinal development by regulation of survival and differentiation. *Invest. Ophthalmol. Vis. Sci.* **52**, 3008–17 (2011).

105. Wu, Q. *et al.* The RNase III enzyme DROSHA is essential for microRNA production and spermatogenesis. *J. Biol. Chem.* **287**, 25173–90 (2012).

106. Korhonen, H. M. *et al.* DICER Regulates the Formation and Maintenance of Cell-Cell Junctions in the Mouse Seminiferous Epithelium. *Biol. Reprod.* **93**, 139 (2015).

107. Singh, U., Malik, M. A., Goswami, S., Shukla, S. & Kaur, J. Epigenetic regulation of human retinoblastoma. *Tumour Biol.* **37**, 14427–14441 (2016).

108. Kaneko, H. *et al.* DICER1 deficit induces Alu RNA toxicity in age-related macular degeneration. *Nature* **471**, 325–330 (2011).

109. Damiani, D. *et al.* Dicer inactivation leads to progressive functional and structural degeneration of the mouse retina. *J. Neurosci.* **28**, 4878–87 (2008).

110. Aldunate, E. Z. *et al.* Conditional Dicer1 depletion using Chrnb4-Cre leads to cone cell death and impaired photopic vision. *Sci Rep* **9**, 2314 (2019).

111. Polesskaya, O. *et al.* The role of Alu-derived RNAs in Alzheimer's and other neurodegenerative conditions. *Med. Hypotheses* **115**, 29–34 (2018).

112. Bodak, M., Cirera-Salinas, D., Yu, J., Ngondo, R. P. & Ciaudo, C. Dicer, a new regulator of pluripotency exit and LINE-1 elements in mouse embryonic stem cells. *FEBS Open Bio* **7**, 204–220 (2017).

113. Singh, R. K. *et al.* Dnmt1, Dnmt3a and Dnmt3b cooperate in photoreceptor and outer plexiform layer development in the mammalian retina. *Exp. Eye Res.* **159**, 132–146 (2017).

114. Deininger, P. L. & Batzer, M. A. Mammalian retroelements. *Genome research* **12**, 1455–1465 (2002).

115. Hong, H., Kim, B. S. & Im, H.-I. Pathophysiological role of neuroinflammation in neurodegenerative diseases and psychiatric disorders. *International neurourology journal* **20**, S2 (2016).

116. Metcalfe, M. J., Huang, Q. & Figueiredo-Pereira, M. E. Coordination between proteasome impairment and caspase activation leading to TAU pathology: neuroprotection by cAMP. *Cell Death Dis* **3**, e326 (2012).

117. Smets, M. *et al.* DNMT1 mutations found in HSANIE patients affect interaction with UHRF1 and neuronal differentiation. *Hum. Mol. Genet.* **26**, 1522–1534 (2017).

118. Kiesel, P. *et al.* Transcription of Alu DNA elements in blood cells of sporadic Creutzfeldt-Jakob disease (sCJD). *Prion* **4**, 87–93 (2010).

119. Nasonkin, I. O. *et al.* Conditional knockdown of DNA methyltransferase 1 reveals a key role of retinal pigment epithelium integrity in photoreceptor outer segment morphogenesis. *Development* **140**, 1330–1341 (2013).

120. Tittle, R. K. *et al.* Uhrf1 and Dnmt1 are required for development and maintenance of the zebrafish lens. *Dev. Biol.* **350**, 50–63 (2011).

121. Georgi, S. A. & Reh, T. A. Dicer is required for the maintenance of notch signaling and gliogenic competence during mouse retinal development. *Dev Neurobiol* **71**, 1153–69 (2011).

122. Georgi, S. A. & Reh, T. A. Dicer is required for the transition from early to late progenitor state in the developing mouse retina. *J. Neurosci.* **30**, 4048–61 (2010).

123. Kim, Y. *et al.* DICER1/Alu RNA dysmetabolism induces Caspase-8-mediated cell death in age-related macular degeneration. *Proceedings of the National Academy of Sciences* **111**, 16082–16087 (2014).

124. Fischer, A. J., Bosse, J. L. & El-Hodiri, H. M. Reprint of: The ciliary marginal zone (CMZ) in development and regeneration of the vertebrate eye. *Experimental eye*

*research* **123**, 115–120 (2014).

125. Wehman, A. M., Staub, W., Meyers, J. R., Raymond, P. A. & Baier, H. Genetic dissection of the zebrafish retinal stem-cell compartment. *Developmental biology* **281**, 53–65 (2005).

126. Casarosa, S. *et al.* Genetic analysis of metamorphic and premetamorphic Xenopus ciliary marginal zone. *Dev. Dyn.* **233**, 646–51 (2005).

127. Perron, M., Kanekar, S., Vetter, M. L. & Harris, W. A. The genetic sequence of retinal development in the ciliary margin of the Xenopus eye. *Dev. Biol.* **199**, 185–200 (1998).

128. Dixit, R. *et al.* Gene expression is dynamically regulated in retinal progenitor cells prior to and during overt cellular differentiation. *Gene Expr. Patterns* **14**, 42–54 (2014).

129. Tropepe, V. *et al.* Retinal stem cells in the adult mammalian eye. *Science* **287**, 2032–2036 (2000).

130. Del Debbio, C. B., Peng, X., Xiong, H. & Ahmad, I. Adult ciliary epithelial stem cells generate functional neurons and differentiate into both early and late born retinal neurons under non-cell autonomous influences. *BMC neuroscience* **14**, 130 (2013).

131. Das, A. V. *et al.* Retinal properties and potential of the adult mammalian ciliary epithelium stem cells. *Vision research* **45**, 1653–1666 (2005).

132. Ballios, B. G., Clarke, L., Coles, B. L., Shoichet, M. S. & Van Der Kooy, D. The adult retinal stem cell is a rare cell in the ciliary epithelium whose progeny can differentiate into photoreceptors. *Biology open* **1**, 237–246 (2012).

133. Cerveny, K. L. *et al.* The zebrafish flotte lotte mutant reveals that the local retinal environment promotes the differentiation of proliferating precursors emerging from

their stem cell niche. *Development* **137**, 2107–2115 (2010).

134. Borday, C. *et al.* Antagonistic cross-regulation between Wnt and Hedgehog signalling pathways controls post-embryonic retinal proliferation. *Development* **139**, 3499–3509 (2012).

135. Corso-Díaz, X., Jaeger, C., Chaitankar, V. & Swaroop, A. Epigenetic control of gene regulation during development and disease: A view from the retina. *Prog Retin Eye Res* **65**, 1–27 (2018).

136. Aldiri, I. *et al.* The Dynamic Epigenetic Landscape of the Retina During Development, Reprogramming, and Tumorigenesis. *Neuron* **94**, 550–568.e10 (2017).

137. Marques, I. J., Lupi, E. & Mercader, N. Model systems for regeneration: zebrafish. *Development* **146**, (2019).

138. Liu, K., Petree, C., Requena, T., Varshney, P. & Varshney, G. K. Expanding the CRISPR Toolbox in Zebrafish for Studying Development and Disease. *Front Cell Dev Biol* **7**, 13 (2019).

139. Yoder, J. A., Soman, N. S., Verdine, G. L. & Bestor, T. H. DNA (cytosine-5)-methyltransferases in mouse cells and tissues. Studies with a mechanism-based probe. *J. Mol. Biol.* **270**, 385–95 (1997).

140. Bestor, T. H. The DNA methyltransferases of mammals. *Hum. Mol. Genet.* **9**, 2395–402 (2000).

141. Unterberger, A., Andrews, S. D., Weaver, I. C. G. & Szyf, M. DNA methyltransferase 1 knockdown activates a replication stress checkpoint. *Mol. Cell. Biol.* **26**, 7575–86 (2006).

142. Schneider, K. *et al.* Dissection of cell cycle-dependent dynamics of Dnmt1 by FRAP and diffusion-coupled modeling. *Nucleic Acids Res.* **41**, 4860–76 (2013).

143. Maenohara, S. *et al.* Role of UHRF1 in de novo DNA methylation in oocytes and maintenance methylation in preimplantation embryos. *PLoS Genet.* **13**, e1007042 (2017).

144. Anderson, R. M. *et al.* Loss of Dnmt1 catalytic activity reveals multiple roles for DNA methylation during pancreas development and regeneration. *Dev. Biol.* **334**, 213–23 (2009).

145. Kaji, K. *et al.* DNMT1 is a required genomic regulator for murine liver histogenesis and regeneration. *Hepatology* **64**, 582–98 (2016).

146. Liu, X. *et al.* DNA methyltransferase 1 functions through C/ebpa to maintain hematopoietic stem and progenitor cells in zebrafish. *J Hematol Oncol* **8**, 15 (2015).

147. Wanner, N. *et al.* DNA Methyltransferase 1 Controls Nephron Progenitor Cell Renewal and Differentiation. *J. Am. Soc. Nephrol.* **30**, 63–78 (2019).

148. Chen, T. *et al.* Complete inactivation of DNMT1 leads to mitotic catastrophe in human cancer cells. *Nat. Genet.* **39**, 391–6 (2007).

149. Jackson-Grusby, L. *et al.* Loss of genomic methylation causes p53-dependent apoptosis and epigenetic deregulation. *Nat. Genet.* **27**, 31–9 (2001).

150. Walsh, C. P., Chaillet, J. R. & Bestor, T. H. Transcription of IAP endogenous retroviruses is constrained by cytosine methylation. *Nat. Genet.* **20**, 116–7 (1998).

151. Ramesh, V. *et al.* Loss of Uhrf1 in neural stem cells leads to activation of retroviral elements and delayed neurodegeneration. *Genes Dev.* **30**, 2199–2212 (2016).

152. Golshani, P., Hutnick, L., Schweizer, F. & Fan, G. Conditional Dnmt1 deletion in dorsal forebrain disrupts development of somatosensory barrel cortex and thalamocortical long-term potentiation. *Thalamus Relat Syst* **3**, 227–233 (2005).

153. Sheaffer, K. L. *et al.* DNA methylation is required for the control of stem cell differentiation in the small intestine. *Genes Dev.* **28**, 652–64 (2014).

154. Fan, G. *et al.* DNA methylation controls the timing of astrogliogenesis through regulation of JAK-STAT signaling. *Development* **132**, 3345–56 (2005).

155. Georgia, S., Kanji, M. & Bhushan, A. DNMT1 represses p53 to maintain progenitor cell survival during pancreatic organogenesis. *Genes Dev.* **27**, 372–7 (2013).

156. Berghmans, S. *et al.* tp53 mutant zebrafish develop malignant peripheral nerve sheath tumors. *Proc. Natl. Acad. Sci. U.S.A.* **102**, 407–12 (2005).

157. Sidi, S. *et al.* Chk1 suppresses a caspase-2 apoptotic response to DNA damage that bypasses p53, Bcl-2, and caspase-3. *Cell* **133**, 864–77 (2008).

158. Noguchi, H. *et al.* DNA Methyltransferase 1 Is Indispensable for Development of the Hippocampal Dentate Gyrus. *J. Neurosci.* **36**, 6050–68 (2016).

159. Rai, K. *et al.* Zebra fish Dnmt1 and Suv39h1 regulate organ-specific terminal differentiation during development. *Mol. Cell. Biol.* **26**, 7077–85 (2006).

160. Pujic, Z. *et al.* Reverse genetic analysis of neurogenesis in the zebrafish retina. *Dev. Biol.* **293**, 330–47 (2006).

161. Haruta, M. *et al.* Loss of maintenance DNA methylation results in abnormal DNA origin firing during DNA replication. *Biochemical and biophysical research communications* **469**, 960–966 (2016).

162. El Yakoubi, W. *et al.* Hes4 controls proliferative properties of neural stem cells during retinal ontogenesis. *Stem Cells* **30**, 2784–95 (2012).

163. Chalopin, D., Naville, M., Plard, F., Galiana, D. & Volff, J.-N. Comparative analysis of transposable elements highlights mobilome diversity and evolution in vertebrates. *Genome Biol Evol* **7**, 567–80 (2015).

164. Gao, B. *et al.* The contribution of transposable elements to size variations between four teleost genomes. *Mobile DNA* **7**, 4 (2016).

165. Maugeri, A. *et al.* Characterization of SIRT1/DNMTs Functions and LINE-1 Methylation in Patients with Age-Related Macular Degeneration. *J Clin Med* **8**, (2019).

166. Li, S.-Y. *et al.* DNMT1 in Six2 Progenitor Cells Is Essential for Transposable Element Silencing and Kidney Development. *J. Am. Soc. Nephrol.* **30**, 594–609 (2019).

167. Liang, G. *et al.* Cooperativity between DNA methyltransferases in the maintenance methylation of repetitive elements. *Mol. Cell. Biol.* **22**, 480–91 (2002).

168. Baillie, J. K. *et al.* Somatic retrotransposition alters the genetic landscape of the human brain. *Nature* **479**, 534–7 (2011).

169. Upton, K. R. *et al.* Ubiquitous L1 mosaicism in hippocampal neurons. *Cell* **161**, 228–39 (2015).

170. Thomas, C. A. *et al.* Modeling of TREX1-Dependent Autoimmune Disease using Human Stem Cells Highlights L1 Accumulation as a Source of Neuroinflammation. *Cell Stem Cell* **21**, 319–331.e8 (2017).

171. Tam, O. H., Ostrow, L. W. & Gale Hammell, M. Diseases of the nERVous system: retrotransposon activity in neurodegenerative disease. *Mob DNA* **10**, 32 (2019).

172. Wylie, A. *et al.* p53 genes function to restrain mobile elements. *Genes \& development* **30**, 64–77 (2016).

173. Ostertag, E. M., Luning Prak, E. T., DeBerardinis, R. J., Moran, J. V. & Kazazian Jr, H. H. Determination of L1 retrotransposition kinetics in cultured cells. *Nucleic Acids Research* **28**, 1418–1423 (2000).

174. Ostertag, E. M. *et al.* A mouse model of human L1 retrotransposition. *Nature genetics* **32**, 655 (2002).

175. Galluzzi, L. *et al.* Essential versus accessory aspects of cell death: recommendations of the NCCD 2015. *Cell Death Differ.* **22**, 58–73 (2015).

176. Viringipurampeer, I. A. *et al.* Rip3 knockdown rescues photoreceptor cell death in blind pde6c zebrafish. *Cell Death Differ.* **21**, 665–75 (2014).

177. Viringipurampeer, I. A. *et al.* Pax2 regulates a fadd-dependent molecular switch that drives tissue fusion during eye development. *Hum. Mol. Genet.* **21**, 2357–69 (2012).

178. Liu, X. & Lieberman, J. A Mechanistic Understanding of Pyroptosis: The Fiery Death Triggered by Invasive Infection. *Adv. Immunol.* **135**, 81–117 (2017).

179. Hato, T. & Dagher, P. C. How the Innate Immune System Senses Trouble and Causes Trouble. *Clin J Am Soc Nephrol* **10**, 1459–69 (2015).

180. Muotri, A. R. *et al.* Somatic mosaicism in neuronal precursor cells mediated by L1 retrotransposition. *Nature* **435**, 903–10 (2005).

181. Coufal, N. G. *et al.* L1 retrotransposition in human neural progenitor cells. *Nature* **460**, 1127 (2009).

182. Erwin, J. A. *et al.* L1-associated genomic regions are deleted in somatic cells of the healthy human brain. *Nat. Neurosci.* **21**, 1016 (2018).

183. Percharde, M. *et al.* A LINE1-Nucleolin Partnership Regulates Early Development and ESC Identity. *Cell* **174**, 391–405.e19 (2018).

184. Yang, F. *et al.* DUX-miR-344-ZMYM2-Mediated Activation of MERVL LTRs Induces a Totipotent 2C-like State. *Cell Stem Cell* **26**, 234–250.e7 (2020).

185. Zhao, K. *et al.* Modulation of LINE-1 and Alu/SVA retrotransposition by Aicardi-Goutières syndrome-related SAMHD1. *Cell Rep* **4**, 1108–15 (2013).

186. Pereira, G. C. *et al.* Properties of LINE-1 proteins and repeat element expression in the context of amyotrophic lateral sclerosis. *Mob DNA* **9**, 35 (2018).

187. Li, S. *et al.* Hypomethylation of LINE-1 elements in schizophrenia and bipolar disorder. *J Psychiatr Res* **107**, 68–72 (2018).

188. Bronner, C., Alhosin, M., Hamiche, A. & Mousli, M. Coordinated Dialogue between UHRF1 and DNMT1 to Ensure Faithful Inheritance of Methylated DNA Patterns. *Genes (Basel)* **10**, (2019).

189. Zhang, Z. *et al.* Micro RNA-29b regulates DNA methylation by targeting Dnmt3a/3b and Tet1/2/3 in porcine early embryo development. *Development, growth \& differentiation* **60**, 197–204 (2018).

190. Seritrakul, P. Functional analysis of DNA methylation and hydroxymethylation during eye development. (2018).

191. Jain, D. *et al.* rahu is a mutant allele of Dnmt3c, encoding a DNA methyltransferase homolog required for meiosis and transposon repression in the mouse male germline. *PLoS Genet.* **13**, e1006964 (2017).

192. Aravin, A. A. *et al.* A piRNA pathway primed by individual transposons is linked to de novo DNA methylation in mice. *Mol. Cell* **31**, 785–99 (2008).

193. Ai, L. *et al.* Myeloid-derived suppressor cells endow stem-like qualities to multiple myeloma cells by inducing piRNA-823 expression and DNMT3B activation. *Mol. Cancer* **18**, 88 (2019).

194. Desai, M., Han, G., Li, T. & Ross, M. G. Programmed Epigenetic DNA Methylation-Mediated Reduced Neuroprogenitor Cell Proliferation and Differentiation in Small-for-Gestational-Age Offspring. *Neuroscience* **412**, 60–71 (2019).

195. Shimoda, N., Yamakoshi, K., Miyake, A. & Takeda, H. Identification of a gene required for de novo DNA methylation of the zebrafish no tail gene. *Developmental dynamics: an official publication of the American Association of Anatomists* **233**, 1509–1516 (2005).

196. Postlethwait, J. H. *et al.* Vertebrate genome evolution and the zebrafish gene map. *Nat. Genet.* **18**, 345–9 (1998).

197. Campos, C., Valente, L. M. P. & Fernandes, J. M. O. Molecular evolution of zebrafish dnmt3 genes and thermal plasticity of their expression during embryonic development. *Gene* **500**, 93–100 (2012).

198. Liu, J., Hu, H., Panserat, S. & Marandel, L. Evolutionary history of DNA methylation related genes in chordates: new insights from multiple whole genome duplications. *Sci Rep* **10**, 970 (2020).

199. Seritrakul, P. & Gross, J. M. Expression of the de novo DNA methyltransferases (dnmt3 - dnmt8) during zebrafish lens development. *Dev. Dyn.* **243**, 350–6 (2014).

200. Cermak, T. *et al.* Efficient design and assembly of custom TALEN and other TAL effector-based constructs for DNA targeting. *Nucleic Acids Res.* **39**, e82 (2011).

201. Albadri, S., Del Bene, F. & Revenu, C. Genome editing using CRISPR/Cas9-based knock-in approaches in zebrafish. *Methods* **121**, 77–85 (2017).

202. Bedell, V. M. *et al.* In vivo genome editing using a high-efficiency TALEN system. *Nature* **491**, 114–118 (2012).

203. Li, T. *et al.* Modularly assembled designer TAL effector nucleases for targeted gene knockout and gene replacement in eukaryotes. *Nucleic acids research* **39**, 6315–6325 (2011).

204. Auer, T. O. & Del Bene, F. CRISPR/Cas9 and TALEN-mediated knock-in approaches in zebrafish. *Methods* **69**, 142–150 (2014).

205. Cade, L. *et al.* Highly efficient generation of heritable zebrafish gene mutations using homo- and heterodimeric TALENs. *Nucleic Acids Res.* **40**, 8001–10 (2012).

206. Lalonde, S. *et al.* Frameshift indels introduced by genome editing can lead to in-frame exon skipping. *PLoS One* **12**, (2017).

207. Seritrakul, P. & Gross, J. M. Tet-mediated DNA hydroxymethylation regulates retinal neurogenesis by modulating cell-extrinsic signaling pathways. *PLoS genetics* **13**, e1006987 (2017).

208. Tsumura, A. *et al.* Maintenance of self-renewal ability of mouse embryonic stem cells in the absence of DNA methyltransferases Dnmt1, Dnmt3a and Dnmt3b. *Genes Cells* **11**, 805–14 (2006).

209. Kato, Y. *et al.* Role of the Dnmt3 family in de novo methylation of imprinted and repetitive sequences during male germ cell development in the mouse. *Human molecular genetics* **16**, 2272–2280 (2007).

210. Kaneda, M. *et al.* Essential role for de novo DNA methyltransferase Dnmt3a in paternal and maternal imprinting. *Nature* **429**, 900–903 (2004).

211. Tadokoro, Y., Ema, H., Okano, M., Li, E. & Nakauchi, H. De novo DNA methyltransferase is essential for self-renewal, but not for differentiation, in hematopoietic stem cells. *J. Exp. Med.* **204**, 715–22 (2007).

212. Meyer, S. E. *et al.* DNMT3A Haploinsufficiency Transforms FLT3ITD Myeloproliferative Disease into a Rapid, Spontaneous, and Fully Penetrant Acute Myeloid Leukemia. *Cancer Discov* **6**, 501–15 (2016).

213. Kimura, H., Suetake, I. & Tajima, S. Exogenous expression of mouse Dnmt3 induces apoptosis in Xenopus early embryos. *J. Biochem.* **131**, 933–41 (2002).

214. Rai, K. *et al.* Dnmt3 and G9a cooperate for tissue-specific development in zebrafish. *Journal of Biological Chemistry* **285**, 4110–4121 (2010).

215. Yang, G. *et al.* DNA methyltransferase 3, a target of microRNA-29c, contributes to neuronal proliferation by regulating the expression of brain-derived neurotrophic factor. *Mol Med Rep* **12**, 1435–42 (2015).

216. Patterson, K. I., Brummer, T., O'brien, P. M. & Daly, R. J. Dual-specificity phosphatases: critical regulators with diverse cellular targets. *Biochemical Journal* **418**, 475–489 (2009).

217. Caprara, G., Zamponi, R., Melixetian, M. & Helin, K. Isolation and characterization of DUSP11, a novel p53 target gene. *Journal of cellular and molecular medicine* **13**, 2158–2170 (2009).

218. Galvao, J. *et al.* The Krüppel-Like Factor Gene Target Dusp14 Regulates Axon Growth and Regeneration. *Investigative ophthalmology \& visual science* **59**, 2736–2747 (2018).

219. Pérez-Sen, R. *et al.* Dual-Specificity Phosphatase Regulation in Neurons and Glial Cells. *Int J Mol Sci* **20**, (2019).

220. Lang, R. & Raffi, F. A. M. Dual-Specificity Phosphatases in Immunity and Infection: An Update. *Int J Mol Sci* **20**, (2019).

221. Amador-Cañizares, Y., Bernier, A., Wilson, J. A. & Sagan, S. M. miR-122 does not impact recognition of the HCV genome by innate sensors of RNA but rather protects the 5′ end from the cellular pyrophosphatases, DOM3Z and DUSP11. *Nucleic acids research* **46**, 5139–5158 (2018).

222. Yuan, Y., Li, D. M. & Sun, H. PIR1, a novel phosphatase that exhibits high affinity to RNA . ribonucleoprotein complexes. *J. Biol. Chem.* **273**, 20347–53 (1998).

223. Deshpande, T., Takagi, T., Hao, L., Buratowski, S. & Charbonneau, H. Human PIR1 of the protein-tyrosine phosphatase superfamily has RNA 5'-triphosphatase and diphosphatase activities. *J. Biol. Chem.* **274**, 16590–4 (1999).

224. Kincaid, R. P., Lam, V. L., Chirayil, R. P., Randall, G. & Sullivan, C. S. RNA triphosphatase DUSP11 enables exonuclease XRN-mediated restriction of hepatitis C virus. *Proc. Natl. Acad. Sci. U.S.A.* **115**, 8197–8202 (2018).

225. Zhao, Y., Ye, X., Dunker, W., Song, Y. & Karijolich, J. RIG-I like receptor sensing of host RNAs facilitates the cell-intrinsic immune response to KSHV infection. *Nature communications* **9**, 1–14 (2018).

226. Häsler, R. *et al.* Alterations of pre-mRNA splicing in human inflammatory bowel disease. *Eur. J. Cell Biol.* **90**, 603–11.

227. Hornung, V. *et al.* 5'-Triphosphate RNA is the ligand for RIG-I. *Science* **314**, 994–7 (2006).

228. Hwang, S.-Y. *et al.* 5'-Triphosphate-RNA-independent activation of RIG-I via RNA aptamer with enhanced antiviral activity. *Nucleic Acids Res.* **40**, 2724–33 (2012).

229. Conti, A. *et al.* Identification of RNA polymerase III-transcribed Alu loci by computational screening of RNA-Seq data. *Nucleic Acids Res.* **43**, 817–35 (2015).

230. Panning, B. & Smiley, J. R. Activation of RNA polymerase III transcription of human Alu elements by herpes simplex virus. *Virology* **202**, 408–17 (1994).

231. Burke, J. M. & Sullivan, C. S. DUSP11 - An RNA phosphatase that regulates host and viral non-coding RNAs in mammalian cells. *RNA Biol* **14**, 1457–1465 (2017).

232. Burke, J. M., Kincaid, R. P., Nottingham, R. M., Lambowitz, A. M. & Sullivan, C. S. DUSP11 activity on triphosphorylated transcripts promotes Argonaute association with noncanonical viral microRNAs and regulates steady-state levels of cellular noncoding RNAs. *Genes Dev.* **30**, 2076–2092 (2016).

233. Tarallo, V. *et al.* DICER1 loss and Alu RNA induce age-related macular degeneration via the NLRP3 inflammasome and MyD88. *Cell* **149**, 847–59 (2012).

234. Kerur, N. *et al.* TLR-independent and P2X7-dependent signaling mediate Alu RNA-induced NLRP3 inflammasome activation in geographic atrophy. *Invest. Ophthalmol. Vis. Sci.* **54**, 7395–401 (2013).

235. Wright, C. B. *et al.* Chronic Dicer1 deficiency promotes atrophic and neovascular outer retinal pathologies in mice. *Proc. Natl. Acad. Sci. U.S.A.* (2020) doi:10.1073/pnas.1909761117.

236. Mattapallil, M. J. *et al.* The Rd8 mutation of the Crb1 gene is present in vendor lines of C57BL/6N mice and embryonic stem cells, and confounds ocular induced mutant phenotypes. *Invest. Ophthalmol. Vis. Sci.* **53**, 2921–7 (2012).

237. Brown, S. D. M. & Moore, M. W. The International Mouse Phenotyping Consortium: past and future perspectives on mouse phenotyping. *Mamm. Genome* **23**, 632–40 (2012).

238. Garcia Garrido, M. *et al.* Towards a quantitative OCT image analysis. *PLoS ONE* **9**, e100080 (2014).

239. Srinivasan, P. P., Heflin, S. J., Izatt, J. A., Arshavsky, V. Y. & Farsiu, S. Automatic segmentation of up to ten layer boundaries in SD-OCT images of the mouse retina with and without missing layers due to pathology. *Biomed Opt Express* **5**, 348–65 (2014).

240. Cuenca, N., Ortuño-Lizarán, I. & Pinilla, I. Cellular characterization of OCT and outer retinal bands using specific immunohistochemistry markers and clinical implications. *Ophthalmology* **125**, 407–422 (2018).

241. Dysli, C., Enzmann, V., Sznitman, R. & Zinkernagel, M. S. Quantitative Analysis of Mouse Retinal Layers Using Automated Segmentation of Spectral Domain Optical Coherence Tomography Images. *Transl Vis Sci Technol* **4**, 9 (2015).

242. Sundermeier, T. R. *et al.* DICER1 is essential for survival of postmitotic rod photoreceptor cells in mice. *FASEB J.* **28**, 3780–91 (2014).

243. Berger, A. *et al.* Spectral-domain optical coherence tomography of the rodent eye: highlighting layers of the outer retina using signal averaging and comparison with histology. *PLoS ONE* **9**, e96494 (2014).

244. Foulkes, W. D., Priest, J. R. & Duchaine, T. F. DICER1: mutations, microRNAs and mechanisms. *Nature Reviews Cancer* **14**, 662–672 (2014).

245. Finco, I. & Hammer, G. D. Isolation, Fixation, and Immunofluorescence Imaging of Mouse Adrenal Glands. *J Vis Exp* (2018) doi:10.3791/58530.

246. Whittington, N. C. & Wray, S. Suppression of Red Blood Cell Autofluorescence for Immunocytochemistry on Fixed Embryonic Mouse Tissue. *Curr Protoc Neurosci* **81**, 2.28.1–2.28.12 (2017).

247. Valiunas, V. *et al.* Connexin-specific cell-to-cell transfer of short interfering RNA by gap junctions. *J. Physiol. (Lond.)* **568**, 459–68 (2005).

248. Lim, P. K. *et al.* Gap junction-mediated import of microRNA from bone marrow stromal cells can elicit cell cycle quiescence in breast cancer cells. *Cancer Res.* **71**, 1550–60 (2011).

249. Zong, L., Zhu, Y., Liang, R. & Zhao, H.-B. Gap junction mediated miRNA intercellular transfer and gene regulation: A novel mechanism for intercellular genetic communication. *Sci Rep* **6**, 19884 (2016).

250. Zhu, Y., Zong, L., Mei, L. & Zhao, H.-B. Connexin26 gap junction mediates miRNA intercellular genetic communication in the cochlea and is required for inner ear development. *Sci Rep* **5**, 15647 (2015).

251. Hong, X., Sin, W. C., Harris, A. L. & Naus, C. C. Gap junctions modulate glioma invasion by direct transfer of microRNA. *Oncotarget* **6**, 15566–77 (2015).

252. Thuringer, D. *et al.* Transfer of functional microRNAs between glioblastoma and microvascular endothelial cells through gap junctions. *Oncotarget* **7**, 73925–73934 (2016).

253. Dong, D., Xie, W. & Liu, M. Alteration of cell junctions during viral infection. *Thorac Cancer* **11**, 519–525 (2020).

254. Sasaki, T. *et al.* Aberrant autolysosomal regulation is linked to the induction of embryonic senescence: differential roles of Beclin 1 and p53 in vertebrate Spns1 deficiency. *PLoS Genet.* **10**, e1004409 (2014).

255. He, C. & Klionsky, D. J. Regulation mechanisms and signaling pathways of autophagy. *Annu. Rev. Genet.* **43**, 67–93 (2009).

256. Choi, A. M. K., Ryter, S. W. & Levine, B. Autophagy in human health and disease. *N. Engl. J. Med.* **368**, 1845–6 (2013).

257. Dermaut, B. *et al.* Aberrant lysosomal carbohydrate storage accompanies endocytic defects and neurodegeneration in Drosophila benchwarmer. *J. Cell Biol.* **170**, 127–39 (2005).

258. Fleming, A. & Rubinsztein, D. C. Zebrafish as a model to understand autophagy and its role in neurological disease. *Biochim. Biophys. Acta* **1812**, 520–6 (2011).

259. Li, J., Kim, S. G. & Blenis, J. Rapamycin: one drug, many effects. *Cell Metab.* **19**, 373–9 (2014).

260. Pang, J. *et al.* Sirtuin 1 and Autophagy Attenuate Cisplatin-Induced Hair Cell Death in the Mouse Cochlea and Zebrafish Lateral Line. *Front Cell Neurosci* **12**, 515 (2018).

261. Schulz, N. K. E. *et al.* Dnmt1 has an essential function despite the absence of CpG DNA methylation in the red flour beetle Tribolium castaneum. *Sci Rep* **8**, 16462 (2018).

262. Hoang, T. V. *et al.* Lens development requires DNMT1 but takes place normally in the absence of both DNMT3A and DNMT3B activity. *Epigenetics* **12**, 27–40 (2017).

263. Dai, Y.-J. *et al.* Conditional knockin of Dnmt3a R878H initiates acute myeloid leukemia with mTOR pathway involvement. *Proc. Natl. Acad. Sci. U.S.A.* **114**, 5237–5242 (2017).

264. Brand, A. H. & Perrimon, N. Targeted gene expression as a means of altering cell fates and generating dominant phenotypes. *Development* **118**, 401–15 (1993).

265. Kwan, K. M. *et al.* The Tol2kit: a multisite gateway-based construction kit for Tol2 transposon transgenesis constructs. *Dev. Dyn.* **236**, 3088–99 (2007).

266. Ornitz, D. M., Moreadith, R. W. & Leder, P. Binary system for regulating transgene expression in mice: targeting int-2 gene expression with yeast GAL4/UAS control elements. *Proc. Natl. Acad. Sci. U.S.A.* **88**, 698–702 (1991).

267. Das, A. T., Tenenbaum, L. & Berkhout, B. Tet-On Systems For Doxycycline-inducible Gene Expression. *Curr Gene Ther* **16**, 156–67 (2016).

268. Buchholz, D. R. Tet-On binary systems for tissue-specific and inducible transgene expression. *Methods Mol. Biol.* **917**, 265–75 (2012).

269. Thakore, P. I. *et al.* Highly specific epigenome editing by CRISPR-Cas9 repressors for silencing of distal regulatory elements. *Nat. Methods* **12**, 1143–9 (2015).

270. Ma, Y., Zhang, L. & Huang, X. Genome modification by CRISPR/Cas9. *FEBS J.* **281**, 5186–93 (2014).

271. Hata, K., Okano, M., Lei, H. & Li, E. Dnmt3L cooperates with the Dnmt3 family of de novo DNA methyltransferases to establish maternal imprints in mice. *Development* **129**, 1983–1993 (2002).

272. Sendvzikaite, G., Hanna, C. W., Stewart-Morgan, K. R., Ivanova, E. & Kelsey, G. A DNMT3A PWWP mutation leads to methylation of bivalent chromatin and growth retardation in mice. *Nature communications* **10**, 1–16 (2019).

273. Itou, D. *et al.* Induction of DNA methylation by artificial piRNA production in male germ cells. *Curr. Biol.* **25**, 901–6 (2015).

274. Lucifero, D. *et al.* Coordinate regulation of DNA methyltransferase expression during oogenesis. *BMC developmental biology* **7**, 36 (2007).

275. Kobayashi, H. *et al.* Contribution of intragenic DNA methylation in mouse gametic DNA methylomes to establish oocyte-specific heritable marks. *PLoS Genet.* **8**, e1002440 (2012).

276. Terry, D. M. & Devine, S. E. Aberrantly High Levels of Somatic LINE-1 Expression and Retrotransposition in Human Neurological Disorders. *Front Genet* **10**, 1244 (2019).

277. Shpyleva, S., Melnyk, S., Pavliv, O., Pogribny, I. & Jill James, S. Overexpression of LINE-1 Retrotransposons in Autism Brain. *Mol. Neurobiol.* **55**, 1740–1749 (2018).

278. Lou, C., Goodier, J. L. & Qiang, R. A potential new mechanism for pregnancy loss: considering the role of LINE-1 retrotransposons in early spontaneous miscarriage. *Reprod. Biol. Endocrinol.* **18**, 6 (2020).

279. Siomi, M. C., Sato, K., Pezic, D. & Aravin, A. A. PIWI-interacting small RNAs: the vanguard of genome defence. *Nat. Rev. Mol. Cell Biol.* **12**, 246–58 (2011).

280. Ablasser, A. *et al.* RIG-I-dependent sensing of poly(dA:dT) through the induction of an RNA polymerase III-transcribed RNA intermediate. *Nat. Immunol.* **10**, 1065–72 (2009).

281. Kinoshita, J. & Peachey, N. S. Noninvasive Electroretinographic Procedures for the Study of the Mouse Retina. *Curr Protoc Mouse Biol* **8**, 1–16 (2018).

282. Uribe, R. A. & Gross, J. M. Immunohistochemistry on cryosections from embryonic and adult zebrafish eyes. *CSH Protoc* **2007**, pdb.prot4779 (2007).

283. Jowett, T. Whole-mount in situ hybridization on zebrafish embryos using a mixture of digoxigenin-and fluorescein-labelled probes. *Trends. Genet.* **10**, 73–74 (1994).

284. Neff, K. L. *et al.* Mojo Hand, a TALEN design tool for genome editing applications. *BMC bioinformatics* **14**, 1 (2013).

285. Cermak, T. *et al.* Efficient design and assembly of custom TALEN and other TAL effector-based constructs for DNA targeting. *Nucleic acids research* **39**, e82–e82

(2011).

286. Gabriele, M. L. *et al.* Reproducibility of spectral-domain optical coherence tomography total retinal thickness measurements in mice. *Invest. Ophthalmol. Vis. Sci.* **51**, 6519–23 (2010).

287. Schindelin, J. *et al.* Fiji: an open-source platform for biological-image analysis. *Nature methods* **9**, 676–682 (2012).